

**Photophysical Behavior of 1,8-Diaminonaphthalene
in Acidic Aqueous Solutions and in Zeolite Sieves**

BY

ABDUL-RAHMAN FAISAL AL-BETAR

A Thesis Presented to the
DEANSHIP OF GRADUATE STUDIES

KING FAHD UNIVERSITY OF PETROLEUM & MINERALS

DHAHRAN, SAUDI ARABIA

In Partial Fulfillment of the
Requirements for the Degree of

MASTER OF SCIENCE

In

CHEMISTRY

May 2004

UMI Number: 1420921

INFORMATION TO USERS

The quality of this reproduction is dependent upon the quality of the copy submitted. Broken or indistinct print, colored or poor quality illustrations and photographs, print bleed-through, substandard margins, and improper alignment can adversely affect reproduction.

In the unlikely event that the author did not send a complete manuscript and there are missing pages, these will be noted. Also, if unauthorized copyright material had to be removed, a note will indicate the deletion.

UMI[®]

UMI Microform 1420921

Copyright 2004 by ProQuest Information and Learning Company.

All rights reserved. This microform edition is protected against unauthorized copying under Title 17, United States Code.

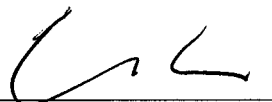
ProQuest Information and Learning Company
300 North Zeeb Road
P.O. Box 1346
Ann Arbor, MI 48106-1346

**KING FAHD UNIVERSITY OF PETROLEUM AND MINERALS
DHAHRAN, SAUDI ARABIA**

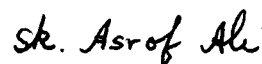
DEANSHIP OF GRADUATE STUDIES

This thesis, written by **Mr. Abdul-Rahman Faisal Al-Betar** under the direction of his thesis advisor and approved by his thesis committee, has been presented to and accepted by the dean of graduate studies, in partial fulfillment of the requirements for the degree of **MASTER OF SCIENCE IN CHEMISTRY.**

Thesis Committee



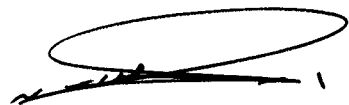
Prof. Uwe K. A. Klein
Thesis Advisor



Prof. Shaikh A. Ali
Member



Dr. Than Htun
Member

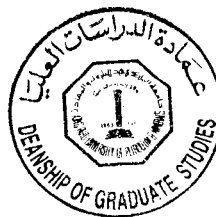


Dr. Assad A Al. Thukair
Department Chairman



Prof. Osama A. Jannadi
Dean, College of Graduate Studies

Date: 9/6/2004



الإهداء

إلى أبي الفاضل الذي ما فتئ يرعاني ويشملني بنصحه...

إلى أمي الحبيبة التي أظلتني بعطفها وحنانها...

إلى إخواني و أخواتي الأفاضل الذين شجعوني على رحلتي العلمية...

إلى أساتذتي الكرام الذين تعلمت منهم المثابرة في المسيرة العلمية...

إليهم جميعاً أهدي هذه الرسالة ،

محمد الرحمن...

ACKNOWLEDGMENT

All praise and glory be to Allah for his limitless help and guidance. Peace pleasing of Allah be upon his prophet Mohammed.

Acknowledgment is due to the King Fahd University of Petroleum & Minerals and the Chemistry Department for supporting this research. I would like to express my profound gratitude and appreciation to my advisor Prof. Uwe K.A. Klein, for his guidance and patience throughout this thesis, his continuous support and encouragement can never be forgotten. It was a great experience working and learning with him. I am also grateful to the other members, Prof. Shaikh A. Ali and Dr. Than Htun. I would like to extend my thanks to Dr. Ali El-Rayyes and Dr. Mohammed Fettouhi for helpful discussions and consultations.

I am also grateful to Dr. Asaad Al-Thukair, Chairman of the Chemistry Department, and Dr. Mahmoud Nagadi, Dean of the College of Sciences at KFUPM, for their support and encouragement.

Finally, my special and deep thanks to my wonderful parents, brothers and sisters for their encouragement and moral support.

TABLE OF CONTENTS

Acknowledgements	i
Table of Contents	ii
List of Tables	vii
List of Figures	ix
Thesis Abstract (English)	xiv
Thesis Abstract (Arabic)	xv
1. INTRODUCTION	1
1.1 General Overview	1
1.2 Purpose of This Work	3
1.3 Literature Review	7
1.4 Reaction Scheme of Proton Transfer	13

1.5	Laser Amplification	15
1.6	Stimulated Emission	18
1.7	Characterization of Zeolite Y (Faujasite)	19
1.7.1	Synthesis of Zeolite Y	19
1.7.2	Applications of Zeolite Y	19
2.	EXPERIMENTAL	21
2.1	Materials	21
2.2	Purification and Stability	22
2.3	Solution Preparations	22
2.4	Catalyst Preparations	22
2.5	Catalyst-Probe Complex Preparations	23
2.6	Poly Dimethylsiloxane ‘PDMS’ Membrane Preparations	23
2.7	UV-Vis Absorption Measurements	24
2.8	Fluorescence Emission Measurements	24
2.9	Fluorescence Decay Time Measurements	24

2.10 Laser Sources of the System	27
2.10.1 The Neodymium-YAG Laser	27
2.10.2 Dye Lasers	27
2.11 Frequency Doubling	30
2.12 Acousto-Optic Mode Locking of Nd:YAG Lasers	31
2.13 Synchronously-Pumped Dye Lasers	32
2.14 Cavity-Dumping of a Continuous Wave (CW) Laser	33
2.15 Cavity-Dumping of Dye Lasers	33
2.16 Single Photon-Counting Technique	34
3. RESULTS AND DISCUSSIONS	36
3.1 Absorption Spectra	36
3.2 Emission Spectra	43
3.3 Relaxation Energy Levels of 1,8-DAN	48
3.4 Fluorescence Decay Measurements	49
3.5 Validity of Lambert Beer's Law	57

3.5.1 Determination of Extinction Coefficient (ϵ)	59
3.6 Determination of the Dissociation Equilibrium Constants, pK_a and pK_a^*	62
3.6.1 Determination of the Dissociation Constants in the Ground State, pK_a	62
3.6.2 Determination of the Dissociation Constants in the Excited State, pK_a^*	67
3.7 Determination of Fluorescence Quantum Yield	74
3.8 Determination of Free Water $[H_2O]_{free}$	76
3.9 Determination of the Quenching Constants, k_q	87
3.9.1 Determination of k_q for the Neutral Form Using Quantum Yield Intensities	87
3.9.2 Determination of k_q for the Neutral Form Using Lifetime Measurements	92
3.9.3 Determination of the Quenching Constant for the Protonated Form, k'_q	94
3.10 Energy Surface Diagrams of 1,8-DAN	100
3.11 Normal and Natural lifetime (τ , τ_0)	103
3.12 Kinetic Model of the Proton Transfer Reactions For 1,8-DAN	105
3.13 1,8-DAN in Zeolite Y Sieves	107
4. CONCLUSION	113

REFERENCES	116
Appendix	120
Vita	129

LIST OF TABLES

3.1 Lifetimes of the different forms of 1,8-DAN	49
3.2 Fluorescence decay time for 1,8-DAN*	52
3.3 Absorption versus [DAN]	59
3.4 Extinction coefficient of different forms 1,8-DAN	61
3.5 Determination of pK_{a1}	63
3.6 Determination of pK_{a2}	65
3.7 Acidity constants in the ground and first excited states of 1,8-DAN	67
3.8 Quantum yields of different forms of 1,8-DAN	75
3.9 Weight % at different $HClO_4$ concentrations	77
3.10 Mole fractions at different $HClO_4$ concentrations	79
3.11 Mole fractions of $[H_2O]_{free}$ at different mole fractions $HClO_4$ (Literature values)	81

3.12 Mole fractions of $[\text{H}_2\text{O}]_{\text{free}}$ at different mole fractions HClO_4	83
3.13 Mole fractions of $[\text{H}_2\text{O}]_{\text{free}}$ at different HClO_4 concentrations	85
3.14 Acid concentrations range 0.01-1.2 M, Emission wavelength fixed at $\lambda_{\text{EM}} = 455 \text{ nm}$	90
3.15 Stern-Volmer plot	93
3.16 Acid concentrations range 1-11.8 M, Emission wavelength fixed at $\lambda_{\text{EM}} = 340 \text{ nm}$	95
3.17 Normal and natural lifetimes and extinction coefficients of 1,8-DAN	104
3.18 Normal and natural lifetimes and extinction coefficients of 1-AN	104
3.19 Edge of unit cell and the number of unit cells per gram of zeolite Y	108
3.20 Loading level of the probe molecule 1,8-DAN	108

LIST OF FIGURES

1.1 1,8-DAN [Neutral Form]	5
1.2 1,8-DANH ⁺ [Mono-cation Form]	5
1.3 1,8-DANH ₂ ²⁺ [Di-cation Form]	6
1.4 Mono-cation scheme of 1,8-DAN suggested by Paul	6
1.5 Laser Four-Level System	15
1.6 Nd-YAG Laser (Full picture)	17
1.7 Nd-YAG Laser cylinder	17
1.8 FAU Structure	20
2.1 Block diagram of mode-locked Nd:YAG laser with a cavity-dumped synchronously-pumped dye laser	26
2.2 Energy levels in: a) free Nd ³⁺ and b) Nd ³⁺ split by crystal field interactions.	28
2.3 One of the Resonance Structures of the Rhodamine 6G Cation, used in the Picosecond Dye Laser System.	29

3.1 Absorption spectra of 1,8-DAN different forms, by Paul et al.	37
3.2 Absorption spectra of the three different forms 1,8-DAN at $8.0 \cdot 10^{-5}$ M	38
3.3 Absorption spectra of three different forms 1,8-DAN at $8.0 \cdot 10^{-5}$ M In terms of the Extinction Coefficient (ϵ)	39
3.4 Absorption spectra of 1,8-DAN at different acidic concentrations, from neutral to pH 2.0	40
3.5 Absorption spectra of 1,8-DAN at different acidic concentrations, From pH 1.5 to pH -1.0	41
3.6 Proposed structure for mono-cation 1,8-DAN which has two transitions.	42
3.7 Proposed structure by Paul et al. for the mono-cation of 1,8-DAN [9] which has only one transition.	42
3.8 Fluorescence emission spectra of different forms of 1,8-DAN, $\lambda_{EM}=340$ nm	44
3.9 Fluorescence emission spectra of different forms of 1,8-DAN, $\lambda_{EM}=300$ nm	45
3.10 Emission spectra of 1,8-DAN of the three different forms, by Paul et al.	46
3.11 Emission spectra of 1,8-DAN at different acid concentrations, 1) pH 0, 2) pH -0.3, 3) pH -0.7, 4) pH -1.0	47
3.12 Shifted energy levels after relaxation. Dashes lines are the relaxation levels	48
3.13 Emission decay profiles of different forms of 1,8-DAN	50
3.14 Natural logarithm emission decay profiles of different forms of 1,8- DAN	51

3.16 Natural logarithm emission decay profiles of 1,8-DAN and the pump pulse	54
3.17 Natural logarithm emission decay profiles of 1,8-DAN at different acid concentrations	55
3.18 Natural logarithm emission decay profiles of 1,8-DAN at different acid concentrations	56
3.19 Absorption increase with concentration	57
3.20 Absorption increase with concentration [Full scale]	58
3.21 Absorption versus [DAN]	60
3.22 Δ Abs versus pH values in the range pH 9.18 to pH 0	64
3.23 Δ Abs versus pH values in the range pH 1.0 to pH -1.1	66
3.24 Absorption and fluorescence spectra of the neutral form of 1,8-DAN expressed in wavelength (nm)	68
3.25 Absorption and fluorescence spectra of the neutral form of 1,8-DAN expressed in wavenumber (cm^{-1})	69
3.26 Absorption and fluorescence spectra of the mono-cation of 1,8-DAN expressed in wavelength (nm)	70
3.27 Absorption and fluorescence spectra of the mono-cation of 1,8-DAN expressed in wavenumber (cm^{-1})	71
3.28 Absorption and fluorescence spectra of the di-cation of 1,8-DAN expressed in wavelength (nm)	72
3.29 Absorption and fluorescence spectra of the di-cation of 1,8-DAN expressed in wavenumber (cm^{-1})	73

3.30 Weight % versus $[\text{HClO}_4]$	78
3.31 Mole fractions of HClO_4 versus $[\text{HClO}_4]$	80
3.32 Mole fractions of $[\text{H}_2\text{O}]_{\text{free}}$ versus mole fractions of HClO_4 (literature values)	82
3.33 Mole fractions of $[\text{H}_2\text{O}]_{\text{free}}$ versus mole fractions of HClO_4	84
3.34 Mole fractions of $[\text{H}_2\text{O}]_{\text{free}}$ versus concentration of HClO_4	86
3.35 $1/I$ versus $[\text{H}^+]$	91
3.36 Stern-Volmer plot, τ_0/τ vs. $[\text{H}^+]$	93
3.37 I_0/I versus mole fraction $[\text{H}_2\text{O}]_{\text{free}}$	96
3.38 Quenching of the neutral form, from 0.01M to 1.0M	97
3.39 Intermediate emission, from 1M to 6M	98
3.40 Quenching of the diprotonated form, from 11.8M to 8.0M	99
3.41 Energy surface diagram for the mono-cation form in the ground and excited state	101
3.42 Energy surface of the di-cation form in the presence and absence of free water molecules	102
3.43 Protonation process of 1,8-DAN adsorbed on zeolite Y at a Bronsted acid site	109
3.44 Emission spectrum of 1,8-DAN/NaY	110

3.45 Emission spectrum of 1,8-DAN/HY-34	111
3.46 Emission spectrum of 1,8-DAN/HY-96	112

THESIS ABSTRACT

NAME Abdul-Rahman Faisal Akram Al-Betar

TITLE Photophysical Behavior of 1,8-Diaminonaphthalene in Acidic Aqueous Solutions and in Zeolite Sieves

FIELD Physical Chemistry

DATE May 2004

The proton-transfer reaction of 1,8-Diaminonaphthalene (1,8-DAN) in acidic medium and in zeolite sieves was studied by means of laser-induced picosecond spectroscopy. It has been found that there are three clear different forms of 1,8-DAN in the ground state, but only two different forms in the excited state. The absorption of the mono-cation form of 1,8-DAN is found to be a mixture of the neutral form and the di-cation form. However, the emission is found to be only from the neutral form, due to the fast dissociation of the mono-cation form once it is excited. The mono-cation form of 1,8-DAN behaves as dual fluorescence under different excitation wavelengths. The di-cation form only fluoresces if no free water cluster is available as a proton acceptor. The reaction in the excited state was shown to be a diabatic quenching reaction. With the help of quantum yields and fluorescence lifetime measurements these results are interpreted in terms of a new photochemical scheme. All dissociation and quenching rate constants, pK_a and k_q , have been determined. 1,8-DAN was investigated inside zeolite Y sieves and has been shown that it may be used as a probe molecule to assess zeolite acidity.

MASTER OF SCIENCE DEGREE
KING FAHD UNIVERSITY OF PETROLEUM AND MINERALS
DHAHRAN, SAUDI ARABIA

خلاصة الرسالة

الاسم	عبد الرحمن فيصل أكرم البيطار
عنوان الرسالة	السلوك الفيزيائي الضوئي لمادة 8,1-ثنائي أمينونفتالين في المحاليل الحمضية و في الزيوليت
التخصص	كيمياء فيزيائية
التاريخ	مايو 2004

لقد تم دراسة تفاعل الانتقال البروتوني من الحالة المثارة لمادة 8,1-ثنائي أمينونفتالين في المحاليل الحمضية و في المواد ذات التجايف الجزئية -الزيوليت- وسجل تلاشي الفلورية وطيف الزمن التحليلي بواسطة نبض الليزر بيكوسكند. و بناء على أشعة الامتصاص و طيف الانبعاث، وجد أن المادة 8,1-ثنائي أمينونفتالين لها ثلاثة أشكال في الحالة الأرضية و شكلان فقط في الحالة المثارة. وتم رصد أشعة الامتصاص لشكل أحادي البروتون بأنها مزيج من امتصاص الشكل المتعادل و امتصاص الشكل ثنائي البروتون. بالرغم من أن طيف الانبعاث يصدر فقط من الشكل المتعادل، وذلك بسبب التفكك السريع للشكل أحادي البروتون ما إن يثار. إن الشكل أحادي البروتون يسلك سلوكاً مزدوجاً للانبعاث وفقاً لطول موجة المثير. يمكن للشكل ثنائي البروتون أن يشع انبعاثاً فلورياً في غياب جزيئات الماء الحرة فقط. وقد تم وصف التفاعل في الحالة المثارة بأنه تفاعل إخمادي فاقده للطاقة. وباستخدام الناتج الكمي و قياس تلاشي الفلورية، تم تفسير هذه النتائج على شكل مخطط كيميائي ضوئي جديد. حيث تم إيجاد كل ثوابت التفكك و الإخماد (k_q و pK_a). وقد تم تحري 8,1-ثنائي أمينونفتالين في داخل تجايف مادة الزيوليت ووجد أنه يمكن أن يستخدم كجزيء مجس لتحديد حامضية مادة الزيوليت.

درجة الماجستير في العلوم

جامعة الملك فهد للبترول والمعادن

الظهران- المملكة العربية السعودية

CHAPTER I

INTRODUCTION

1.1 General Overview

Proton transfer reactions have been the subject of many studies over the years [1-20].

Eigen measured for the first time the fast recombination of H^+ and OH^- using a relaxation method [16, 17]. Forster and Weller were the first to explain the difference between the ground state and the excited state dissociation constants by means of an excited state proton transfer [10, 18-20]. Intermolecular proton transfer between the excited molecules and the solvent has been investigated in the past few years by means of the picosecond spectroscopic technique. Studies were extended to alcohol-water mixtures [10-15].

With the advent of short pulses it becomes possible to directly measure proton transfer of excited organic acids. Ultra short pulse laser spectroscopy has become one of the chief ways for studying the rapid kinetics of proton transfer reactions [10]. By using the short pulse method, the nature of the accepting cluster of water molecules can be described. Four water molecules (H_8O_4) were suggested to be a model of proton acceptor [10]. In the presence of excess of free water, an average of nine water molecules is used for the hydration of one proton [6]. The idea of free water already existed in the late 1970s [1].

The proton transfer reaction from the excited state of 4-hydroxy-1-naphthalenesulphonate has been investigated in alcohol-water mixtures at different temperatures [10-15]. Two new models and two possible mechanisms are proposed to explain the proton transfer process of the probe molecule in methanol- and ethanol-water mixtures [10].

Recently there has been renewed interest in the photophysical behavior of 1-Aminonaphthalene (1-AN) [6, 7]. 1-ANH^+ is a very strong acid in the excited state and was shown to have, besides the expected excited acidic form, a new form X which is an adduct between the excited acid and the anion ClO_4^- i.e. $X \equiv \text{RNH}_2\text{---H}^+\text{---ClO}_4^-$. This molecule in the acidic form and the X-form was successfully applied to study the acidity of zeolite Y (NaY, HY) catalysts [7, 8]. Proton transfer reactions were shown for 1-AN in acidic aqueous solutions at the excited state [7]. The completely protonated 1,8-DAN has also been shown to be a very strong acid in the excited state [9]. However, some of the findings are controversial.

Determination of the surface acidity of solid acids, e.g. zeolite, based on photochemical properties is the result of more recent research work. Zeolite acidity can be evaluated by a number of techniques such as the temperature-programmed desorption of bases, calorimetric methods, FTIR, or the use of test catalytic reactions. These techniques give qualitative or semi-quantitative evaluation of acidity but can be used to rank a closely related set of zeolite catalysts. In the 1970's, Hammett indicators were used to establish an acidity scale for zeolite based on the pK_a values. The limitations of this method were the

use of bulky indicator molecules that interacted with the surface of the catalyst and gave unrepresentative readings [8].

Therefore, the present work was carried out in two parts: first, to set up the reaction scheme of 1,8-DAN in the ground and excited state with varying acidity. Second, photochemical characterizations of zeolite, based on fluorescence properties. These were done by measuring the interaction of the probe molecules with the acidic site of the catalyst, i.e. proton transfer reactions between the zeolite and 1,8-DAN in the ground and excited state, using laser-induced picosecond spectroscopy.

Transparent films of the zeolite in polydimethylsiloxane (PDMS) were used, as results obtained using zeolite powder are prone to difficulties due to scattered light. PDMS was used first by El-Rayyes in his work on 1-Aminonaphthalene(1-AN) [7,8].

1.2 Purpose of This Work

Paul et al. have studied the 1,8-DAN in sulphuric acid solutions and present absorption and fluorescence spectra as well as some fluorescence lifetime data [9]. However, there is no complete analysis of the overall reaction scheme and it is not shown how the various forms of 1,8-DAN were separated. Also, no excitation spectra are shown and the lifetime data are very scattered.

It is, therefore, the objective of this master thesis to complete the analysis of the photophysical parameters of this molecule, 1,8-DAN, in HClO₄ solutions with various pH values according to scheme 1.1. In particular, detailed absorption, fluorescence and lifetime studies should reveal whether 1,8-DAN shows similar behavior like 1-AN, i.e. quenching of the neutral and singly protonated forms and the formation of an X-like adduct. Also, this study may show whether 1,8-DAN could be used as a probe molecule for the assessment of intra-cavity acidities of zeolite catalysts. Hence, we may be able to check the acidity scale for zeolites proposed by El-Rayyes et al. [7,8].

By varying the acid concentration of HClO₄ and measuring absorption and emission spectra of 1,8-DAN we want to prove the structure of the protonated forms, i.e. monoprotonated, diprotonated or whether the proton is shared between the two amino groups, see Figures 1.1 – 1.4.

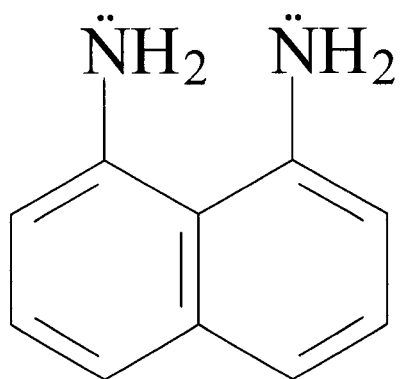


Fig 1.1 1,8-DAN [Neutral Form]

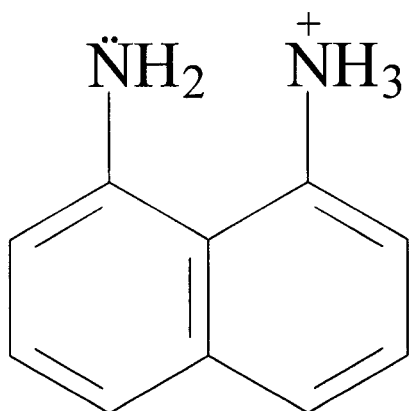


Fig 1.2 1,8-DANH⁺ [Mono-cation Form]

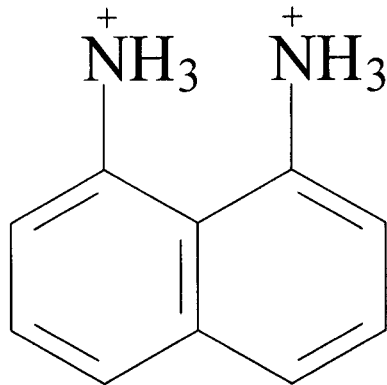


Fig 1.3 1,8-DANH₂²⁺ [Di-cation Form]

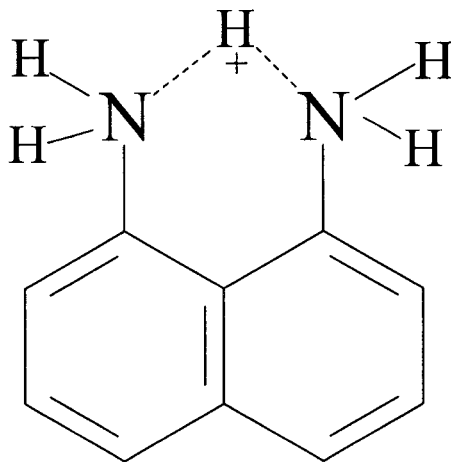


Fig 1.4 Mono-cation scheme of 1,8-DAN suggested by Paul [9].

1.3 Literature Review

Literature studies revealed that 1,8-DAN is heavily studied with respect to its electrochemical properties and its organic reactions [21, 22]. However, there is no complete information available on the photophysical behavior of 1,8-DAN.

Its unique properties has made poly-1,8-diaminonaphthalene (poly-1,8-DAN) an object of interesting studies over the past decade. Its most remarkable characteristic, the ability to extract and form complexes with certain cations, such as Ag^+ , Cu^{2+} and Hg^{2+} , has drawn most attention since it creates an opportunity for possible applications of poly-1,8-DAN in heavy metal sensors. This exceptional property has been explained through the investigation of the molecular structure of poly-1,8-DAN, which has shown a presence of the free amino groups which enable poly-1,8-DAN to form strong complexes with metal ions. As interesting as the properties of poly-1,8-DAN are, there is still a serious drawback, common for all conducting polymers, that limits its practical application. All of the conducting polymers have inadequate processability. It is difficult to obtain these materials in the form of specific structures [23].

Poly (1,8-diaminonaphthalene) films, poly(1,8-DAN), were electrosynthesized on a Pt electrode to study their utility in extracting Cr(VI) (as dichromate ions) from acidic aqueous solution. The electrodeposition procedure was improved by acidification of the acetonitrile electropolymerization bath with $\text{CCl}_3\text{CO}_2\text{H}$. Possible molecular structures of electrosynthesized poly (1,8-diaminonaphthalene) were determined by means of IR spectroscopy. The mechanism of dichromate ion removal was studied by

potentiometric measurements in the system Ag/AgCl/Cl-(std)/0.1 M HClO₄/p (1,8-DAN)/Pt, upon addition of K₂Cr₂O₇ solution. The presence and oxidation state of chromium in the polymer matrix was explored by means of energy dispersive X-ray (EDX) spectrometry [24].

The electrochemical behavior and charge transport processes of poly-1,8-diaminonaphthalene were studied by a cyclic potential sweep method in aqueous solution. At scan rates less than 100 mV/s the film shows semi-infinite diffusion behavior and then the electrode reaction can be considered in the same manner as of a solution phase redox species at an uncoated electrode. The effects of pH and temperature on the peak currents and peak potentials were studied. The kinetic parameters of the polymeric film were established and a redox mechanism of poly-1,8-diaminonaphthalene film was proposed [25].

Carbon paste electrodes modified with conducting polymers for sensitive and selective determination of lead are presented. A novel method for generating a reproducible polymer-coated electrode surface is developed. 1,8-diaminonaphthalene (1,8-DAN) was mixed with a carbon paste electrode leading to a conducting polymer in acidic medium while, in the same medium, this polymer is known to be non-conducting on a platinum electrode. The electrode behavior of poly(1,8-DAN), electropolymerised into carbon paste, was investigated by cyclic voltammetry in the presence of the ferri-ferrocyanide couple. A carbon paste electrode modified with poly(1,8-DAN) was used to determined Pb²⁺ in aqueous solutions [26].

Nitrogen -15 NMR was determined for 1,8-DAN and 1,2-DAN and their monoprotinated species [27].

A new naphthalene derivative containing an urea group at the 1,8-position of naphthalene was synthesized and showed unique absorption and fluorescence peaks in the presence of fluoride ions. Calculations suggested that the new peak was attributed to the increased anionic character of the urea nitrogen due to the strong interaction of the fluoride and N-H protons [28].

The reaction of 1,8-diaminonaphthalene with trimethylchlorosilane and tri(isopropyl)chlorosilane gives N,N'-disilylated products in moderate yields. Double deprotonation of the products with n-BuLi yields the dilithiated products in 78-85% yield [21].

Using 1- and 3-aminonaphthalene as model substrates, Cheung et al. investigated the effect of insertion of a second amino group on mutagenicity, binding to the cytosolic Ah receptor and CYP1A inducibility, and the effects were compared to those elicited by 3,3'-diaminobenzidine and 1-naphthylethylenediamine. 1,5- And 1,8-diaminonaphthalene were effective inducers of CYP1A activity, more potent than 1-aminonaphthalene. 2,3-Diaminonaphthalene was also an inducer of CYP1A, but the effect was similar to that elicited by 2-aminonaphthalene. In contrast, 3,3'-diaminobenzidine and 1-naphthylethylenediamine did not induce CYP1A activity [29].

The acidity difference of 1,8- and 1,5-diaminonaphthalenes is due to intra molecule nitranion stabilization through homoconjugate H bonding, the first example of amide ion

homoconjugation. The high basicity of 1,8-bis(dimethylamino)naphthalene is an inappropriate model for the enhanced acidity of 1,8-diaminonaphthalene. Deprotonation in K 3-aminopropylamide removes the difference between the acidities of the diamines and is attributed to di-deprotonation [30].

Activities of catalysts obtained by reaction of $[MCl(C_8H_{14})_2]_2$, (C_8H_{14} = cyclooctene, M = Rh, Ir) with $H_2N(CH_2)_nNH_2$, ($n = 2-5$), $Me_2NC_2H_4NMe_2$, and 1,8-diaminonaphthalene in hydrogenation of ten alkenes, alkynes, and cycloalkenes were determined. The most efficient catalyst was obtained with 1,3-diaminopropane [22].

Ni(II) complexes containing 2 and 3 molecules of the aromatic diamines, o-phenylenediamine, 1,8-diaminonaphthalene, and 2,2'-diaminobiphenyl are described. The complexes were characterized by magnetic resonance and IR and visible spectral measurements [31].

Phenylboronic acid reacts quantitatively by ball-milling in the solid state with o-phenylenediamine, 1,8-diaminonaphthalene, anthranilic acid, pyrocatechol, pyrogallol, pinacol, bicyclic cis-diols, mannitol, and inositol to form the five- or six-membered cyclic phenylboronic amides or esters. Catalysts or other auxiliaries are strictly excluded, as they are not required and would have to be removed after the reactions. These varied model reactions provide pure protected products without the necessity of further purifying workup and the potential for protection chemistry is demonstrated. Some of the reactions can also be quantitatively performed if stoichiometric mixtures of the reactants are co-ground or co-milled and heated to appropriate temperatures either below the eutectics or

above the melting points. The temperatures are much higher in the latter case. Similar reactions in solution suffer from less than 100 % yield of the mostly sensitive compounds that are difficult to purify and thus create much waste. The hydrolysis (deprotection) conditions of the products are rather mild in most cases. Therefore, this particularly easy access to heteroboroles, heteroborolanes, heteroborinones, heteroborines, and heteroborinines is highly valuable for their more frequent use in protective syntheses [32].

1,8-Diaminonaphthalene reacts selectively with 1 equiv of 9-BBN to form a bridging amine-aminoborane, and with 2 equiv of 9-BBN to form a nonbridging bis(aminoborane). These aminoboranes give rise to a novel diaminoborate (4e,1-) ligand system by reactions with dimethylamides of titanium and zirconium [33].

The H-bond interaction between 1,8-diaminonaphthalene and phenol derivatives has been investigated in C₂Cl₄ by IR spectroscopy. The thermodynamic parameters and the IR data in the ν OH and ν NH₂ range suggest that H-bond formation occurs at one of the two NH₂ groups. These results are in complete contrast with those obtained for the proton sponge 1,8-bis (dimethylamino) naphthalene [34].

The kinetic and equilibrium protonation of ten alkylated 1,8-diaminonaphthalene mono-cations was studied using ¹³C NMR. The trimethylammonium compound was protonated at N, C-2, and C-4 in a 1:15:4 ratio at equilibrium but kinetically controlled protonation was exclusively at N. Deuteration was more rapid at C-4 than at C-2 and involved rate limiting ring inversion in the non planar C-protonated ions. Deprotonation of cyclic alkylated compounds at equilibrium occurred mainly at N,N, or N,p-C depending on the

alkyl groups [35].

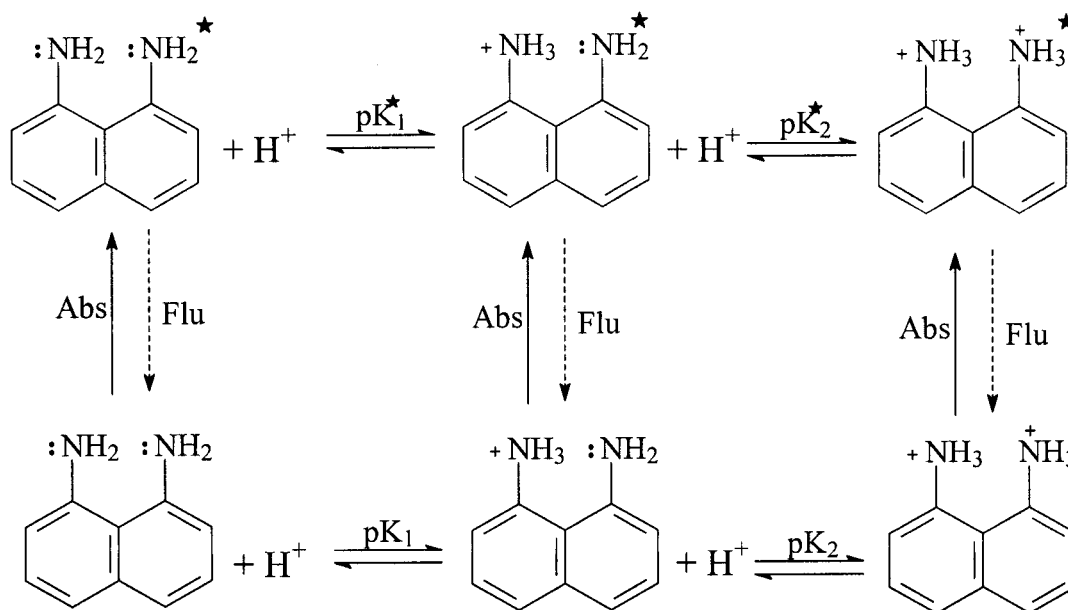
AM1, PM3 and SAM1 calculations have been carried out on eight compounds related to 1,8-diaminonaphthalene, five known proton sponges and three new compounds (a quinolizine, an isoquinoline and a 2,7-naphthyridine) have been calculated. The acceptable results obtained for the correlation between pK_a and protonation enthalpies for the first five compounds using either the AM1 or the SAM1 method, gives confidence to the predicted high basicity (between 19 and 22 pK_a units) for the unknown compounds [36].

Absorption and fluorescence spectra of 1,4-diaminonaphthalene (1,4-DAN), 1,5-diaminonaphthalene (1,5-DAN) and 1,8-diaminonaphthalene (1,8-DAN) were recorded in eleven different solvents and at various acid concentrations ($H_0/pH/H^-$, -10 to 16). These studies have indicated that the two amino groups are coplanar to the naphthalene ring in 1,5-DAN, are twisted with respect to each other, but coplanar to the ring in 1,8-DAN and are non planar with respect to the naphthalene ring in 1,4-DAN. Based on molar absorption coefficient data, the long wavelength band is found to be a mixture of the $^1A_g \rightarrow ^1L_a$ and $^1A_g \rightarrow ^1L_b$ transitions in non-polar solvents, whereas in aqueous solvents it is due to the $^1A_g \rightarrow ^1L_b$ transition. The change in dipole moment on excitation is zero for 1,5-DAN and greatest for 1,4-DAN. Prototropic equilibrium was not established between mono-cation and neutral species in the S_1 state. This is because the radiative decay rate is greater than the protonation / deprotonation rates. Proton-induced fluorescence quenching was not observed for the neutral species, whereas it is observed for the mono-cations before these are protonated to form di-cations. K'_q for 1,5-DAN and

1,8-DAN are $2.6 \cdot 10^8$ and $1.0 \cdot 10^9 \text{ cm}^3 \text{ mol}^{-1} \text{ s}^{-1}$, respectively. Lifetime data have shown that the proton-induced fluorescence quenching is dynamic in nature. $-\text{NH}_2$ and $-\text{NH}_3^+$ are stronger acids in the S_1 state than in S_0 state [9].

1.4 Reaction Scheme of Proton Transfer

1,8-Diaminonaphthalene (1,8-DAN) has two amino groups that could be protonated according to scheme 1.1.



Scheme 1.1 1,8-DAN Kinetics Models of the Proton Transfer Reactions

Where

pK_1, pK_2 Dissociation constants in the ground state

pK_1^*, pK_2^* Dissociation constants in the excited state

The dissociation constants and recombination constants vary with environmental parameters such as pH, solvent polarity and temperature [10].

The lifetime (τ) of the first excited state is determined by:

$$\tau = \frac{1}{k_r + k_{nr} + k_1^*} \quad (1.1)$$

For intramolecular process:

$$\tau_0 = \frac{1}{k_r + k_{nr}} \quad (1.2)$$

$$k_1^* = \frac{1}{\tau} - \frac{1}{\tau_0} \quad (1.3)$$

where

k_r : radiative rate constant

k_{nr} : non-radiative rate constant

k_1^* : proton dissociation rate constants in the excited state

1.5 Laser Amplification³⁷⁻⁴⁰

So far, nothing has been mentioned about how an amplifying medium works in a laser. Light can interact with individual atoms within an amplifying medium.

The Nd-YAG laser used in this study is an optically pumped solid-state laser that can produce very high-power emissions. This is a result of its lasing medium operating as a four-level system, Figure 1.5.

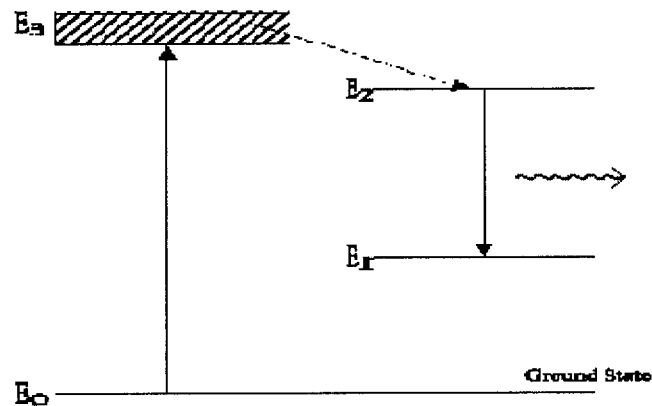


Fig 1.5 Laser Four-Level System

The lasing medium is the colorless, isotropic crystal $\text{Y}_2\text{Al}_5\text{O}_{12}$ (Yttrium-Aluminum Garnet - YAG). When used in a laser, about 1% of the Yttrium is replaced by Neodymium. The energy levels of the Nd^{3+} ion are responsible for the fluorescent properties, i.e., active particles in the amplification process.

Population inversion results from shining light on this crystal. If the light is intense enough, atoms within the crystal that absorb this light undergo a transition from the ground state into the absorption bands. This is often done with a flash lamp, often a quartz tube filled with a noble gas through which high energy stored in a capacitor is discharged, emitting in the blue and ultra-violet.

Atoms undergo transitions efficiently from their broad absorption bands (shown as the E_3 level in Figure 1.5) to the upper energy levels. The radiative decays to the ground-state from these bands have long lifetimes, in the order of microseconds, as compared to the fast transitions to the upper energy levels (in the order of nano-seconds). Approximately 99% of the ions that are excited to the absorption band transfer to the upper energy levels. Due to the long lifetime of the upper energy levels, they de-excite almost solely due to spontaneous emission.

The Nd-YAG laser used in our lab uses a cylindrical crystal. The crystal forms the laser cavity and has reflective ends - one coated so that it is 100% reflective, and the other is either sufficiently reflective, or is coated to allow only part of the amplified light to pass - enough feed-back so that oscillation may occur, Figure 1.6, 1.7.

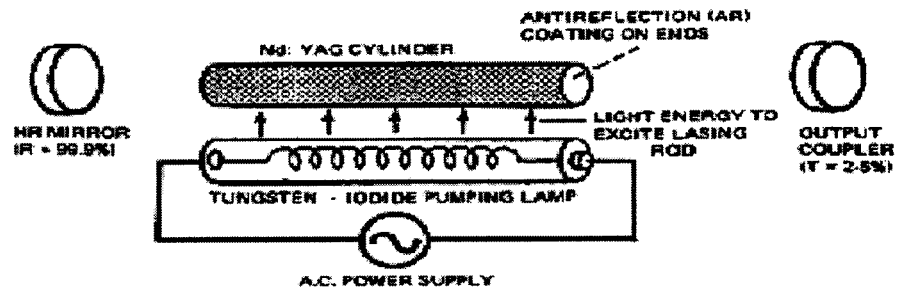


Fig 1.6 Nd-YAG Laser (Full picture)

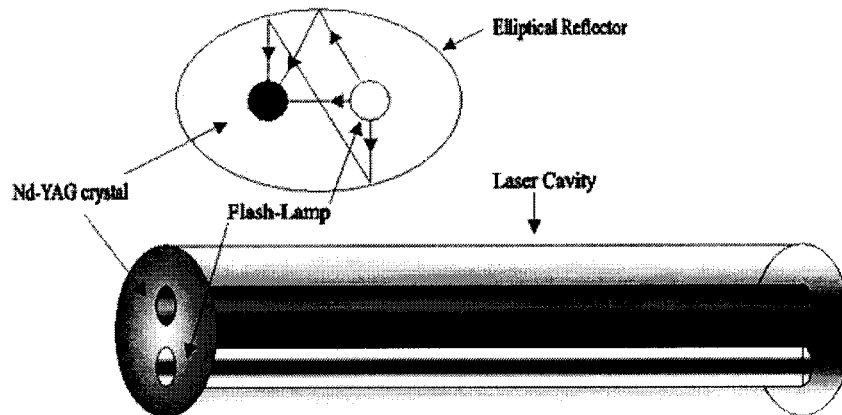


Fig 1.7 Nd-YAG Laser cylinder

1.6 Stimulated Emission

Stimulated emission is a very uncommon process in nature but it is central to the operation of lasers. An atom in a high energy level, or excited state, can return to the lower state spontaneously. However, if a photon of light interacts with the excited atom, it can stimulate a return to the lower state. One photon interacting with an excited atom results in two photons being emitted. Furthermore, the two emitted photons are said to be in phase, i.e. thinking of them as waves, the crest of the wave associated with one photon occurs at the same time as on the wave associated with the other. This feature ensures that there is a fixed phase relationship between light radiated from different atoms in the amplifying medium and results in the laser beam produced having the property of coherence.

1.7 Characterization of Zeolite Y (Faujasite)⁴¹

Zeolite Y exhibits the FAU (faujasite) structure, Figure 1.8. It has a 3-dimensional pore structure with pores running perpendicular to each other in the x, y, and z planes similar to LTA, and is made of secondary building units 4, 6, and 6-6. The pore diameter is large at 7.4 Å since the aperture is defined by a 12 member oxygen ring, and leads into a larger cavity of diameter 12 Å. The cavity is surrounded by ten sodalite cages (truncated octahedral) connected on their hexagonal faces. The unit cell is cubic ($a = 24.7\text{Å}$) with Fd-3m symmetry. Zeolite Y has a void volume fraction of 0.48, with a Si/Al ratio of 2.43. It thermally decomposes at 793°C.

1.7.1 Synthesis of Zeolite Y

Zeolite Y, like zeolite A, is synthesized in a gelling process. Sources of alumina (sodium aluminate) and silica (sodium silicate) are mixed in alkaline (NaOH) aqueous solution to give a gel. The gel is then usually heated to 70-300°C to crystallize the zeolite. The zeolite is present in Na^+ form and can be converted to the acid form. To prevent disintegration of the structure from acid attack, it is first converted to the NH_4^+ form before being converted to acidic form. If a hydrogenation metal such as platinum is needed, it is deposited via impregnation or ion exchange.

1.7.2 Applications of Zeolite Y

The most important use of zeolite Y is as a cracking catalyst. It is used in acidic form in petroleum refinery catalytic cracking units to increase the yield of gasoline and diesel fuel from crude oil feedstock by cracking heavy paraffins into gasoline grade naphthas. Zeolite

Y has superseded zeolite X in this use because it is both more active and more stable at high temperatures due to the higher Si/Al ratio. It is also used in the hydrocracking units as a platinum/palladium support to increase aromatic content of reformulated refinery products.

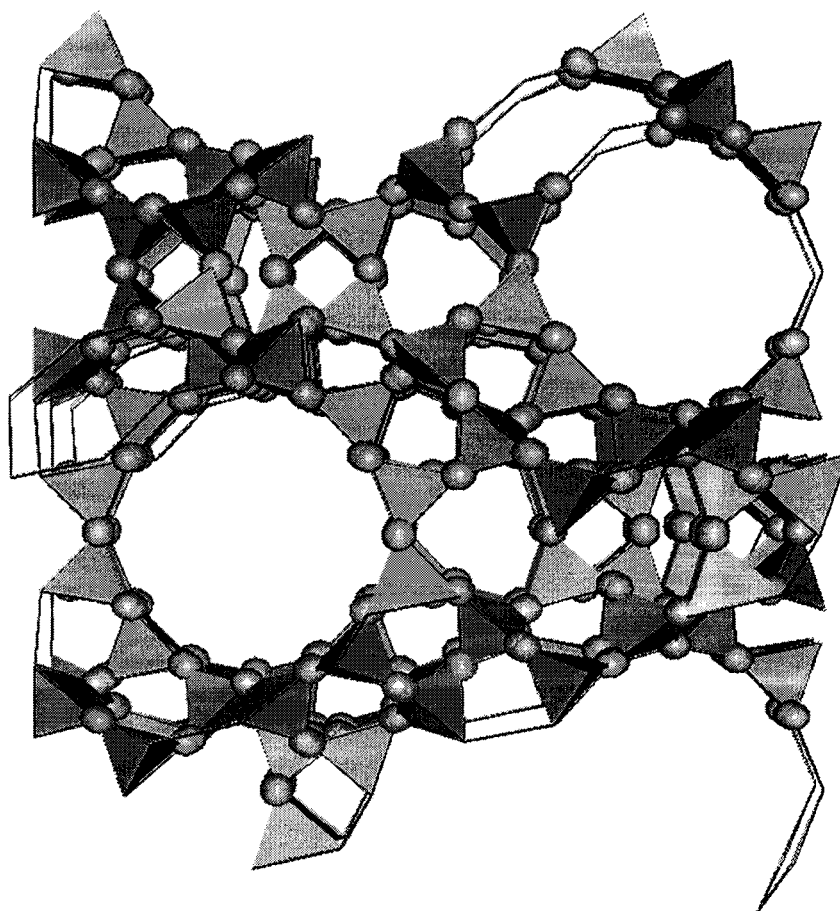


Fig 1.8 FAU Structure

CHAPTER II

EXPERIMENTAL

2.1 Materials

The probe molecule, 1,8-DAN, was provided by Fluka company and was used after recrystallization from ethanol-water followed by sublimation. Perchloric acid, HClO₄ (>70%) Fluka, was used for varying acid concentrations.

The sieves molecule, Zeolite Y, is the sodium form of zeolite Y, denoted as NaY. Samples with varying percentage of the proton form were prepared by ion exchanging the zeolite NaY with ammonium nitrate solution (NH₄⁺ NO₃⁻).

Solvents such as *n*-hexane (spectral grade) are used after drying over molecular sieves 5A. Polydimethylsiloxane (RTV 615 A &B, density 1.02 g/ml) were provided by General Electric silicones.

2.2 Purification and Stability

Since 1,8-Diaminonaphthalene is readily oxidized, it needs to be purified before use. Recrystallization from ethanol-water for many times and sublimation are two possible methods. Deoxygenated water is used to keep the solutions stable for longer time.

2.3 Solution Preparations

1,8-DAN was first dissolved in methanol-water (<1 wt%) and then diluted to different concentrations by distilled water. A diluted solution of the acid was used to prepare samples of pH 5.0 to pH 2.0. For pH values from 3.0 to 9.0, buffer (pH 3, 6, and 9) solutions were used. Highly acidic solutions, pH 1.0 to pH -1.1, of 1,8-DAN were prepared by adding different volumes of concentrated perchloric acid. Different acidic molarities were prepared starting from 0.01 M to 11.8 M. The 1,8-Diaminonaphthalene concentration was kept at $C_0 = 8.0 \times 10^{-5}$ M.

2.4 Catalyst Preparations

A sample containing 34% NH_4^+ and 66% Na^+ was prepared by stirring NaY in 0.25M solution of ammonium nitrate for 30 min at room temperature (24°C). The liquid to zeolite ratio was 4 : 1 by weight. The zeolite was filtered, washed and dried at 110°C for 6 h. It was then calcined at 450°C for 24 h raising the temperature from room temperature at the rate of 1°/min. This sample was denoted as HY-34, 34% of the exchange sites were in the

H-form. Similarly the sample HY-96 was prepared by successive ion exchange with 1.0 M ammonium nitrate solution followed by drying and calcination [8].

2.5 Catalyst-Probe Complex Preparations

Aliquots of zeolite Y were calcined at 500°C overnight and cooled in a desiccator under vacuum. The dried solid was transferred into a solution of the 1,8-DAN in *n*-hexane with a trace of methanol and stirred for about 6 h and kept overnight to reach equilibrium. The complex was then collected by filtration and washed three times with the solvent to remove the externally adsorbed 1,8-DAN molecules and then dried on a vacuum line at 10^{-3} – 10^{-4} Torr. The percent loading of the fluorophore on the molecular sieves is calculated by comparing the UV spectra of the original solution to that of the filtrate. The 1,8-DAN/*n*-hexane concentration used for loading was kept at 1.4×10^{-3} M.

2.6 Poly Dimethylsiloxane ‘PDMS’ Membrane Preparations

The PDMS membrane of the zeolite loaded with 1,8-DAN was prepared as follows: 30–70 mg of the dried zeolite loaded with the 1,8-DAN molecules was transferred into a vial containing 1 g of *n*-hexane. The mixture was sonicated for a period of 1 h to break the zeolite aggregates. Then 1 g of RTV 615 A was added and the mixture was sonicated again for a period of 6 h. Finally, 100 mg of RTV 615 B was added and the mixture was further sonicated for 20 min. The mixture was cast onto a glass plate and heated in an

oven at 60°C overnight. The membrane was removed from the glass plate and further dried at 60°C for a few hours [8].

2.7 UV-Vis Absorption Measurements

Steady-state UV-Vis absorption measurements for solutions were obtained using a Lambda-5 and a Lambda EZ 210 (Perkin-Elmer) Spectrophotometer.

2.8 Fluorescence Emission Measurements

Fluorescence spectra were recorded with a SPF-500 spectrofluorometer from SLM Instruments. The fluorescence spectra were corrected for the intensity of the lamp and the sensitivity of the photomultiplier tube.

2.9 Fluorescence Decay Time Measurements

A mode-locked Nd:YAG laser (Spectra-Physics model 3800) with a mode locker (Spectra-Physics model 451) operating at 41 MHz repetition rate was used to pump a Rhodamine 6G dye laser. Cavity dumping at 4 MHz was performed. The output pulses were frequency doubled (Spectra-Physics model 390 frequency doubler). The excitation wavelength was 300 nm and the fluorescence decay signals of the probe molecule were collected at the wavelength of maximum fluorescence emission, see Figure 2.1. Lifetimes

were measured using the Applied Photophysics photon-counting spectrometer system, model PS 60, equipped with a XP 2020Q photomultiplier. The actual pulse width of the excitation pulse is less than 10 ps; however, due to the response time of the photon counting system it is broadened to 350 ps. Data were collected through a multichannel analyzer and then transferred to a computer for analysis. Time dependent fluorescence decays of the various forms of 1,8-DAN have been recorded to find lifetimes and other kinetic parameter of scheme 1.1.

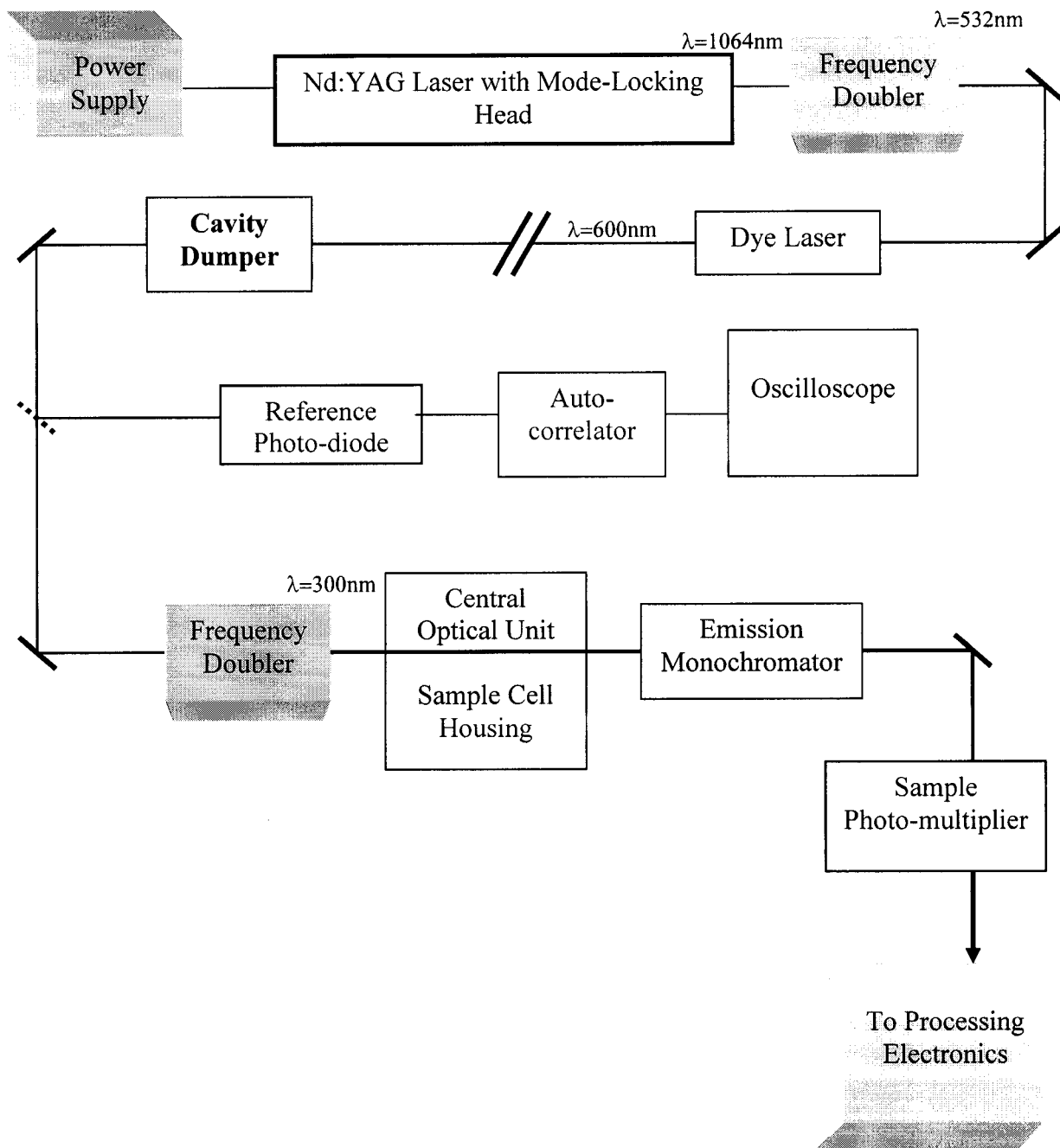


Fig 2.1 Block diagram of mode-locked Nd:YAG laser with a cavity-dumped synchronously pumped dye laser.

Mode-Locking: to make pulse train

Cavity Dumper: time-filter pulse

Auto-correlator: to measure true pulse width

Oscilloscope: to see the pulse

2.10 Laser Sources of the System

2.10.1 The Neodymium-YAG Laser

Nd^{3+} ions doped in the solid matrix of an yttrium aluminum garnet ($\text{Y}_3\text{Al}_5\text{O}_{12}$) is used to induce the laser action in the system. The Nd atom has the ground state configuration of $\dots 4d^{10}, 4f^4, 5s^2, 5p^6, 6s^2$ and $5I^4$ ground state. The Nd^{3+} has $\dots 4d^{10}, 4f^3, 5s^2, 5p^6$, ground state configuration. The 4I term being $L=6$ and $S=3/2$ giving rise to $J=15/2, 13/2, 11/2, 9/2$ in the Russell-Saunders terms. The $^4F_{3/2} - ^4I_{11/2}$ transition is important for the laser action and the laser operates on four level system since $^4I_{11/2}$ is not the ground state.

In the YAG crystal, the $^4I_{11/2}$ and $^4F_{3/2}$ states of Nd^{3+} are split by crystal field interactions into six and two states respectively. Among the eight transitions which are around $1.06 \mu\text{m}$, only transitions 1 and 2 in the Figure 2.2 are of importance. The transition at $1.0648 \mu\text{m}$ (1) and $1.0612 \mu\text{m}$ (2) are dominant at room temperature and 77 K respectively.

2.10.2 Dye Lasers

A wide range of dyes can be used for this purpose. One of the most common dyes is Rhodamine 6G ($\text{C}_{28}\text{H}_{31}\text{N}_2\text{O}_3\text{Cl}$), Figure 2.3, since it has an absorption band in the visible range and a broad fluorescence band. Rhodamine 6G has 186 distinct modes of vibration. Due to the electrostatic perturbations and collisions with solvent molecules, an

energy continuum is formed for each electronic state. This results in broad band absorption and fluorescence. Since fluorescence occurs over a range of wavelengths, tuning of the dye laser is obtained by using various techniques [7].

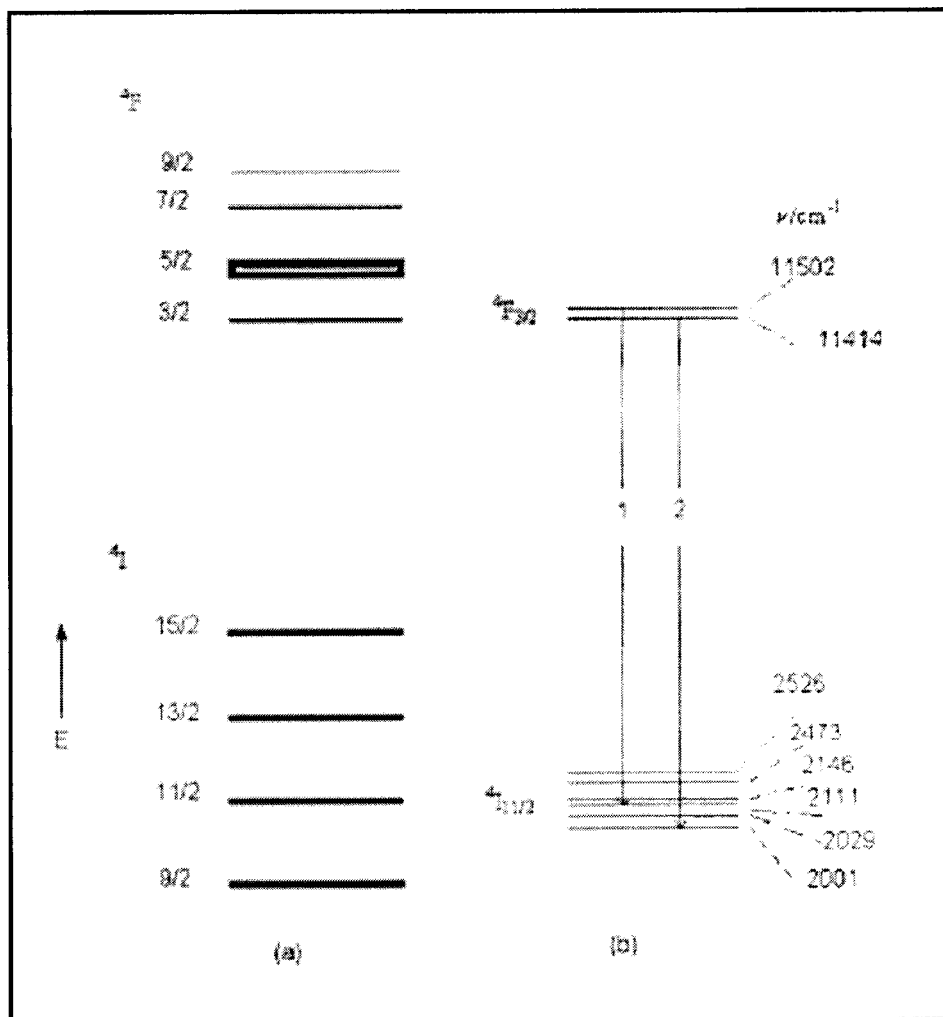


Fig. 2.2 Energy levels in: a) free Nd³⁺ and b) Nd³⁺ split by crystal field interactions.

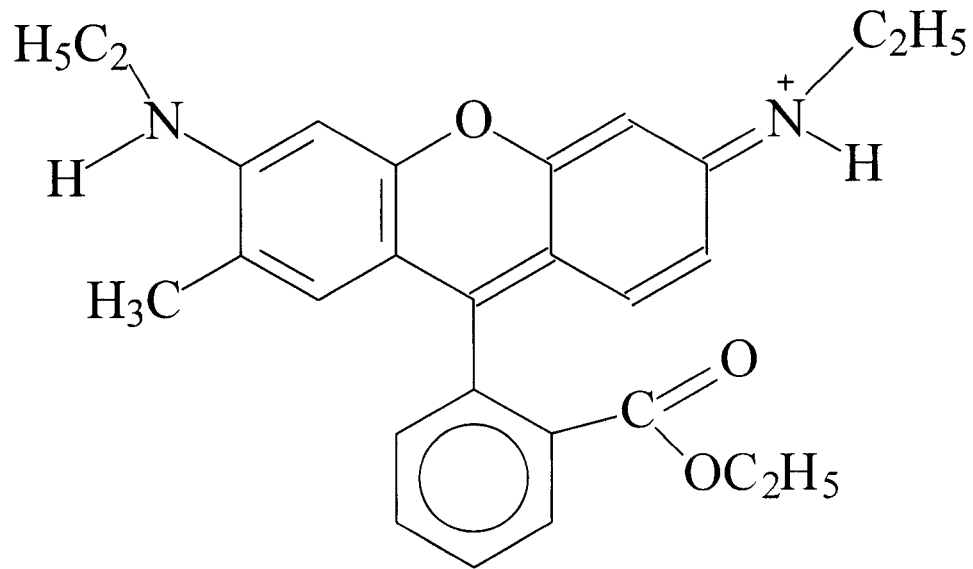


Fig 2.3 One of the Resonance Structures of the Rhodamine 6G Cation, Used in the Picosecond Dye Laser System.

2.11 Frequency Doubling

The induced electric dipole (μ) and the oscillating electric field (E) are related as

$$\mu = \alpha E \quad (2.1)$$

Where α = polarisability

In fact,

$$\begin{aligned} \mu &= \mu^1 + \mu^2 + \mu^3 + \dots \\ &= \alpha E + 1/2 \beta E E + 1/6 \gamma E E E + \dots \end{aligned} \quad (2.2)$$

Where β = hyperpolarizability

γ = the second hyperpolarizability

Any effects due to the second (or higher) terms are referred to as non-linear effects. Since the magnitude of the oscillating electric field is given by:

$$E = A \sin 2 \pi \nu t \quad (2.3)$$

Then,

$$\begin{aligned} E^2 &= A^2 (\sin 2 \pi \nu t)^2 \\ &= 1/2 A^2 (1 - \cos 2 \pi \nu t) \end{aligned} \quad (2.4)$$

Where A = amplitude

ν = frequency

Hence, the radiation scattered by the sample has some radiation with twice the frequency (or half the wavelength) of the incident radiation because of the μ^2 term. This is known as second harmonic generation or frequency doubling [7].

2.12 Acousto-Optic Mode Locking of Nd:YAG Lasers

For Nd:YAG lasers, the modes are coupled by means of an acousto-optic modulator placed inside the optical cavity. The modulator has a prism shape and a piezoelectric transducer is attached to one of the surfaces of the modulator. A standing acoustic wave is generated by driving the piezoelectric transducer at high frequency (41 M Hz). This standing wave induces grating-like periodic variations along the axis perpendicular to the two surfaces of the prism.

As light from the laser cavity enters the prism, a portion is both diffracted and shifted in frequency by an amount equal to the acoustic frequency. After passing through the modulator, the diffracted and undiffracted light rays are reflected by a dielectrically coated end mirror back through the modulator where a portion of each originally diffracted beam is diffracted once again, back into the cavity. As the frequency of the modulator is set to half the $C/2L$ or intracavity mode spacing of the ion laser, the portion of the first diffracted beam, on the second pass through the modulator, now diffracted back into the cavity is either upshifted in frequency to that of an originally adjacent higher mode, or downshifted in frequency to that of an originally adjacent lower mode. As a result, only those modes with correct frequency and phase relationship to match the mode locker frequency are sustained in the cavity and coherent addition between the various modes locks them into a

fixed amplitude, phase, and frequency relationship. Then, Fourier addition between the various frequency components results in a train of pulses with 200 picosecond duration with a periodicity equals to the intracavity mode spacing i.e. about 12.5 ns [42].

2.13 Synchronously Pumped Dye Lasers

In this process, the output pulses of a mode-locked ion laser are used to excite a dye laser whose cavity has been extended such that the intermode frequency spacing is an integral multiple of the mode locker frequency. In this configuration as each laser pulse enters the dye stream, the leading edge of the pulse brings the population of the excited dye molecules up past the threshold to sustain lasing. The dye laser pulse circulating within the cavity is timed to arrive at jet stream just as the dye laser medium reaches threshold. Because of the large stimulated emission cross-section of the dye medium the inverted population is rapidly depleted by the dye laser pulse. This rapid switch off of the gain medium is the reason for the generation of the very short pulses by the dye laser. Following this depletion, the remaining part of the pump pulse has insufficient energy to bring the dye laser medium back above threshold and the resulting dye laser pulse is much shorter in duration than the pump pulse i.e. a few ps [42].

2.14 Cavity Dumping Continuous Wave (CW) Laser

The modulator is placed at the focus of an astigmatically compensated three or four mirror folded cavity in a double pass optical geometry. When CW laser light passes through the modulator, part of the beam is diffracted and frequency shifted by an amount equal to the acoustic frequency. The remainder of the beam passes through the modulator unaffected. In the double pass configuration, both the diffracted and undiffracted beams are then directed back through the modulator by a curved cavity end mirror. On the second pass, a portion of the first diffracted beam is directed back into the laser cavity while a portion of the originally undiffracted beam is now diffracted and frequency shifted on to the remainder of the first diffracted beam. Because the sign of the frequency shift depends on the direction of the laser beam through the modulator, the two diffracted beams interfere resulting in an amplitude modulated output with a beat frequency equal to twice the cavity dumper acoustic frequency. This amplitude modulation is particularly important in the cavity dumping of mode-locked pulsed trains [42].

2.15 Cavity Dumping of Dye Lasers

In a dye laser all of the light is contained within an ultra-short optical pulse circulating back and forth within the laser cavity. Under these conditions, pulse shape or pulse width is unaffected by the cavity dumping process and the acousto-optic modulator acts primarily as a gate which periodically couples a mode-locked pulse out of the laser cavity. The primary function of a cavity dumper when used in this configuration is to generate

variable repetition rate trains of the ultra-short optical pulses. The mode-locked, cavity-dumped pulses have peak power considerably larger than those from a mode-locked only system. In the mode-locked, cavity-dumped configuration, a very fast RF pulse is used to drive the Bragg cell. The frequency of the RF pulse is set to integer + 1/2 times the repetition frequency of the optical pulse train. With this arrangement whenever the desired pulse is centered at the diffraction maximum of the modulation envelope, the preceding and trailing pulses are automatically centered at the diffraction minima. Therefore, background noise due to adjacent pulses is suppressed [42].

2.16 Single Photon-Counting Technique

The single photon counting technique is one of the methods developed to measure fluorescence decays. The sample is excited with frequency doubled pulse from a cavity-dumped synchronously pumped dye laser. The time interval between the lamp pulse and the anode pulse is converted to a voltage by using a time-to-amplitude converter. The time-to-amplitude converter is reset to zero if no photon is detected. A multichannel pulse height analyzer is used to collect such recorded pulses in a form of digital manner. As a statistical method is employed, measurements need to be done repeatedly. Eventually, the multichannel pulse height analyzer gives a histogram approximating the time variation of the fluorescence signal which can be displayed or plotted. The aim of measuring the time-resolved fluorescence decay is to evaluate the impulse response function. By using a computer, the data can be analyzed according to the following equations using an iterative deconvolution.

$$I_E(t) = \int_0^t I_a(t-\theta) I_E^\delta(\theta) d\theta \quad (2.5)$$

Where $I_E(t)$ = time dependent fluorescence emission.

$$I_E^\delta(t) = \sum_i A_i \exp(-t/\tau_i) \quad (2.6)$$

Where $I_E^\delta(t)$ = decay function responding to a δ -shape emission.

The least squares method is used to calculate the value of $I_E^\delta(t)$ given assumed values of pre-exponential factors A_i and lifetimes τ_i . Then calculated $I_E^\delta(t)$ values are compared with observed $I_E(t)$ values until the best fit is obtained [7].

CHAPTER III

RESULTS AND DISCUSSIONS

3.1 Absorption Spectra

By increasing the acidity of the solution from neutral to 11.8 M HClO₄ we found a steady decrease of the band at 330 nm and the appearance of a band at 280 nm with an isosbestic point at 295 nm as shown in figures 3.1 – 3.5.

The absorption spectrum of the neutral form of 1,8-DAN shows a maximum wavelength λ_{\max} at ca.330 nm. The absorption spectrum of the di-cation form, pH -1.0, of 1,8-DAN shows a maximum wavelength λ_{\max} at ca.280 nm. The absorption spectrum of the mono-cation form, pH 2.0, of 1,8-DAN shows a maximum wavelength λ_{\max} at ca.295 nm, which is the isosbestic point of the 1,8-DAN forms.

The absorption spectrum of the mono-cation form is a mixture of two transitions, the neutral transition at 330 nm and the diprotonated transition at 280 nm. A proposed structure of the mono-cation form was suggested according to the absorption spectra, Figure 3.6. However, if the proposed structure by Paul et al., Figure 3.7, is true, only one transition should occur in the absorption spectrum which is not the case.

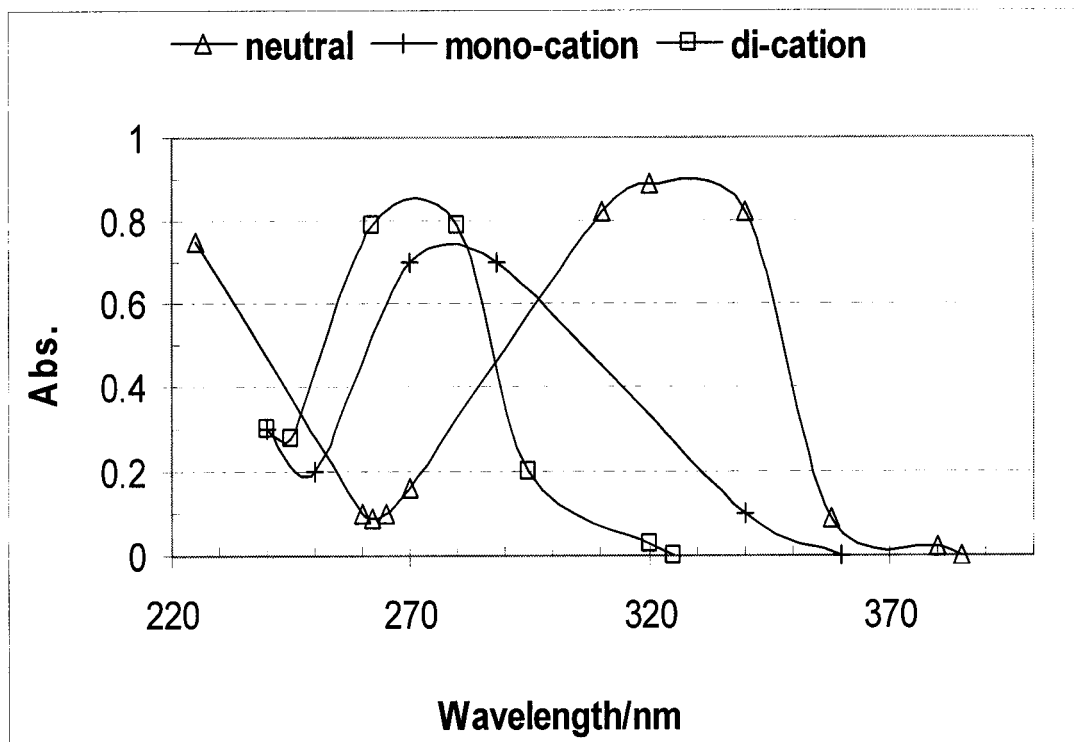


Fig. 3.1

Absorption spectra of 1,8-DAN different forms, by Paul et al. [9]

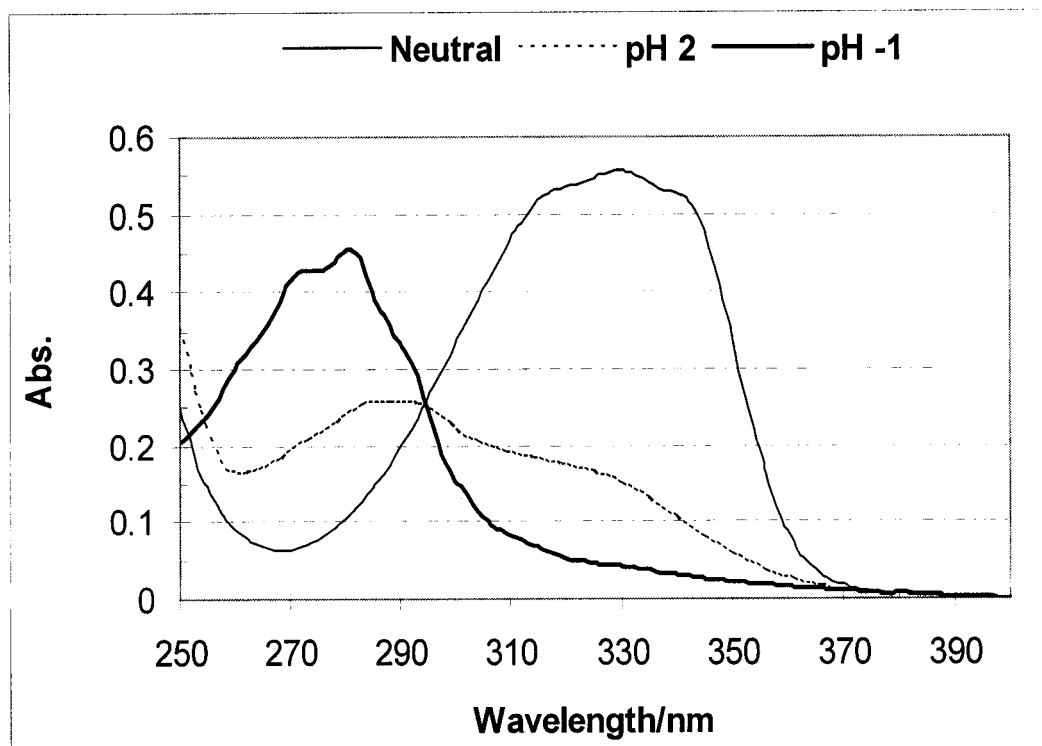


Fig. 3.2

Absorption spectra of the three different forms 1,8-DAN at 8.0×10^{-5} M

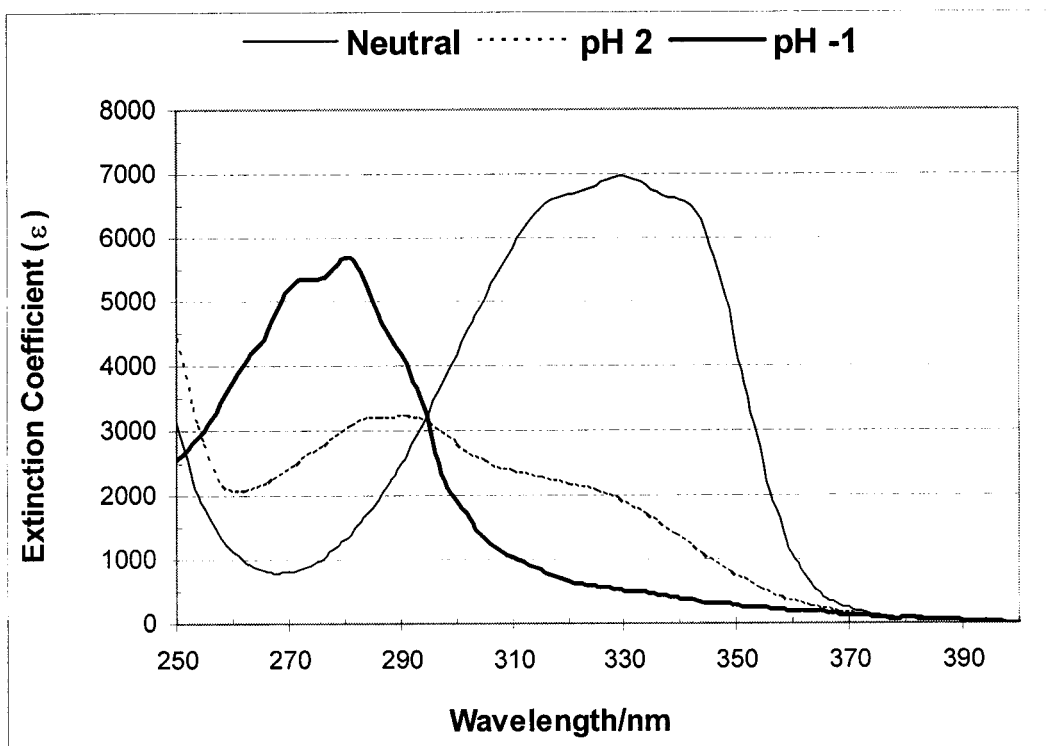


Fig. 3.3

Absorption spectra of the three different forms 1,8-DAN at $8.0 \cdot 10^{-5}$ M
In terms of the Extinction Coefficient (ϵ).

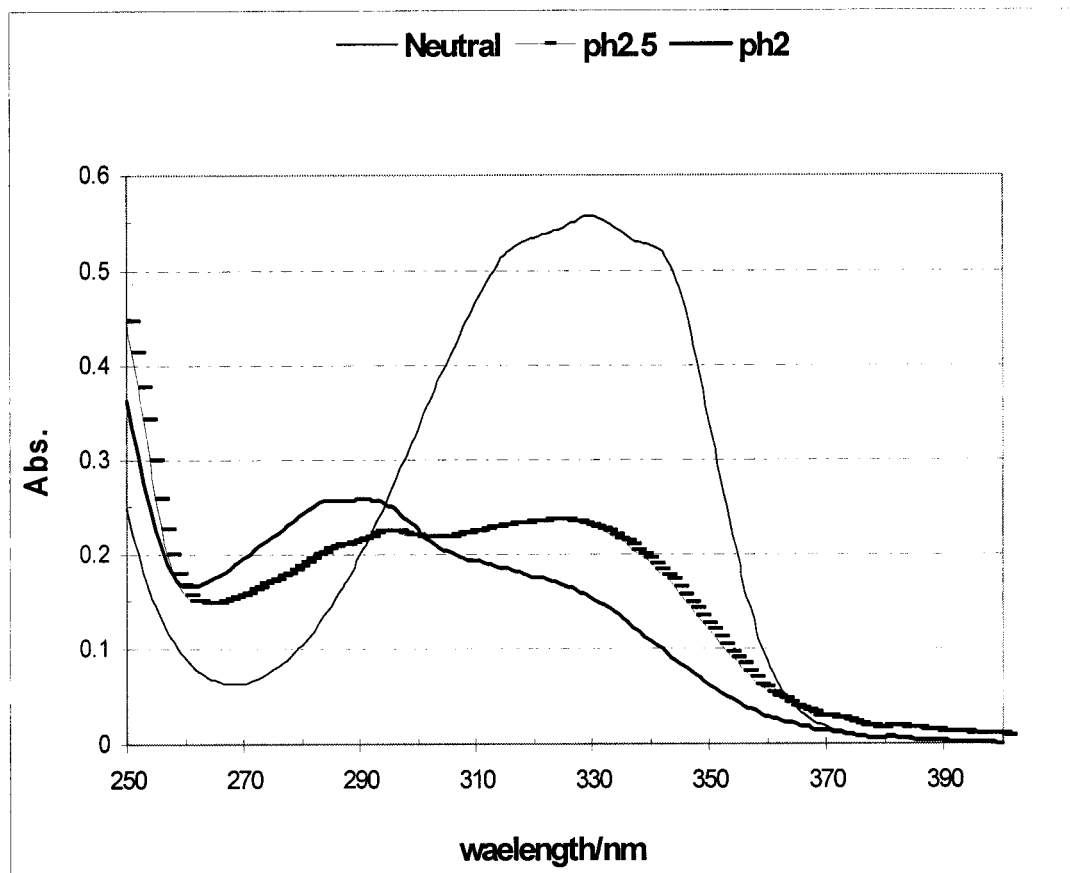


Fig. 3.4

Absorption spectra of 1,8-DAN at different acidic concentrations,
From the neutral form (pH 5.8) to pH 2.0

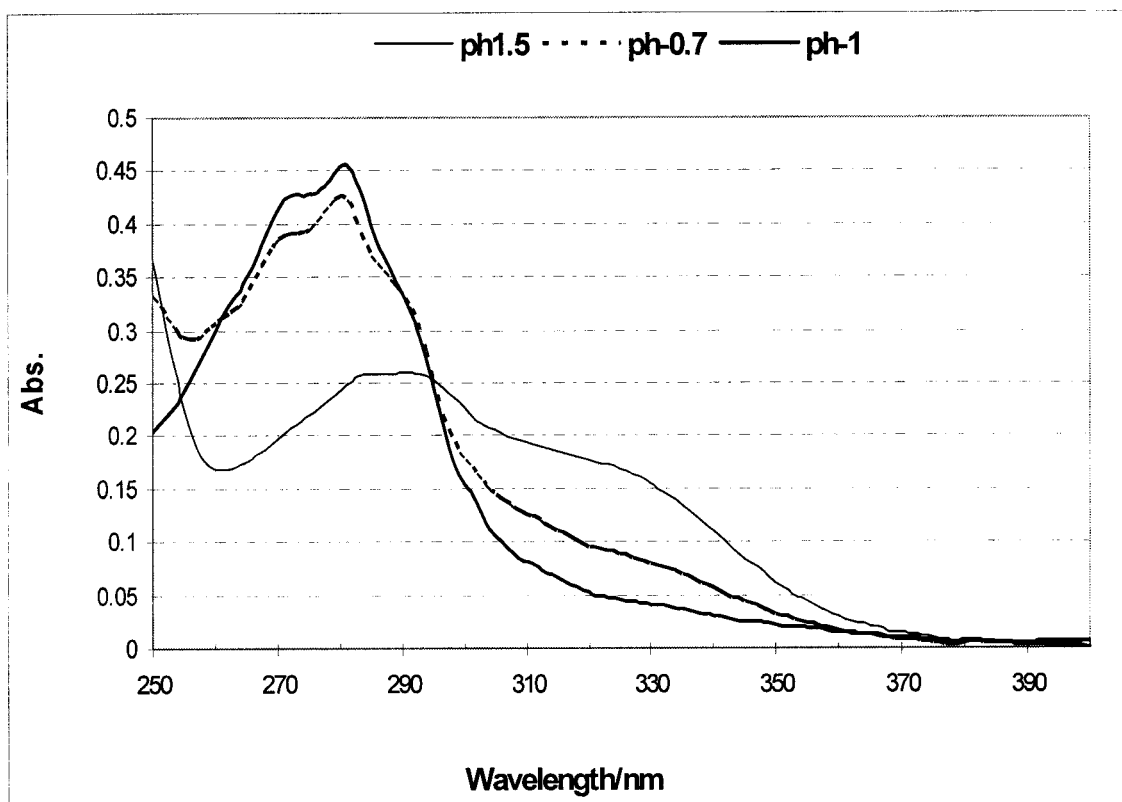


Fig. 3.5

Absorption spectra of 1,8-DAN at different acidic concentrations,
From pH 1.5 to pH -1.0

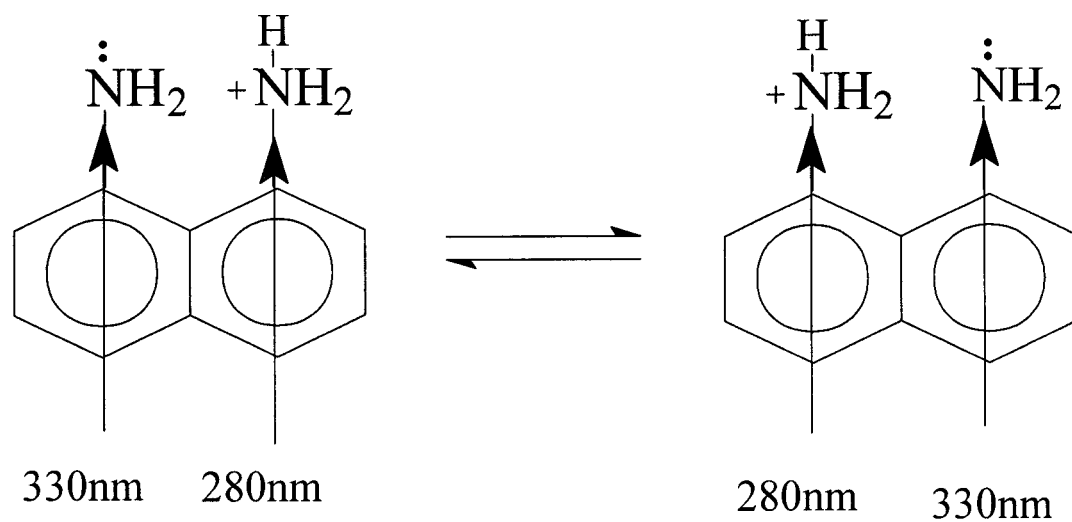


Fig. 3.6

Proposed structure for mono-cation 1,8-DAN which has two transitions.

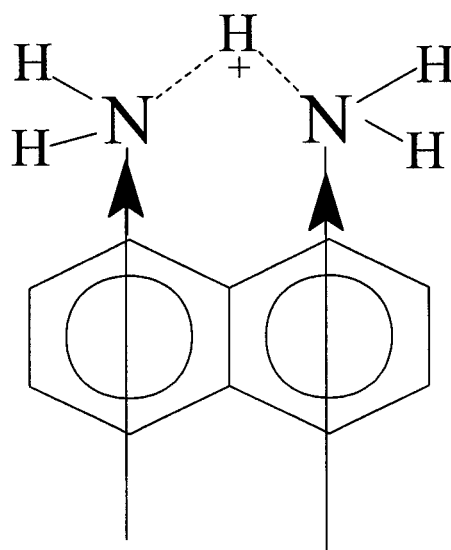


Fig. 3.7

Proposed structure by Paul et al. for the mono-cation of 1,8-DAN [9] which has only one transition.

3.2 Emission Spectra

Emission spectra of the neutral form and the monocation form show the same emission at $\lambda_{Em} = 440$ nm, upon excitation wavelength $\lambda_{Ex} = 340$ nm, Figure 3.8. However, upon excitation wavelength $\lambda_{Ex} = 300$ nm the mono-cation form shows a red shift at $\lambda_{Em} = 452$ nm, which is due to solvent relaxation, Figure 3.9. This red shift is in agreement with what was found by Paul et al, Figure 3.10, [9].

The emission spectrum of the di-cation form shows an emission at $\lambda_{Em} = 340$ nm, which is the expected blue shift due to the blue shift in the absorption spectrum caused by the two extra protons.

Emission spectra of the neutral form of 1,8-DAN show a strong quenching effect upon increasing of the hydrogen ion concentration at the range $0.01 < [H^+] < 1.0$ M, Figure 3.11. This happens without increasing the fluorescence intensity of the di-cation form. The emission of the di-cation form appears at concentration of 1.2 M $HClO_4$ until it reaches the maximum emission at 11.8 M $HClO_4$. However, the quenching effect of the di-cation form is visible upon increasing free water, i.e. diluting the 11.8 M with water, without an increase in the emission of the neutral form.

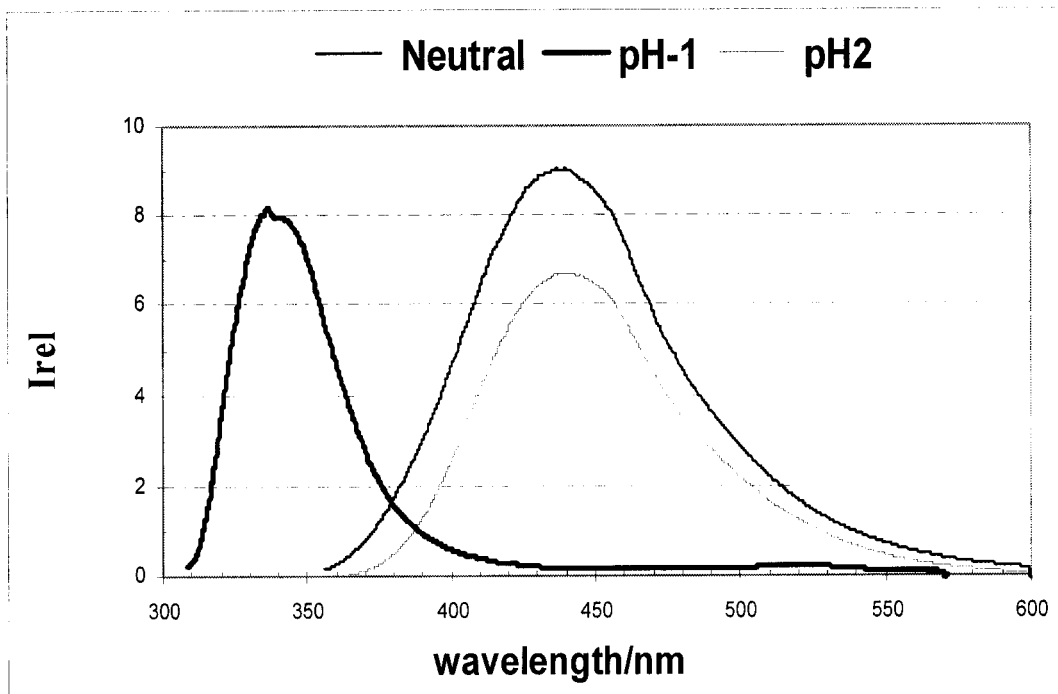


Fig. 3.8

Fluorescence emission spectra of different forms of 1,8-DAN.

Emission of the neutral and pH 2, show the same emission peak at $\lambda_{EX} = 340$ nm.

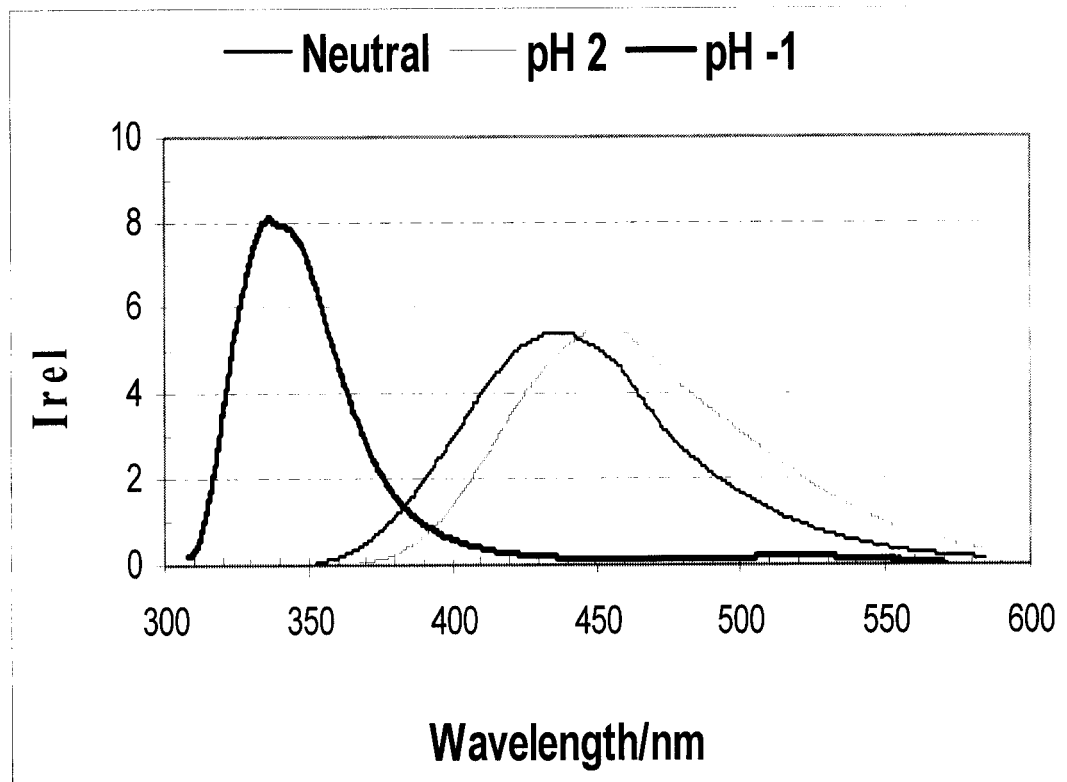


Fig. 3.9

Fluorescence emission spectra of different forms of 1,8-DAN.

Emission of the neutral and pH 2, show different emission peaks if excited at $\lambda_{EX} = 300$ nm, due to solvent relaxation.

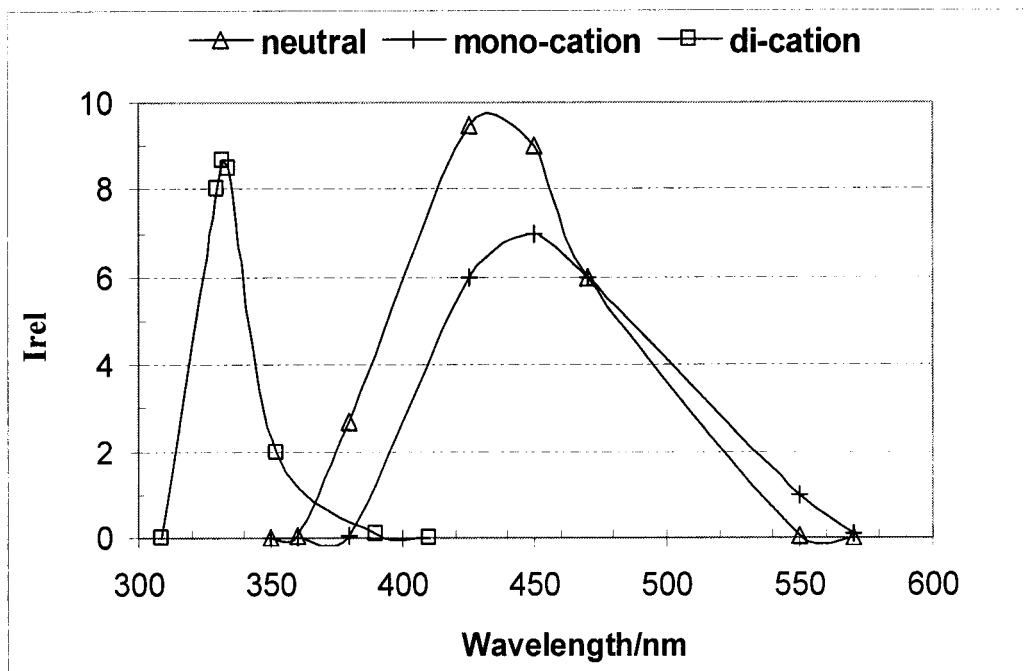


Fig. 3.10

Emission spectra of 1,8-DAN of the three different forms, by Paul et al. [9]

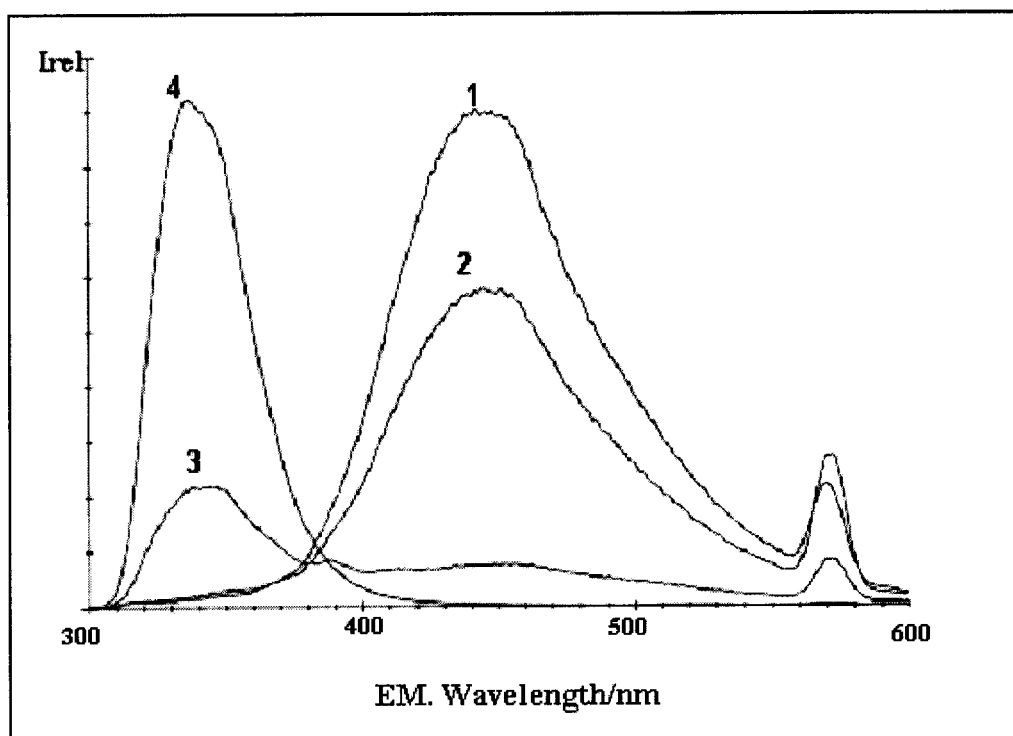


Fig. 3.11

Emission spectra of 1,8-DAN at different acid concentrations

1) pH 0, 2) pH -0.3, 3) pH -0.7, 4) pH -1.0

3.3 Relaxation Energy Levels of 1,8-DAN

It is well known that the solvent relaxation process due to changes of the dipole moment on excitation causes a red shift of the fluorescence spectrum [43], Figure 3.9. Lowering of the energy gap from the excited Frank-Condon state caused by solvent relaxation is the main reason for this red shift. The following figure shows the new energy levels after relaxation, Figure 3.12.

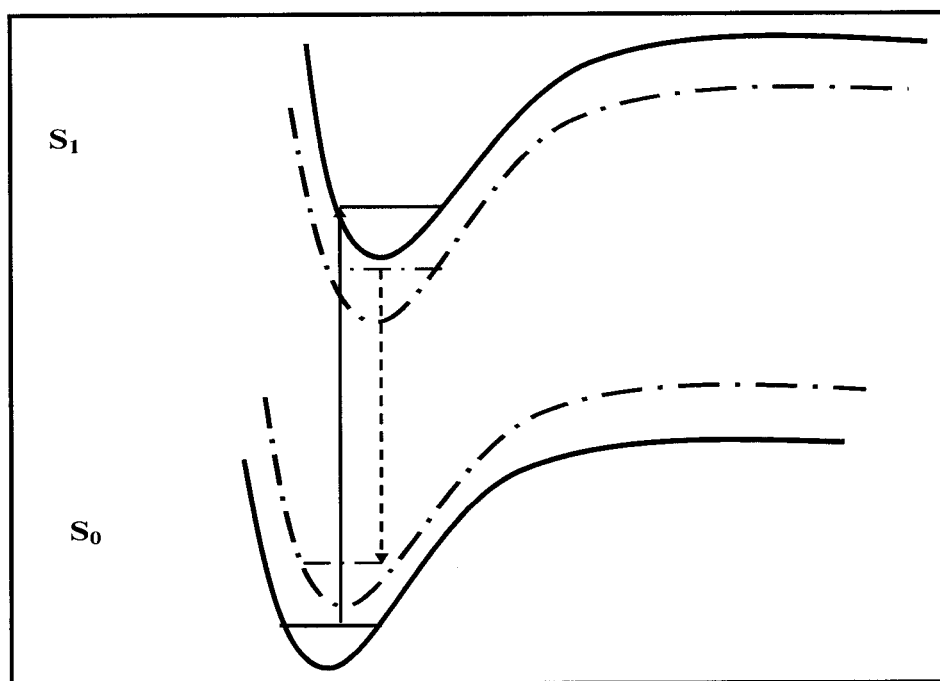


Fig. 3.12

Shifted energy levels after relaxation. Dashed lines are the relaxation levels.

Absorption and emission occur according to the Frank-Condon principle.

3.4 Fluorescence Decay Measurements

All measurements of the fluorescence decays are with fixed excitation wavelength $\lambda_{Ex} = 300$ nm. Fluorescence decays of the neutral form 1,8-DAN, pH 5.8, and the mono-cation form, pH 2.0, have very similar decays, Figures 3.13 and 3.14. The emission wavelength of both is at $\lambda_{Em} = 460$ nm. Both are single-exponential and nicely fit the equation:

$$I(t) = I_0 e^{-t/\tau} \quad (3.1)$$

Fluorescence decay for the di-cation form, pH -1.0, shows a bi-exponential decay with emission wavelength $\lambda_{Em} = 360$ nm and nicely fit the equation:

$$I(t) = A_1 e^{-t/\tau_1} + A_2 e^{-t/\tau_2} \quad (3.2)$$

Table 3.1 Lifetimes of the different forms of 1,8-DAN

pH	τ_1 /ns		τ_2 /ns	
	Paul et al.	our work	Paul et al.	our work
5.8 (Neutral)	1.6	7.7	---	
2.0 (Mono-cation)	7.4	8.3	---	
-1.1 (Di-cation)	---	1.6	---	22.2

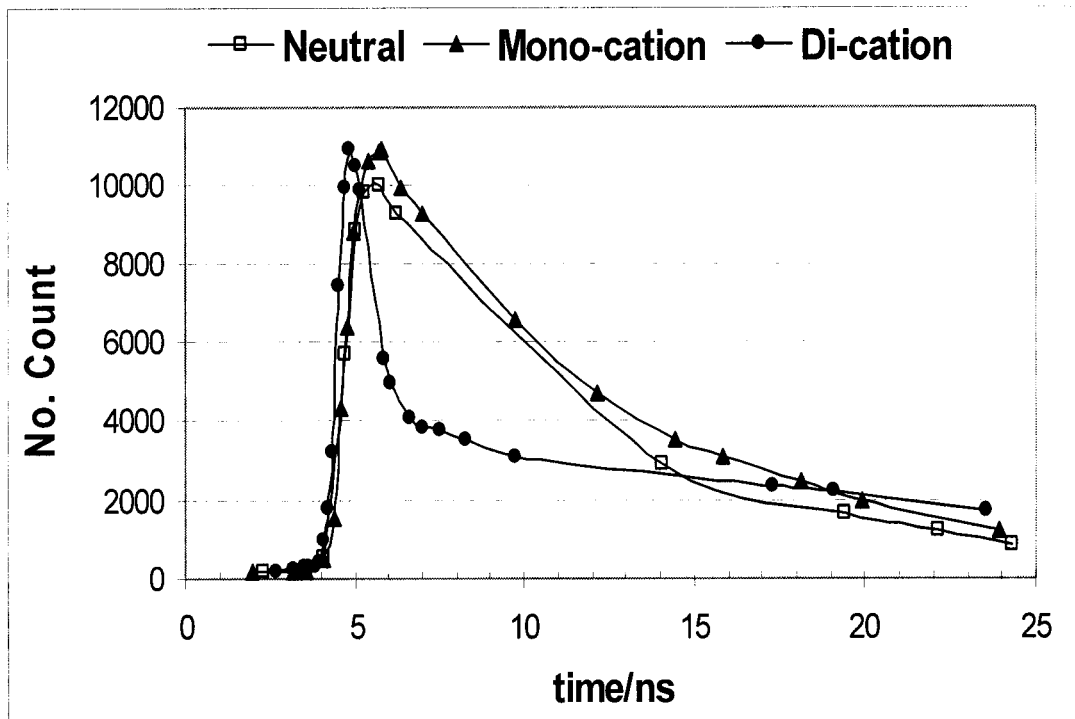


Fig. 3.13

Emission decay profiles of different forms of 1,8-DAN.

It shows similar decays for the neutral form and the mono-cation.

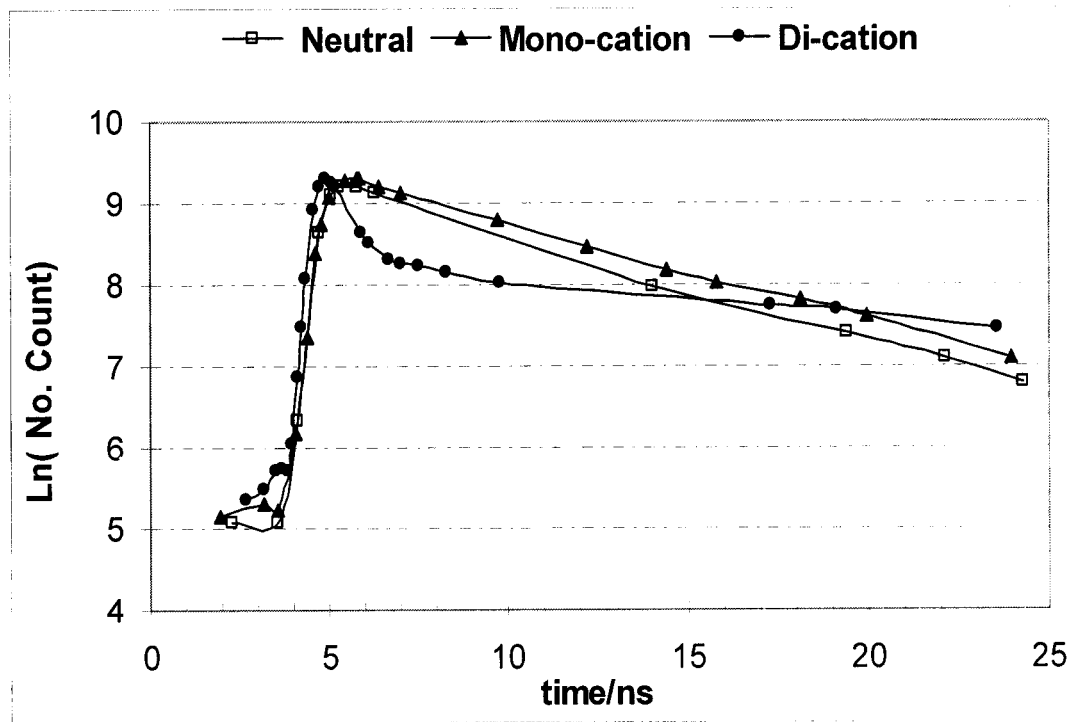


Fig. 3.14

Natural logarithm emission decay profiles of different forms of 1,8-DAN.

$$\tau = 1/\text{slope}$$

Table 3.2 Fluorescence decay time for 1,8-DAN*

pH	τ_1/ns	τ_2/ns
5.0	3.8	---
4.0	4.3	---
3.0	7.9	---
2.0	8.3	---
1.3	5.7	---
1.0	4.3	---
0.3	1.6	---
0	0.7	---
-1.1	1.6	22.2

λ_{Ex} = 300 nm for all measurements

λ_{Em} = 460 nm for the neutral form and mono-protonated form

λ_{Em} = 360 nm for the di-protonated form

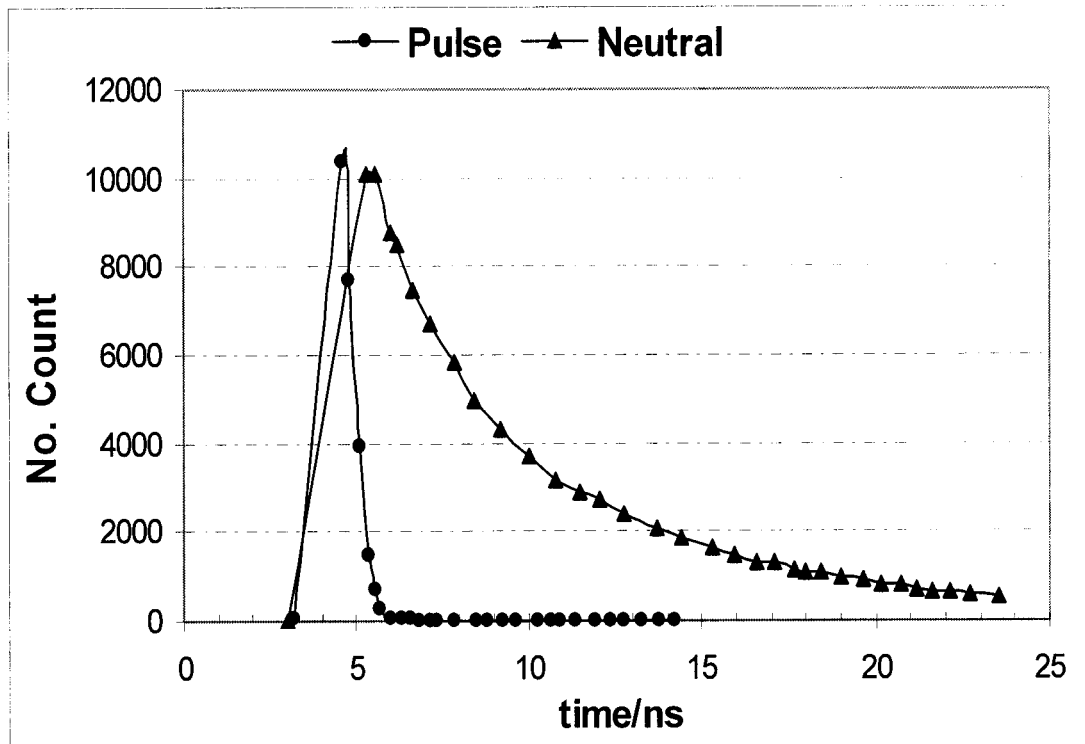


Fig. 3.15

Emission decay profiles of the neutral form of 1,8-DAN and the pump pulse

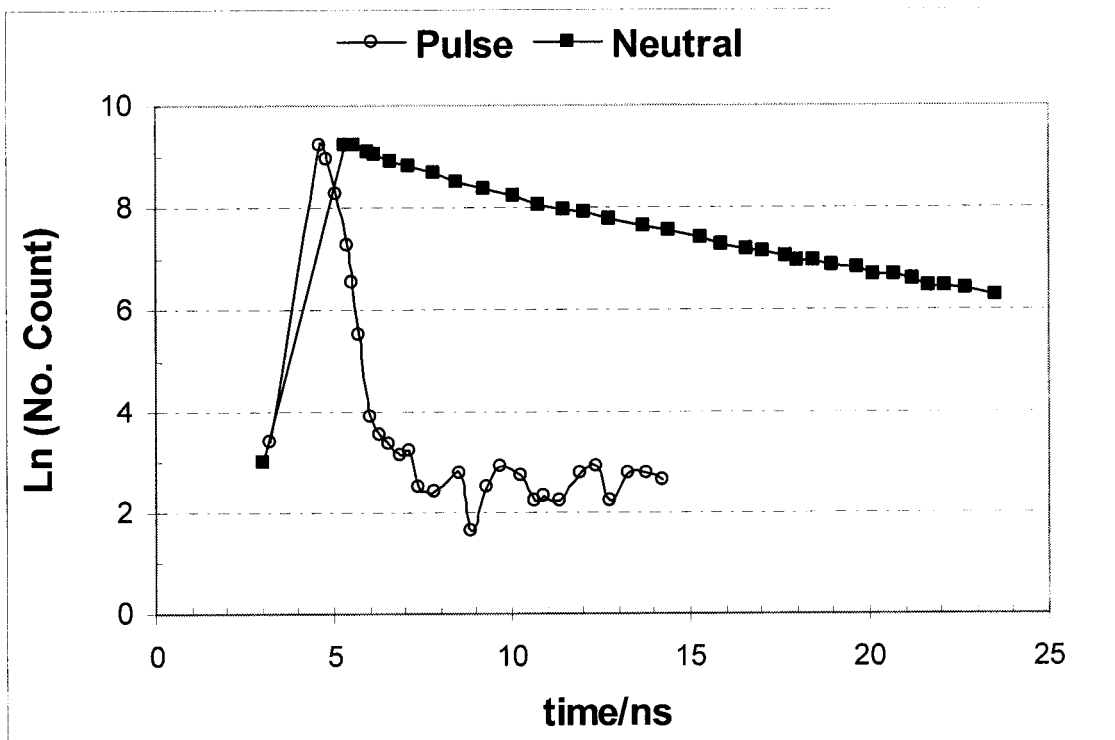


Fig. 3.16

Natural logarithm emission decay profiles of the neutral form of 1,8-DAN and the pump pulse

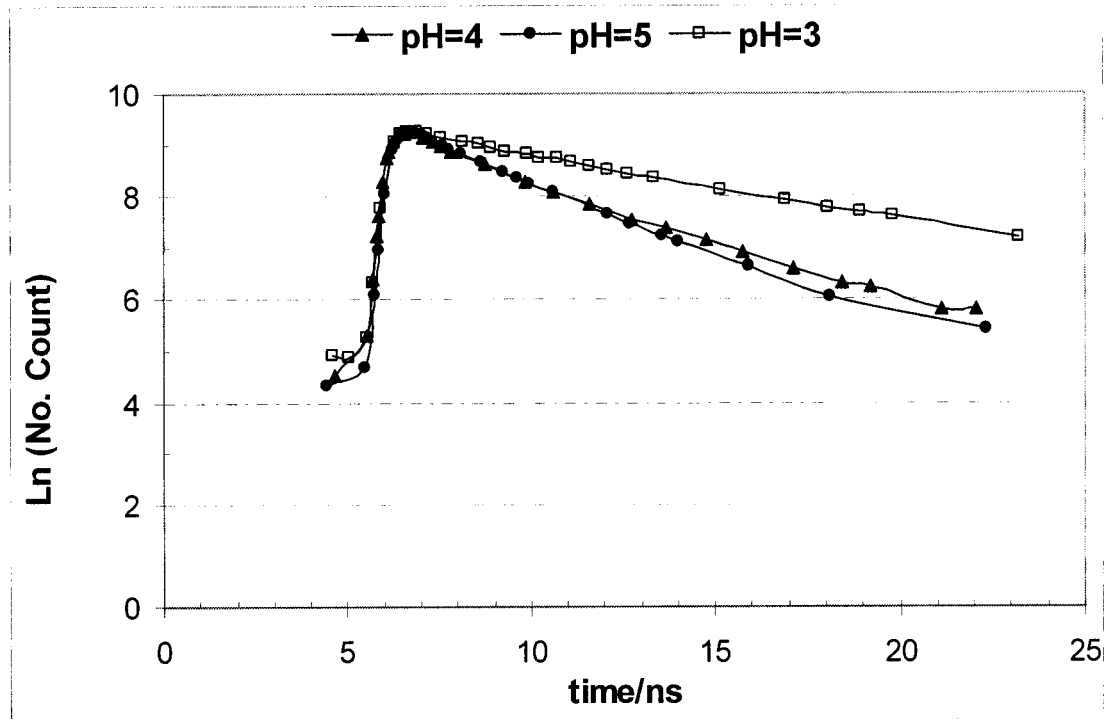


Fig. 3.17

Natural logarithm emission decay profiles of 1,8-DAN at different acid concentrations.

$$\tau = 1 / \text{slope}$$

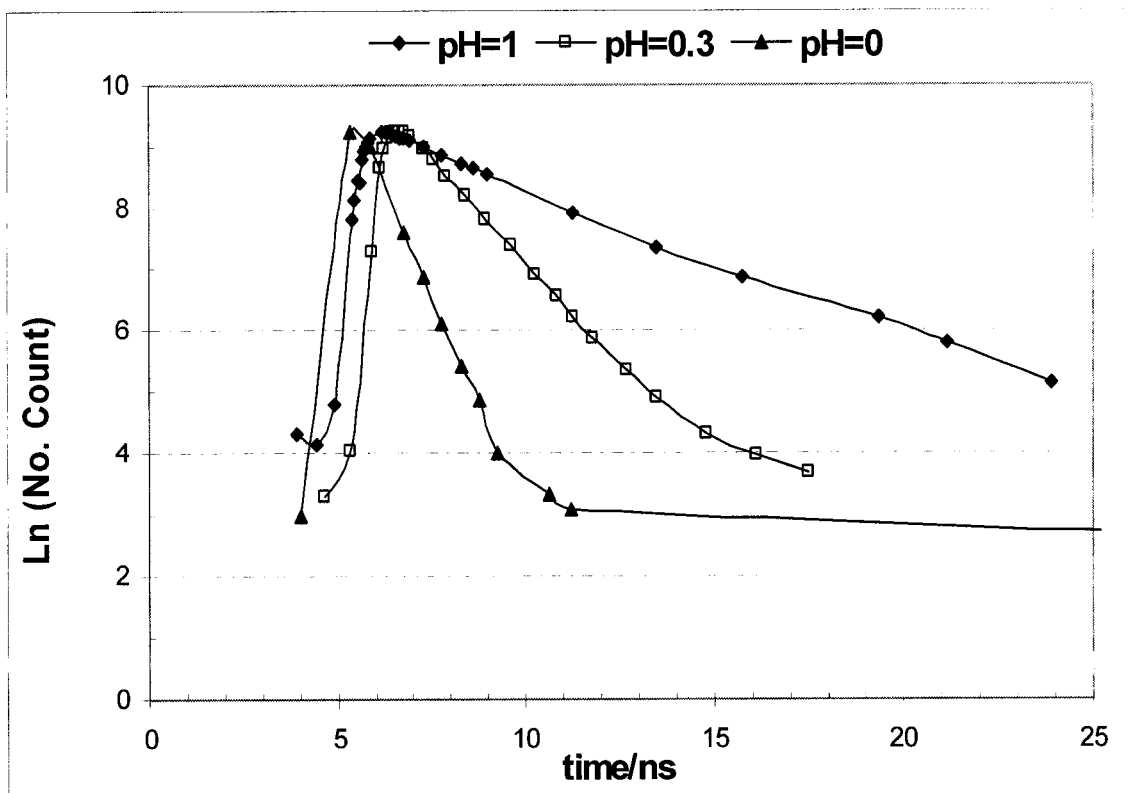


Fig. 3.18

Natural logarithm emission decay profiles of 1,8-DAN at different acid concentrations.

$$\tau = 1/\text{slope}$$

3.5 Validity of Lambert Beer's Law

It is expected that the pure 1,8-DAN follows Lambert Beer's law, with good agreement in the range: 4×10^{-5} M to 10×10^{-5} M.

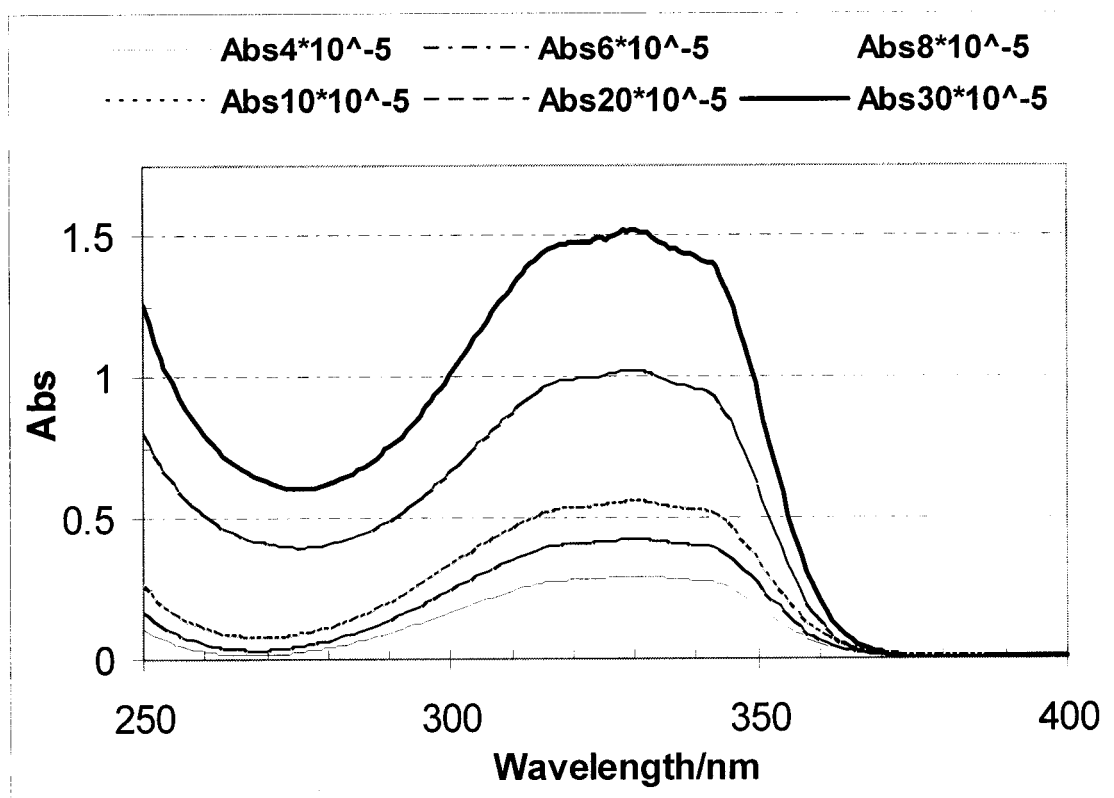


Fig. 3.19

Absorption increase with concentration

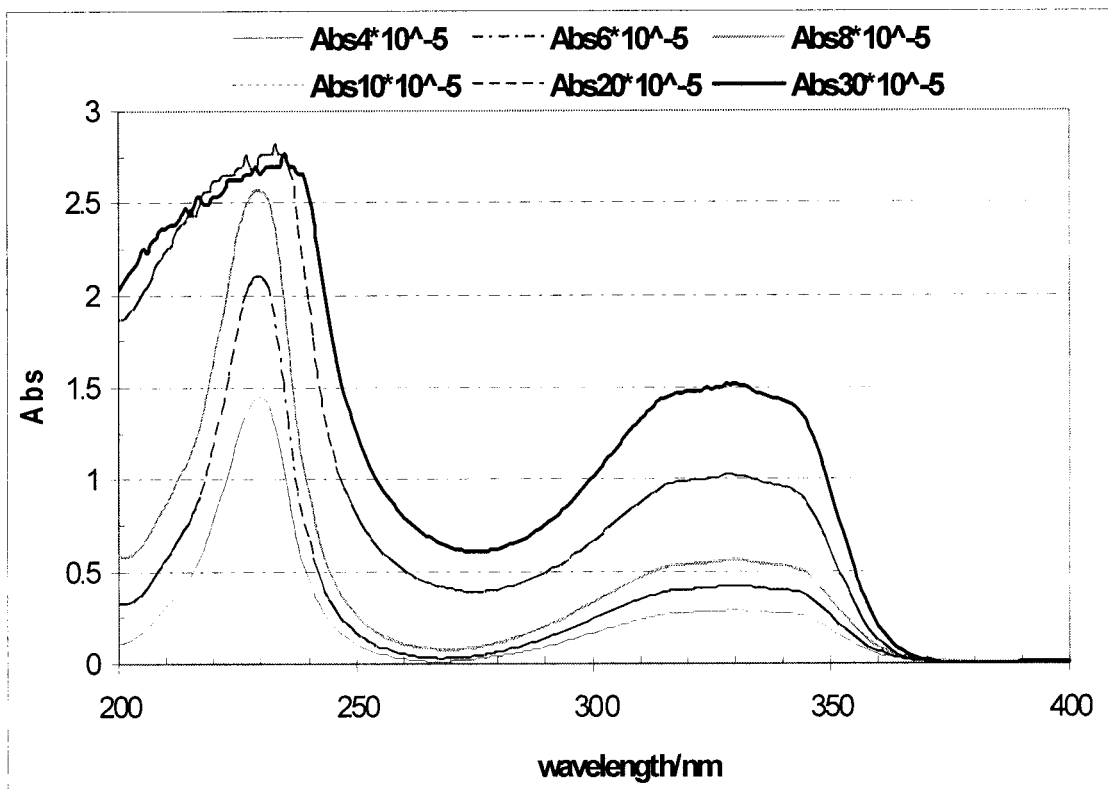


Fig. 3.20

Absorption increase with concentration [Full scale]

3.5.1 Determination of Extinction Coefficient (ϵ)

By plotting absorbance versus concentration of 1,8-DAN we got the extinction coefficient for the neutral form, Figure 3.21. We found that the best fit of the Beer's law validity is in the range $(4 - 10) \times 10^{-5}$ M of 1,8-DAN, table 3.3.

$$A = (\epsilon \cdot l) \cdot C \quad (3.3)$$

If $l = 1$ cm, Then $\epsilon = \text{slope}$

Table 3.3 Absorption versus [DAN]

[DAN]	Abs. ⁺
4.00E-05	0.29
6.00E-05	0.41
8.00E-05	0.59
1.00E-04	0.71

⁺ Wavelength is fixed at 330 nm

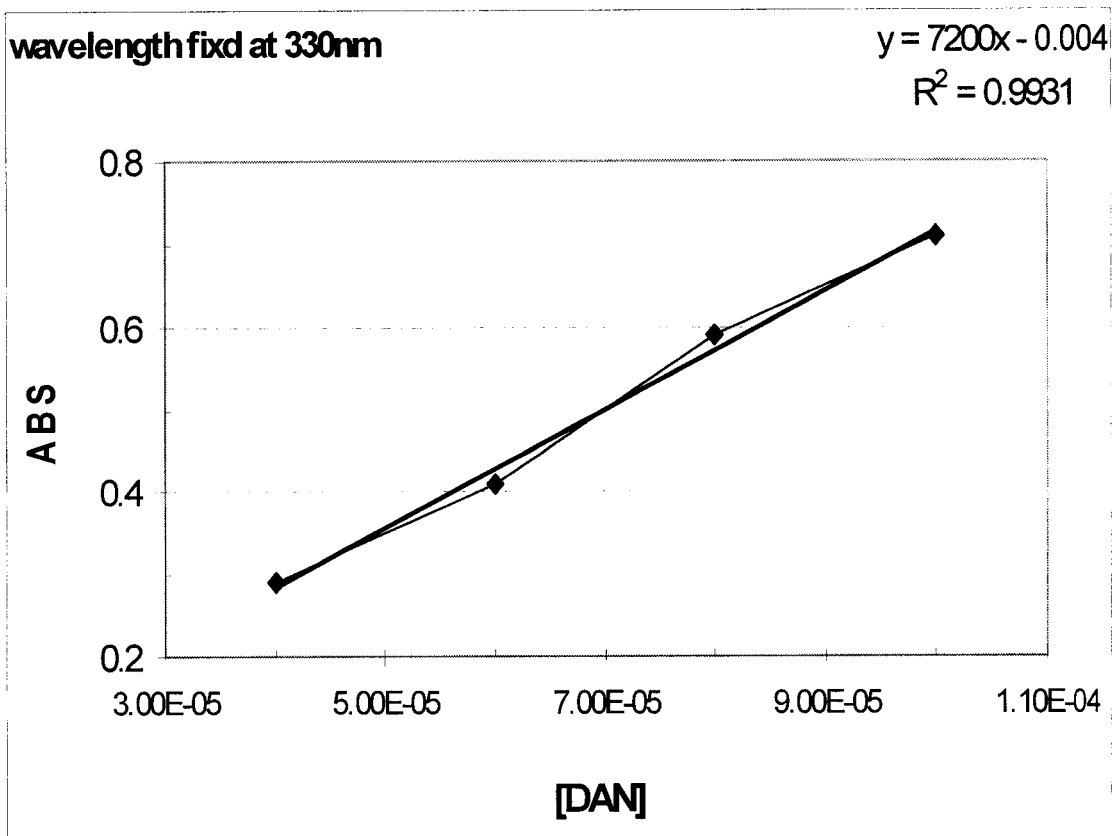


Fig. 3.21

Absorption versus [DAN] with slope = $\epsilon = 7200$

The value of the extinction coefficient of the neutral form 1,8-DAN is $7200 \text{ L mol}^{-1} \text{ cm}^{-1}$, which agrees well with the first findings, see figure 3.3, of the neutral form $\epsilon = 7000$.

The same can be obtained for the other two forms, table 3.4.

Table 3.4 Extinction coefficient of different forms 1,8-DAN

Form of 1,8-DAN	Extinction Coefficient (ϵ)*
Neutral (1,8-DAN)	7000
Mono-Cation (1,8-DANH ⁺)	3200
Di-Cation (1,8-DANH ₂ ²⁺)	5700

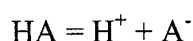
* Corresponding to figure 3.3

3.6 Determination of the Dissociation Equilibrium Constants,

pK_a and pK_a^*

3.6.1 Determination of the Dissociation Constants in the Ground State, pK_a

The values of the dissociation constants, pK_1 and pK_2 , in the ground state (S_0) were determined by plotting the absorbance differences of 1,8-DAN against pH values. A sigmoidal curve with an inflections at pH 4.0 and pH -0.1 were obtained, which are the values of pK_1 and pK_2 at the ground state. These values of 1,8-DAN agree well with the literature values of 4.15 and -0.1 for pK_1 and pK_2 , respectively [4]. The values are reported in table 3.5 and 3.6 and the plots are shown in figures 3.22 and 3.23.



$$K_a = [H^+] [A^-] / [HA]$$

$$\log K_a = \log [H^+] + \log [A^-] - \log [HA]$$

$$pH = pK_a + \log [A^-] / [HA] \quad (3.4)$$

When $[A^-]$ equals $[HA]$

$$pH = pK_a$$

Table 3.5 Determination of pK_{a1}

pH	Abs	ΔAbs^+
9.18	0.46	0.09
4.5	0.41	0.14
4	0.3	0.25
3.5	0.2	0.35
3	0.15	0.4
2	0.15	0.4
1	0.15	0.4
0.3	0.15	0.4
0	0.15	0.4

⁺ ΔAbs were taken with respect to the neutral form $[\text{DAN}] = 8 \cdot 10^{-5} \text{M}$, which has Abs 0.55 at 330 nm.

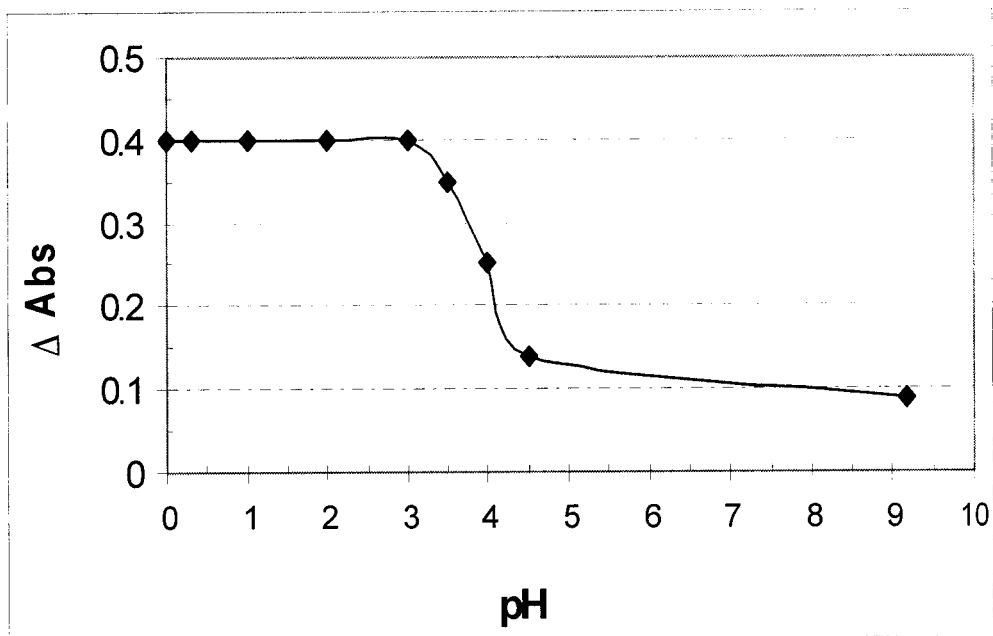


Fig. 3.22

ΔAbs versus pH values in the range pH 9.18 to pH 0

Table 3.6 Determination of pK_{a2}

pH	Abs	Δ Abs⁺
1.0	0.19	0
0.7	0.2	0.01
0.05	0.24	0.05
0	0.28	0.09
-0.3	0.35	0.16
-0.7	0.4	0.21
-0.9	0.41	0.22
-1	0.42	0.23
-1.1	0.42	0.23

⁺ Δ Abs were taken with respect to the monocation form pH 2.0 [DAN]= $8 \cdot 10^{-5}$ M, which has Abs 0.19 at 270 nm.

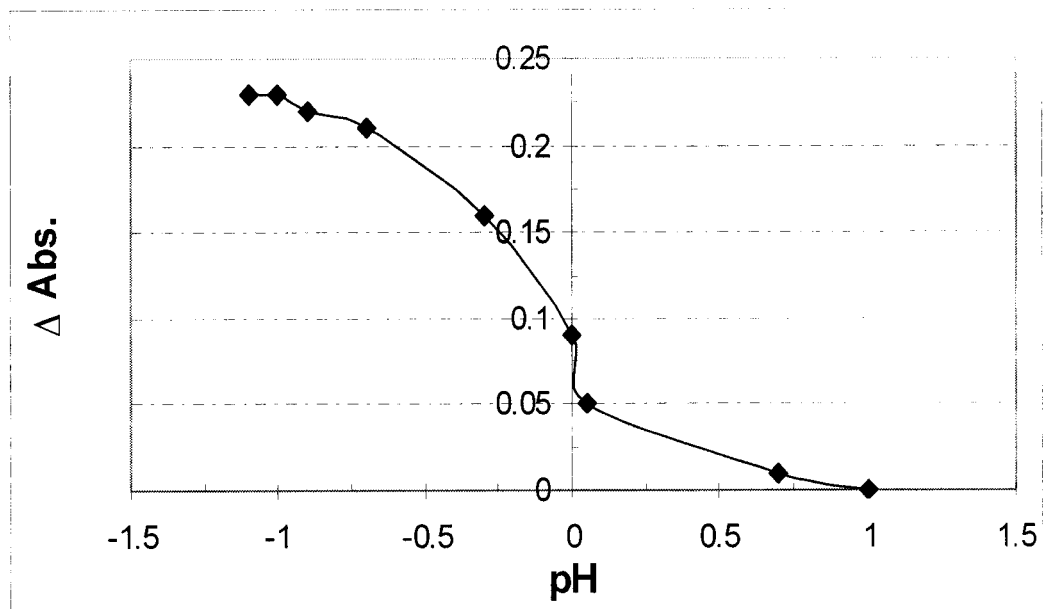


Fig. 3.23

ΔAbs versus pH values in the range pH 1.0 to pH -1.1

3.6.2 Determination of the Dissociation Constants in the Excited State, pK_a^*

From the dissociation constants in the ground state we can determine the dissociation constants in the excited state using the Forster-Cycle [44]:

$$pK_a^* = pK_a - (E_{HA} - E_{A^-}) / 2.303 R T \quad (3.5)$$

Where

E_{HA} and E_{A^-} can be determined from the 0-0 transition

Since $E = hv = h C N_A / \lambda$

So,

$$pK_a^* = pK_a - h C N_A (\lambda_{HA}^{-1} - \lambda_{A^-}^{-1}) / 2.303 R T \quad (3.6)$$

Or,

$$pK_a^* = pK_a - h C N_A (\bar{\nu}_{HA} - \bar{\nu}_{A^-}) / 2.303 R T \quad (3.7)$$

Where

λ is the wavelength taken at the 0-0 transition between absorption and corresponding emission of any form, as in the figures 3.24 to 3.29.

Table 3.7 Acidity constants in the ground and first excited states of 1,8-DAN

Equilibrium	pK_a		pK_a^*	
	Paul et al.	our work	Paul et al.	our work
$DANH^+ \leftrightarrow DAN + H^+$	4.2	4.0	---	-9.7 ⁺
$DANH_2^{2+} \leftrightarrow DANH^+ + H^+$	-0.1	-0.1	-6.5	-10.7

pK_a^* values are theoretical values obtained by Forster-Cycle

⁺ Using 1-Aminonaphthalene spectra

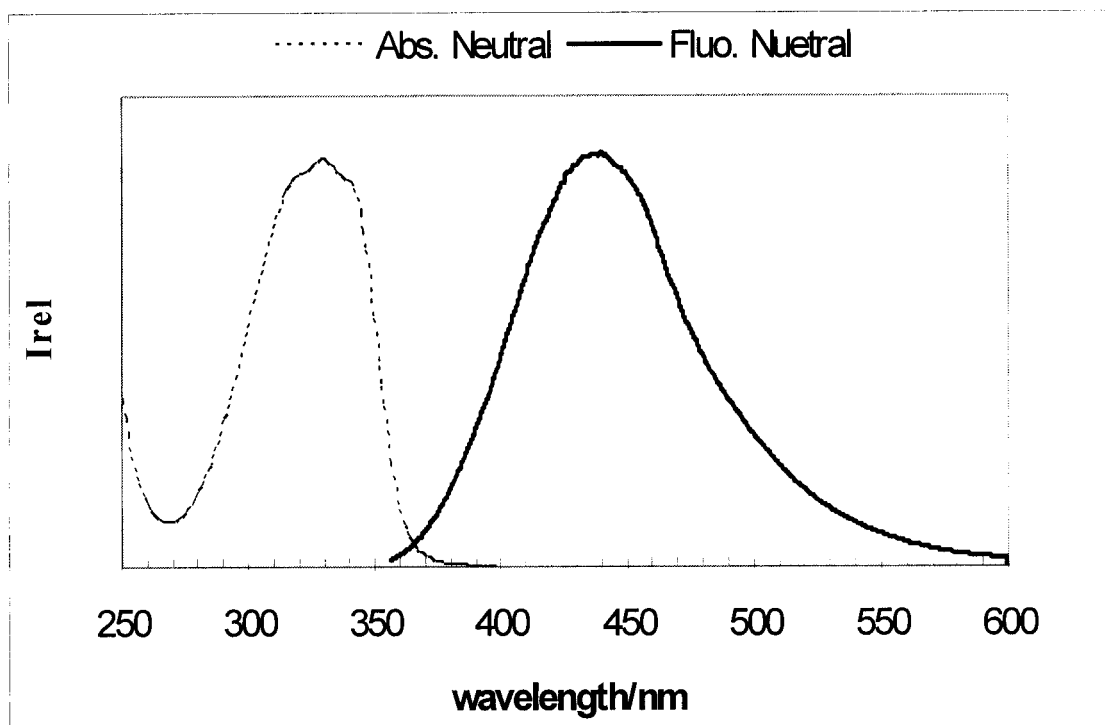


Fig. 3.24

Absorption and fluorescence spectra of the neutral form of 1,8-DAN expressed in wavelength (nm).

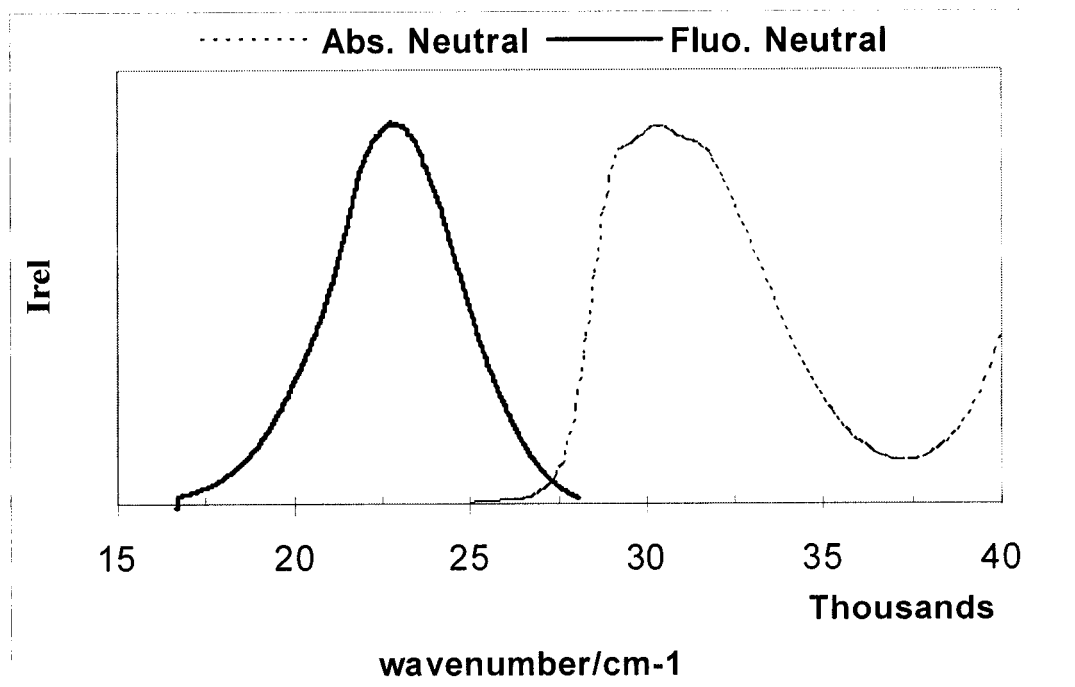


Fig. 3.25

Absorption and fluorescence spectra of the neutral form of 1,8-DAN expressed in wavenumber (cm^{-1}).

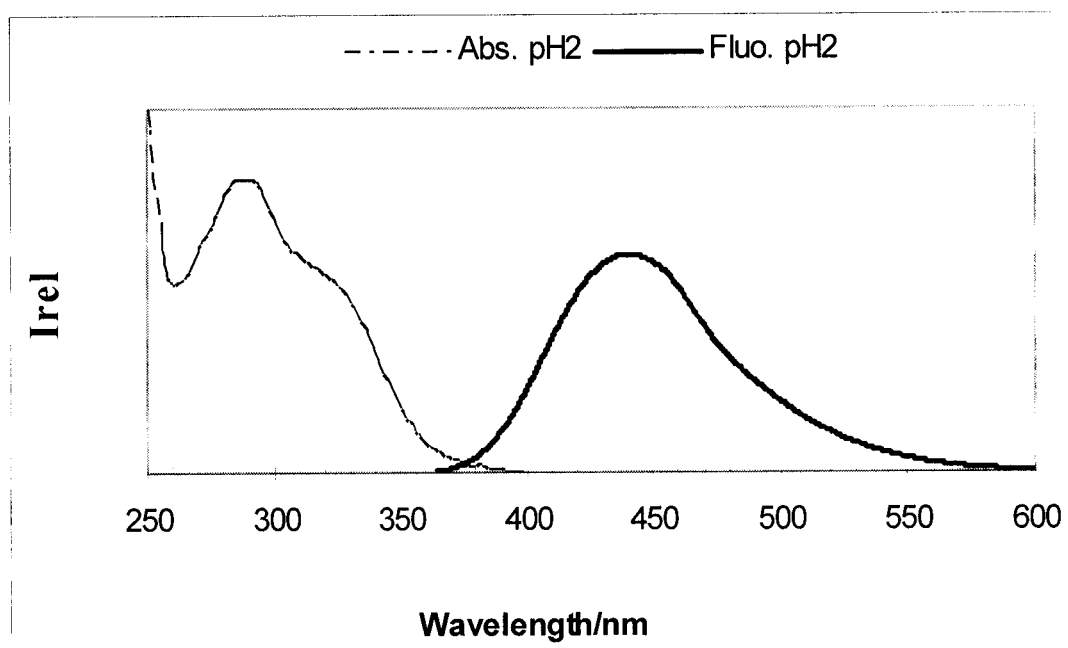


Fig. 3.26

Absorption and fluorescence spectra of the mono-cation of 1,8-DAN expressed in wavelength (nm).

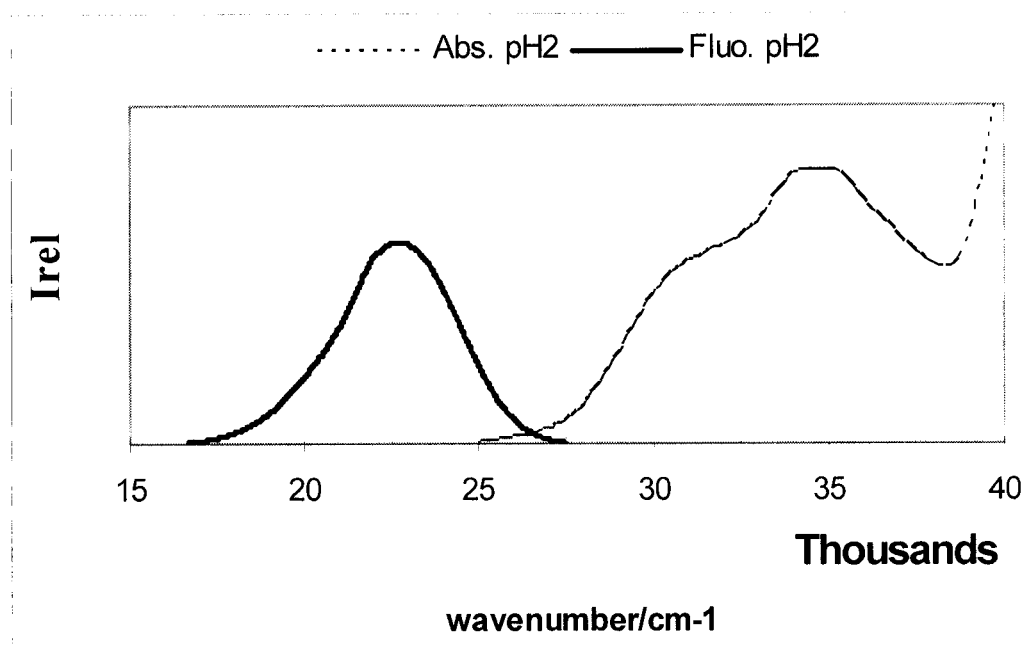


Fig. 3.27

Absorption and fluorescence spectra of the mono-cation of 1,8-DAN expressed in wavenumber (cm^{-1}).

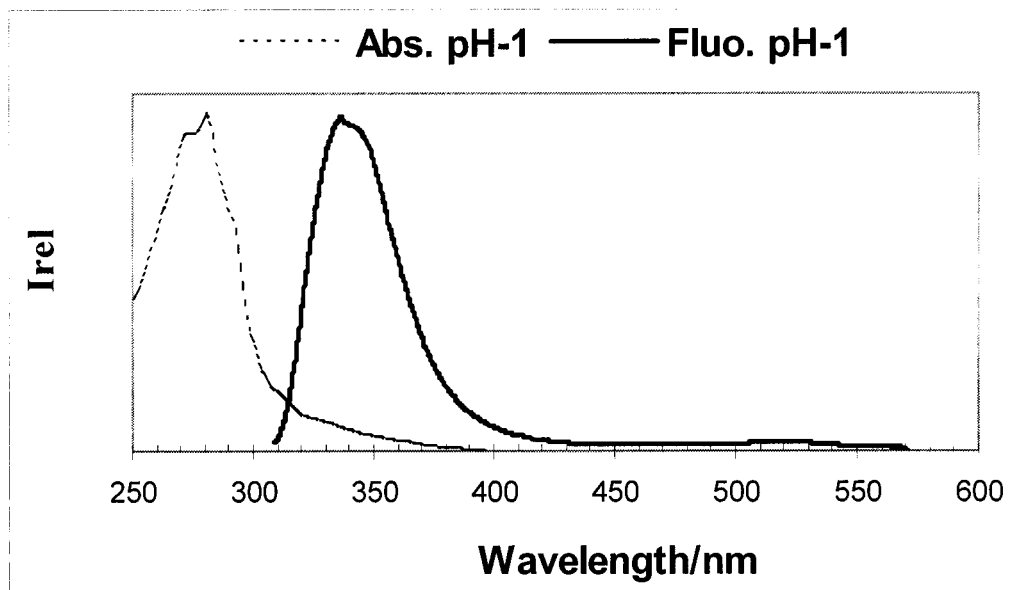


Fig. 3.28

Absorption and fluorescence spectra of the di-cation of 1,8-DAN expressed in wavelength (nm).

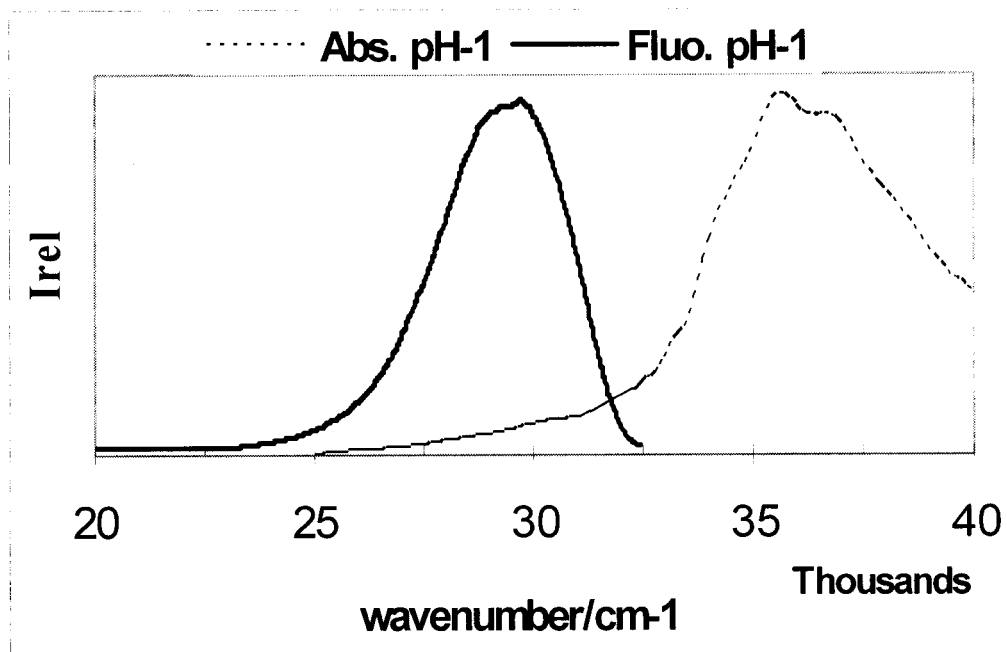


Fig. 3.29

Absorption and fluorescence spectra of the di-cation of 1,8-DAN expressed in wavenumber (cm^{-1}).

3.7 Determination of Fluorescence Quantum Yields

Fluorescence quantum yields were determined by comparing the fluorescence intensity of 1,8-DAN solutions to a reference solution. Quinine sulphate dissolved in 1N H₂SO₄ was used as fluorescence reference. The absorbance of the sample and the reference must be the same at the excitation wavelength.

$$\frac{\Phi_f^s}{\Phi_f^r} = \frac{n_s^2 \int I_s dv}{n_r^2 \int I_r dv} \quad (3.8)$$

Where:

Φ_f^s Fluorescence quantum yield for the substance under investigation.

Φ_f^r Fluorescence quantum yield for the reference.

$\int I_s dv$ Corresponds to the area under the emission peak of the substance.

$\int I_r dv$ Corresponds to the area under the emission peak of the reference.

n_s and n_r Refractive index for the solvent used for the substance and the reference, respectively.

Reported Measurements:

Quantum yield of quinine sulphate $\Phi_f^r = 0.55$

Refractive index of water $n_{H_2O} = 1.33$

Table 3.8 Quantum yields of different forms of 1,8-DAN

Form of 1,8-DAN	Quantum yield Φ_f^s
Neutral (1,8-DAN)	0.061*
Mono-Cation (1,8-DANH ⁺)	0.136
Di-Cation (1,8-DANH ²⁺)	0.047

* Agrees well with the earlier finding by Paul et al. which had a value of 0.061

3.8 Determination of Free Water $[\text{H}_2\text{O}]_{\text{free}}$

Free water $[\text{H}_2\text{O}]_{\text{free}}$ in different acid concentrations can be determined indirectly as function of HClO_4 concentrations. The following determinations have to be done to get the mole fractions of $[\text{H}_2\text{O}]_{\text{free}}$, $\gamma_{\text{H}_2\text{O}(\text{free})}$: from weight percentages of HClO_4 we got the concentrations of HClO_4 , from the concentrations of HClO_4 we got mole fractions of HClO_4 , from mole fractions of HClO_4 we got mole fractions of $[\text{H}_2\text{O}]_{\text{free}}$ according to literature values [6], then plotting mole fractions of $[\text{H}_2\text{O}]_{\text{free}}$ versus mole fractions of HClO_4 and mole fractions of $[\text{H}_2\text{O}]_{\text{free}}$ versus HClO_4 concentrations of our system.

All are listed in tables 3.9 to 3.13 and figures 3.30 to 3.34.

Table 3.9 Weight % at different HClO₄ concentrations

Weight %	[HClO₄] M
6	0.618
10	1.055
14	1.509
20	2.245
24	2.768
30	3.608
40	5.170
45	6.057
50	7.023
60	9.187
70	11.662

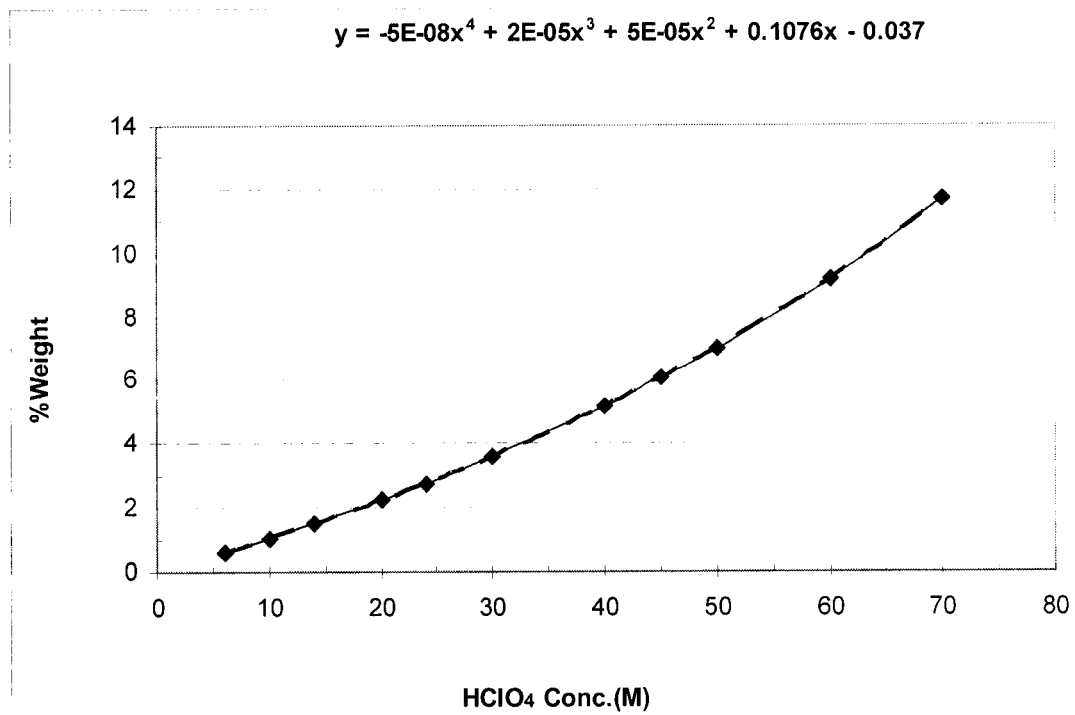


Fig. 3.30

Weight % versus [HClO₄]

Table 3.10 Mole fractions at different HClO₄ concentrations

[HClO₄] M	γ_{HClO_4}
0.618	0.0113
1.055	0.0195
1.509	0.0283
2.245	0.0429
2.768	0.0536
3.608	0.0715
5.17	0.1068
6.057	0.1280
7.023	0.1522
9.187	0.2119
11.662	0.2951

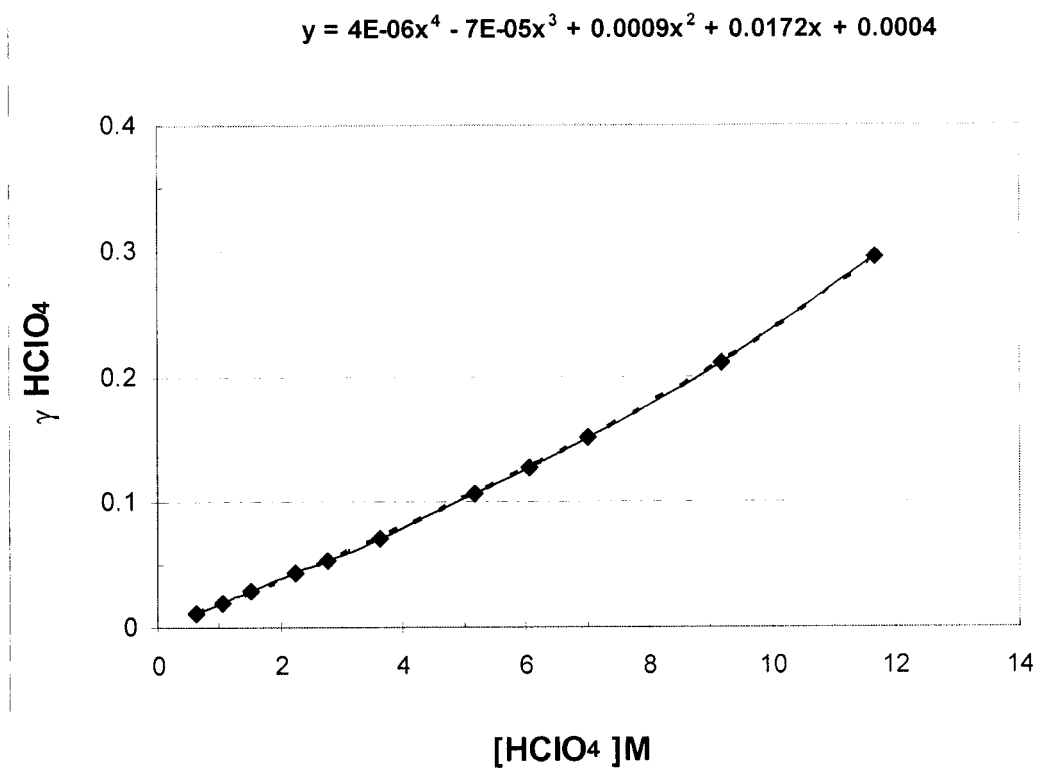


Fig. 3.31

Mole fractions of HClO₄ versus [HClO₄]

Table 3.11 Mole fractions of $[\text{H}_2\text{O}]_{\text{free}}$ at different mole fractions HClO_4 (Literature values⁶)

γ_{HClO_4}	$\gamma_{[\text{H}_2\text{O}]_{\text{free}}}$
0	1
0.02	0.83
0.04	0.62
0.06	0.44
0.08	0.29
0.09	0.19
0.11	0.10
0.13	0.06
0.15	0.03
0.17	0
0.21	0
0.25	0

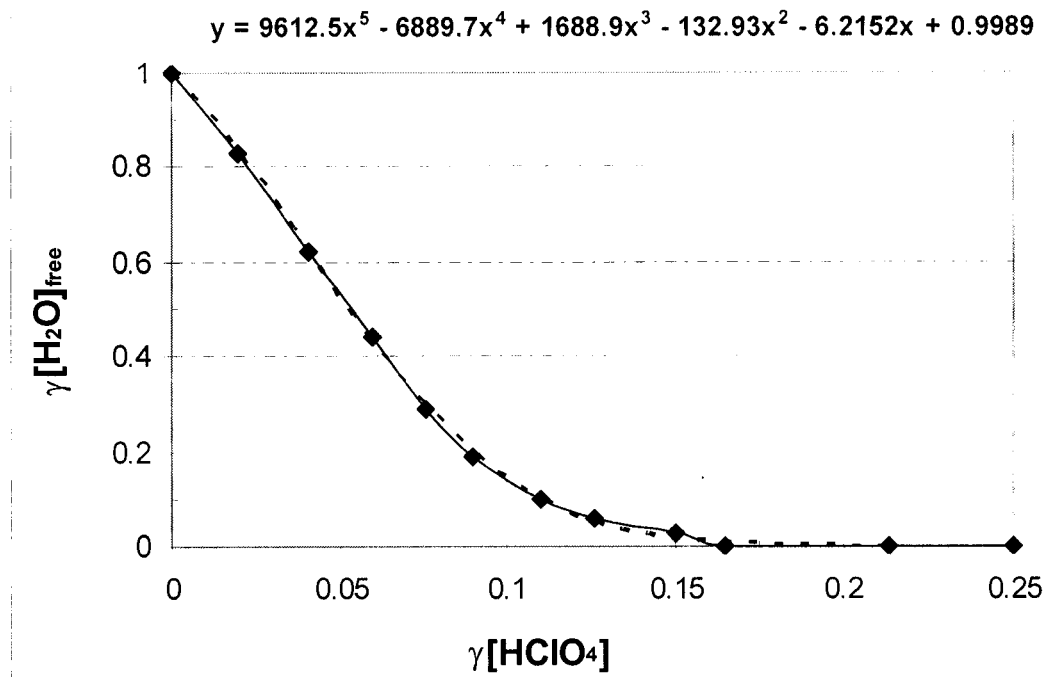


Fig. 3.32

Mole fractions of $[H_2O]_{free}$ versus mole fractions of $HClO_4$ (literature values⁶)

Table 3.12 Mole fractions of $[\text{H}_2\text{O}]_{\text{free}}$ at different mole fractions HClO_4

γHClO_4	$\gamma [\text{H}_2\text{O}]_{\text{free}}$
0.2912	0
0.2324	0
0.2033	0.0013
0.1761	0.0074
0.1505	0.0174
0.1261	0.0524
0.1027	0.1316
0.0801	0.2639
0.0585	0.4441
0.0379	0.6508
0.0184	0.8490
0	1

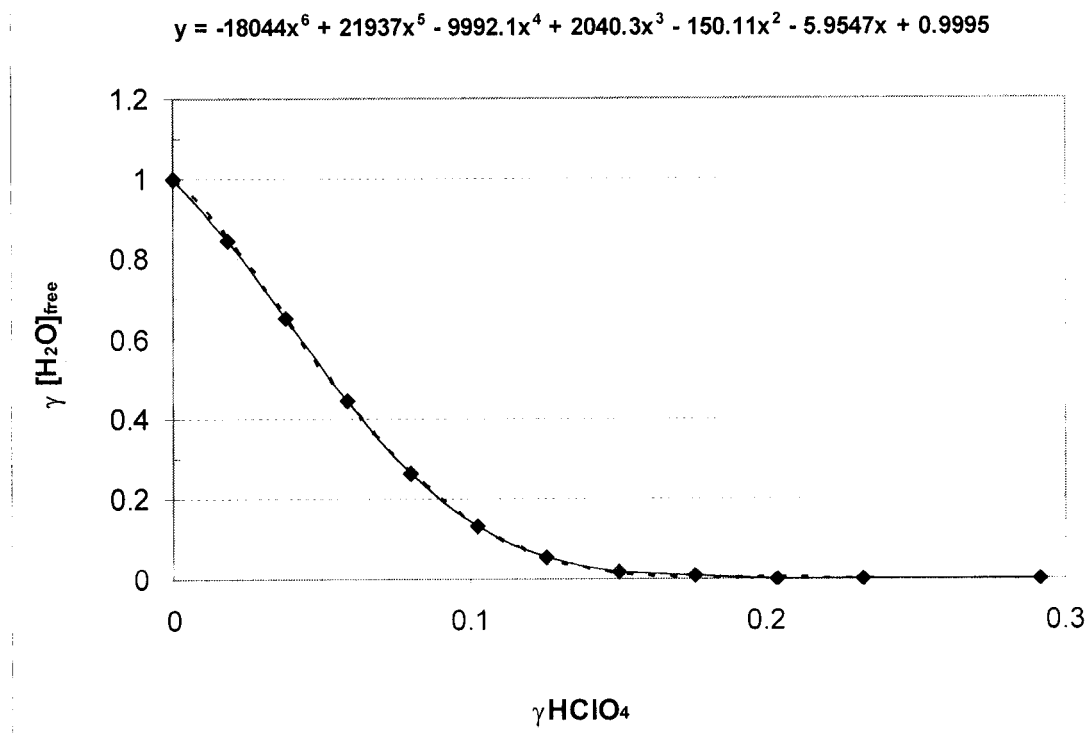


Fig. 3.33

Mole fractions of $[\text{H}_2\text{O}]_{\text{free}}$ versus mole fractions of HClO_4

Table 3.13 Mole fractions of $[\text{H}_2\text{O}]_{\text{free}}$ at different HClO_4 concentrations

$[\text{HClO}_4]$ M	$\gamma [\text{H}_2\text{O}]_{\text{free}}$
11.8	0
10	0
9	0.0013
8	0.0074
7	0.0174
6	0.0524
5	0.1316
4	0.2639
3	0.4441
2	0.6508
1	0.8490
0	1

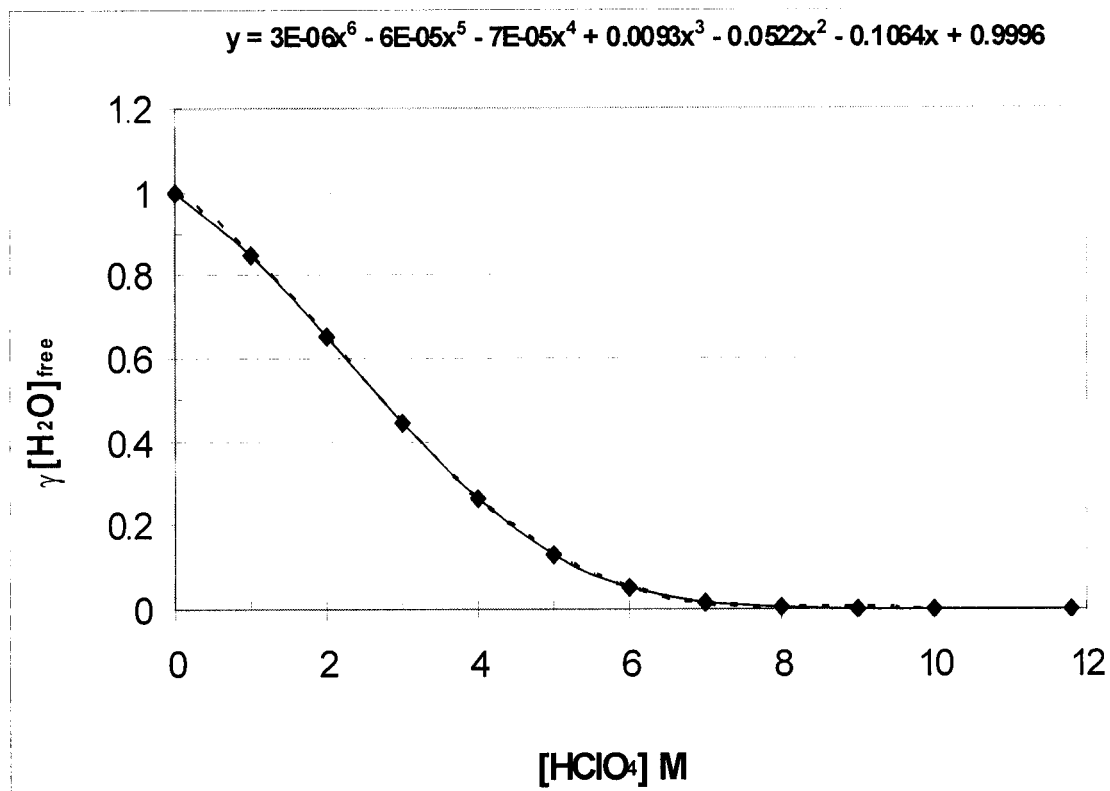


Fig. 3.34

Mole fractions of $[\text{H}_2\text{O}]_{\text{free}}$ versus concentration of HClO_4

3.9 Determination of the Quenching Constants, k_q

3.9.1 Determination of k_q for the Neutral Form Using Quantum Yield Intensities

Appreciable proton-induced quenching has been observed for the fluorescence of the mono-cation form in the proton concentration range 0.01 – 1.2 M, prior to the formation of the di-cation. Further, there was no quenching effect due to the counter ion ClO_4^- under the experimental conditions employed. Quenching constant can be determined using the model suggested by Shizuka et al. [9] or by using a simple Stern-Volmer plot under the condition where the H^+ concentration is too small to give any backward reaction.

Since the intensity of the emission peak is proportional to the fluorescence yield, plotting $1/I$ versus $[\text{H}^+]$ can be used to determine k_q under fixed emission wavelength $\lambda_{\text{EM}} = 455$ nm.

The quencher for the neutral form emission is $[\text{H}^+]$, Figure 3.38 and 3.39. The following equations are used to determine k_{q1} :

$$\eta_0 = \frac{n_e}{n_e + n_r} \quad (3.9)$$

$$\eta = \frac{n_e}{n_e + n_r + k_q [\text{H}^+]} \quad (3.10)$$

Dividing 3.9 over 3.10

$$\frac{\eta_0}{\eta} = 1 + \frac{k_q}{n_e + n_r} [H^+] \quad (3.11)$$

Since $\tau_0 = \frac{1}{n_e + n_r}$

$$\frac{\eta_0}{\eta} = 1 + k_q \tau_0 [H^+] \quad (3.12)$$

Then,

$$\frac{1}{\eta} = \frac{1}{\eta_0} + \frac{k_q \tau_0}{\eta_0} [H^+] \quad (3.13)$$

or,

$$\frac{1}{\eta} = \frac{1}{\eta_0} + \frac{k_q}{\eta_0 (n_e + n_r)} [H^+] \quad (3.14)$$

From equation 3.13

Plotting $1/\eta$ Vs. $[H^+]$, gives slope = $k_q \tau_0 / \eta_0$

Then,

$$k_q = \frac{\text{slope} * \eta_0}{\tau_0}$$

Note Actual quantum yields are not needed. As they are proportional to the height of the spectrum, height can be used directly.

Where

η and η_0 Fluorescence yield with and without quencher, respectively.

k_q Rate constant for proton-induced fluorescence quenching

τ_0 Natural lifetime of the neutral species

Table 3.14 Acid concentrations range 0.01-1.2 M, Emission wavelength fixed at

$\lambda_{EM} = 455 \text{ nm}$.

$[\text{H}^+] \text{ M}$	I	1/I
0.01	14.2	0.070
0.05	10	0.100
0.1	7	0.143
0.2	4.3	0.233
0.3	2.9	0.345
0.4	3.4	0.294
0.5	2.6	0.385
0.6	2.1	0.476
0.7	1.9	0.526
0.8	2.3	0.435
0.9	1.4	0.714
1	0.6	1.667
1.1	0.5	2.0
1.2	0.4	2.5

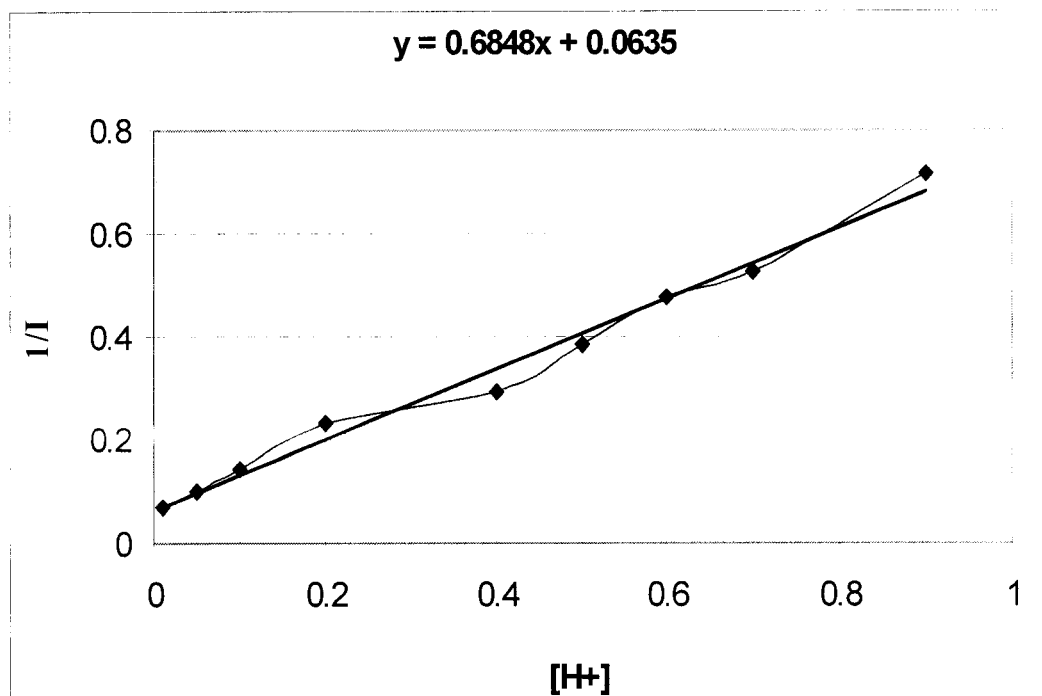


Fig. 3.35

$1/I$ versus $[H^+]$

Using

Slope = 0.685

$\tau_0 = 7.7 \times 10^{-9}$ s

$\eta_0 = 14.2$

Then,

$k_q = 1.26 \times 10^9 \text{ M}^{-1}\text{s}^{-1}$

Which is with good agreement with the value obtained from the Stern-Volmer plot in terms of lifetimes.

3.9.2 Determination of k_q for the Neutral Form Using Lifetime Measurements

The quenching constant k_q can be determined using a Stern-Volmer plot in terms of τ_0/τ vs. $[H^+]$, Figure 3.36. Using a simple Stern-Volmer plot has to be under the conditions where the lifetimes of the mono-cation are short in comparison to those of the di-cation lifetimes and the H^+ concentration is too small to give any backward reaction i.e. from 0.01 M to 1.0 M $HClO_4$.

Stern-Volmer equation:

$$\frac{\tau_0}{\tau} = 1 + k_q \tau_0 [H^+] \quad (3.15)$$

Where

τ_0 Actual lifetime in the neutral species i.e. without quenchers H^+

τ Actual lifetime in the mono-cation species i.e. with quenchers H^+

k_q Quencher rate constant of the neutral form

From equation 3.15

Plotting τ_0/τ vs. $[H^+]$, gives slope = $k_q \tau_0$

So,

$$k_q = \text{slope} / \tau_0$$

Table 3.15 Stern-Volmer plot

$[H^+] \text{ M}$	τ / ns	τ_0/τ
0.01	8.3	0.928
0.05	5.7	1.351
0.1	4.3	1.791
0.5	1.6	4.813
1.0	0.7	11.0

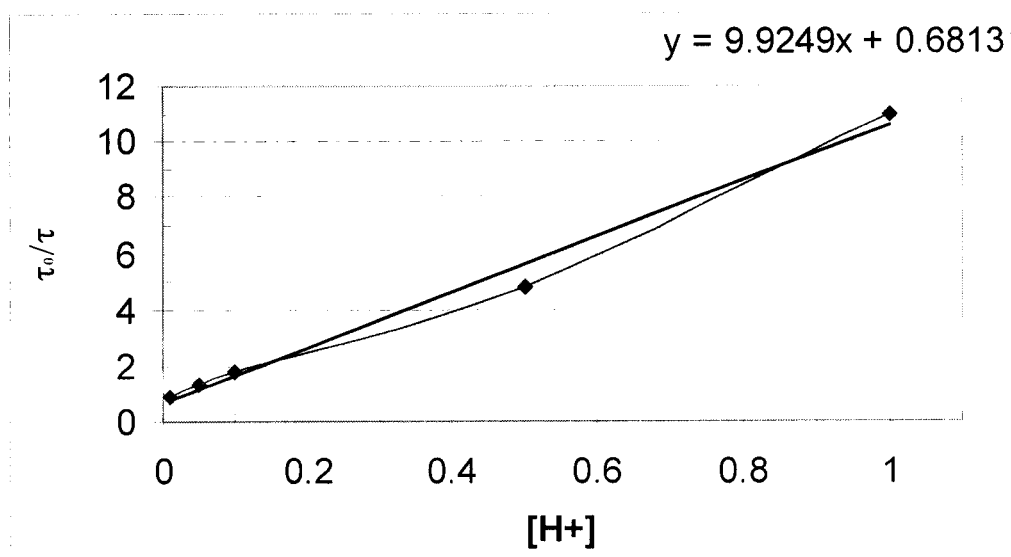


Fig. 3.36

Stern-Volmer plot, τ_0/τ vs. $[H^+]$

Using

Slope = 9.92

$\tau_0 = 7.7 \times 10^{-9} \text{ s}$

Then,

$k_q = 1.29 \times 10^9 \text{ M}^{-1} \text{ s}^{-1}$

Which is in good agreement with the value calculated by intensity values $1/I$ vs. $[H^+]$, which gives $k_q = 1.26 \times 10^9 \text{ M}^{-1}\text{s}^{-1}$. This is the same value within an error of 2%.

3.9.3 Determination of the Quenching Constant for the Protonated Form, k'_q

The quencher for the protonated form is $[H_2O]_{free}$ i.e. the proton acceptor, Figure 3.40. The following equations are used to determine k'_q :

$$\frac{1}{\eta} = \frac{1}{\eta_0} + \frac{k_1}{\eta_0(n_e + n_r)} \gamma[H_2O]_{free} \quad (3.16)$$

Then,

$$\frac{1}{\eta} = \frac{1}{\eta_0} + \frac{k_1 \tau_{acid}}{\eta_0} \gamma[H_2O]_{free} \quad (3.17)$$

or,

$$\frac{\eta_0}{\eta} = 1 + k_1 \tau_{acid} \gamma[H_2O]_{free} \quad (3.18)$$

Where

$$k_1 = k'_q * 55.5$$

Since

$$1000 \text{ g H}_2\text{O} = 55.5 \text{ mol H}_2\text{O}$$

Table 3.16 Acid concentrations range 1-11.8 M, Emission wavelength fixed at

$$\lambda_{EM} = 340 \text{ nm}$$

$[\text{H}^+] \text{ M}$	I	I₀/I	$\gamma [\text{H}_2\text{O}]_{\text{free}}$
11.8	152	1	0
10	61	2.49	0
9	29	5.24	0.0013
8	12	12.67	0.0074
7	3.7	41.08	0.0174
6	4	38.00	0.0524
5	2.4	63.33	0.1316
4	1.5	101.33	0.2639
3	1	152.0	0.4441
2	0.7	217.14	0.6508
1	0.4	380.0	0.8490

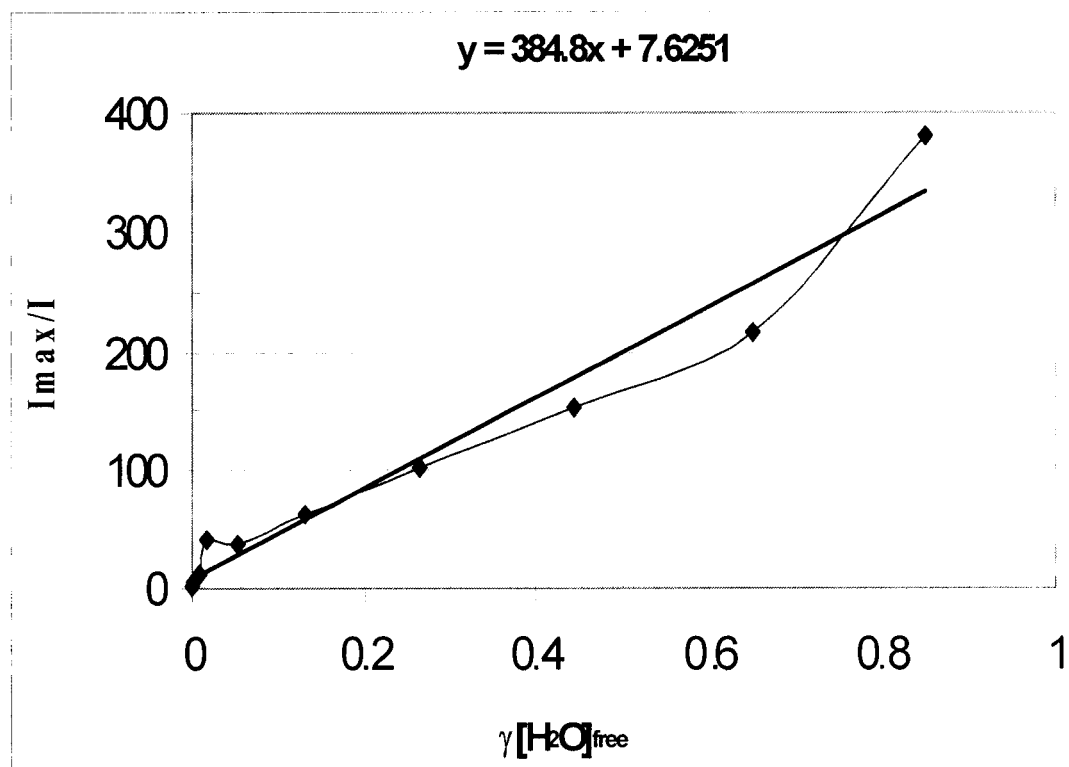


Fig. 3.37

I_0/I versus mole fraction $[\text{H}_2\text{O}]_{\text{free}}$

$$\text{Slope} = k_1 * \tau_{\text{acid}}$$

$$k_1 = 384.8 / 22.2 \times 10^{-9} \text{s} = 1.73 * 10^{10} \text{s}^{-1}$$

$$k'_q = k_1 / 55.5 = 3.12 * 10^8 \text{M}^{-1} \text{s}^{-1}$$

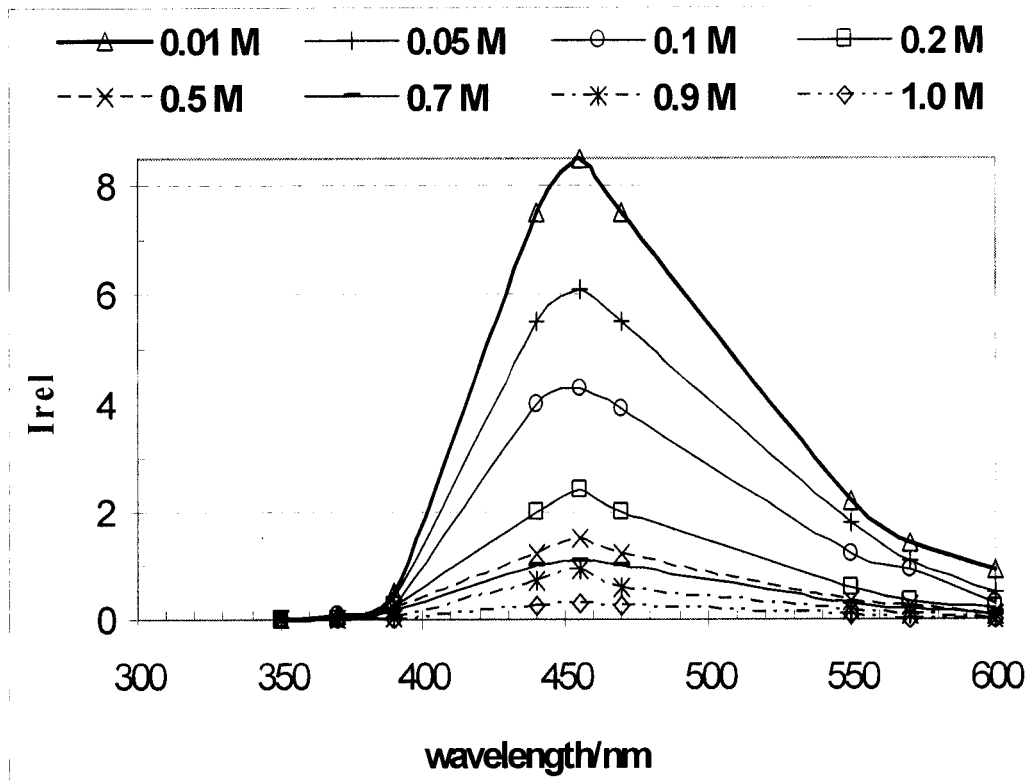


Fig. 3.38

Quenching of the neutral form, from 0.01M to 1.0M

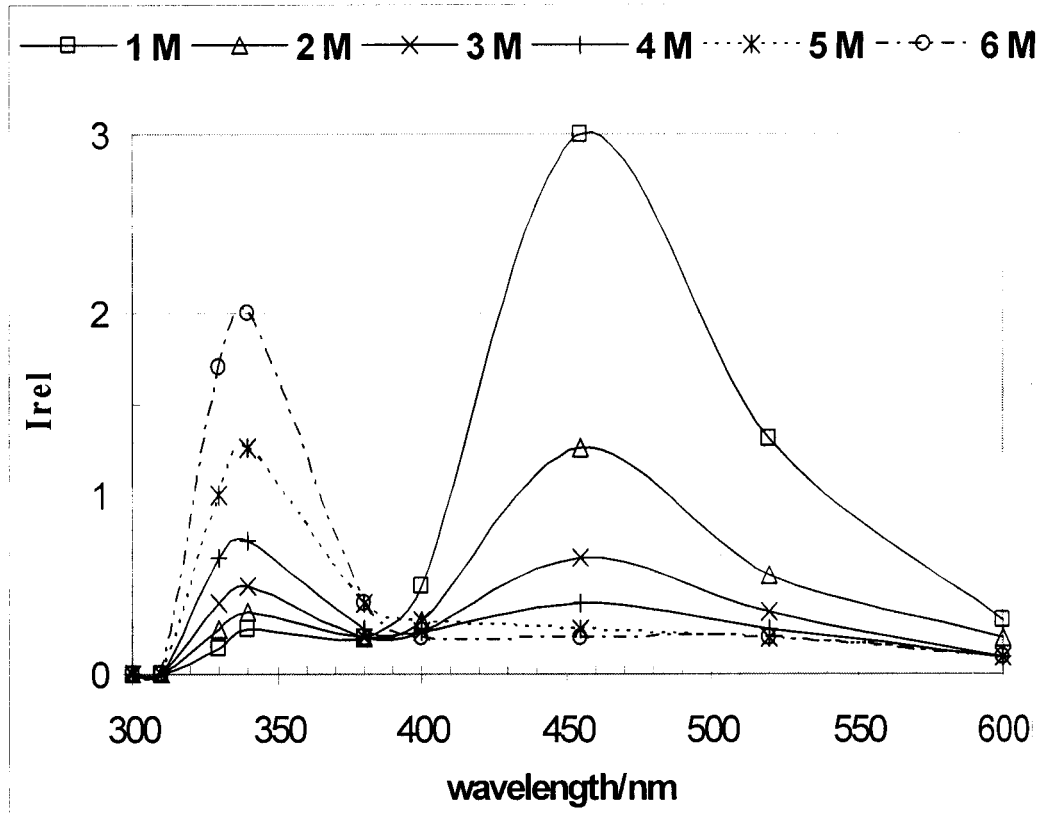


Fig. 3.39

Intermediate emission, from 1M to 6M

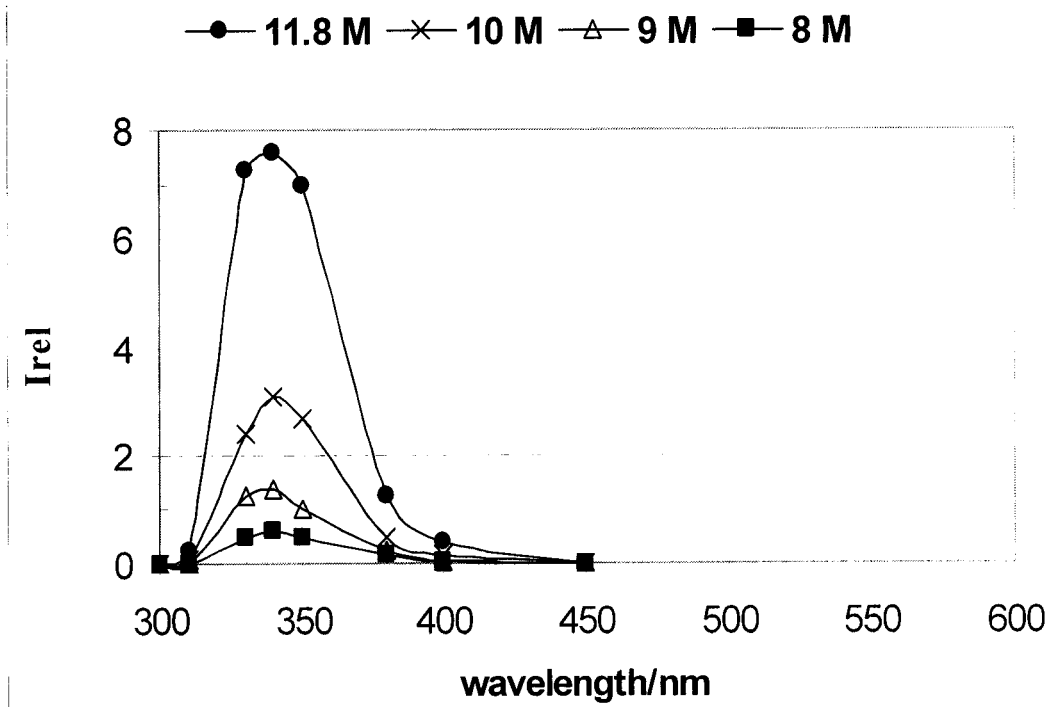


Fig. 3.40

Quenching of the diprotonated form, from 11.8M to 8.0M

3.10 Energy Surface Diagrams of 1,8-DAN

According to the spectroscopic measurements we got, there are three different forms of 1,8-DAN in the ground state, i.e. the neutral, the mono-cation and the di-cation form. However, there are only two different forms of 1,8-DAN in the excited state, i.e. the neutral and the di-cation form. The mono-cation form in the excited state becomes more acidic. The estimated value of k_d^* is 10^{17}s^{-1} , which was estimated by using the $\text{p}k_a^*$ of the Aminonaphthalene (1-AN). Hence, it loses the proton very fast to become the neutral form which actually gives the emission, see Figure 3.8. On the other hand, Figure 3.9 shows a red shift of the mono-cation form due to solvent relaxation. According to these information energy surface diagrams of the mono- and the di-cation form were sketched, Figure 3.41 and 3.42.

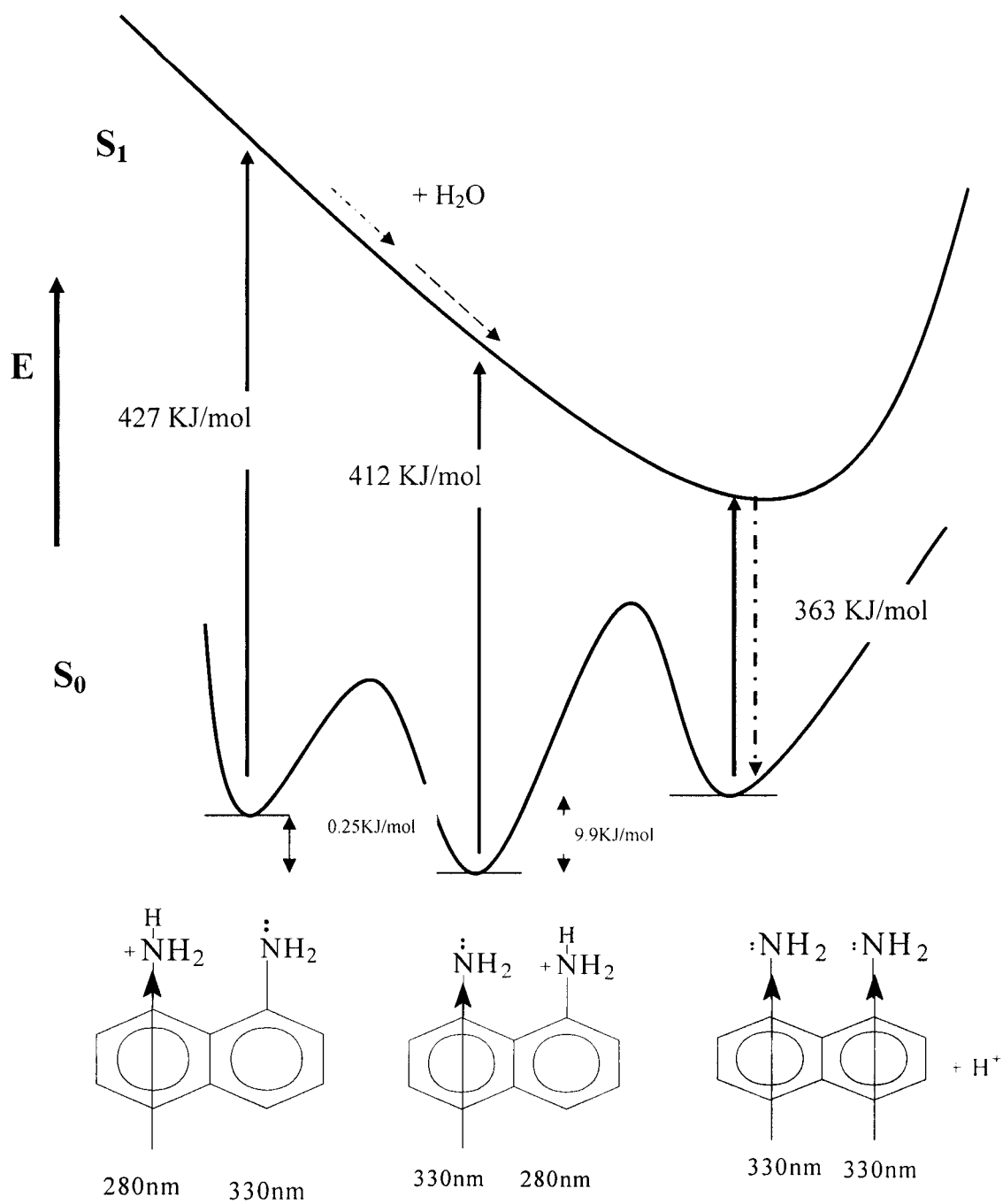


Fig. 3.41

Energy surface diagram for the mono-cation form in the ground and excited state

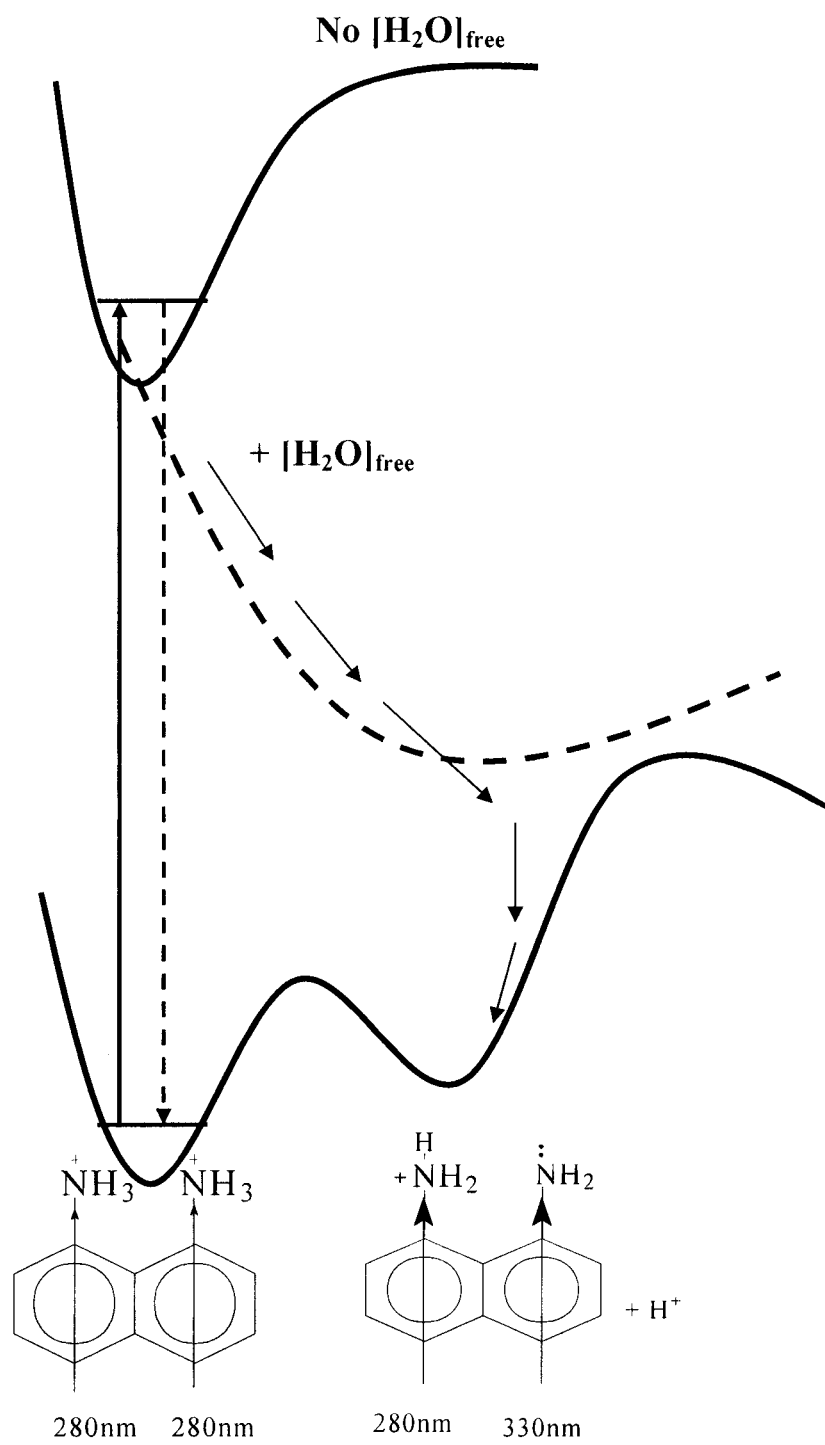


Fig. 3.42

Energy surface of the di-cation form in the presence and absence of free water molecules

3.11 Normal and Natural lifetime (τ , τ_0)

In order to elucidate the nature of the states involved we first calculated the natural lifetimes of the different forms of 1,8-DAN and compared it with aminonaphthalene (1-AN). It is expected that the Strickler-Berg equation is valid, see table 3.17 and 3.18, (though the natural lifetime is not calculated directly from the Strickler-Berg equation).

$$\frac{1}{\tau_0(\text{calc.})} = 2.88 \times 10^{-9} n^2 \frac{\int f(\bar{\nu}) d\bar{\nu}}{\int f(\bar{\nu}) \frac{d\bar{\nu}}{\bar{\nu}^3}} \int \frac{\epsilon}{\bar{\nu}} d\bar{\nu} \quad (3.19)$$

From Strickler-Berg equation

$$\tau_0 \propto \frac{1}{\int \epsilon(\bar{\nu}) d\bar{\nu}} \quad (3.20)$$

The natural lifetime τ_0 can be calculated by

$$\tau_0 = \frac{\tau}{\eta} \quad (3.21)$$

Where

$\tau = 1/k_f + k_r$ (Normal lifetime)

$\tau_0 = 1/k_f$ (Natural lifetime)

Table 3.17 Normal and natural lifetimes and extinction coefficients of 1,8-DAN

Sample	Lifetime τ/ns	Quantum yield η	Nat. lifetime τ_0/ns	Ext. coeff. $\epsilon/\text{M}^{-1}\text{cm}^{-1}$
DAN	7.7	0.061	126.2	7000
DANH⁺	8.3	0.136	61.0	3200
DANH₂²⁺	22.2	0.047	472.3	5700

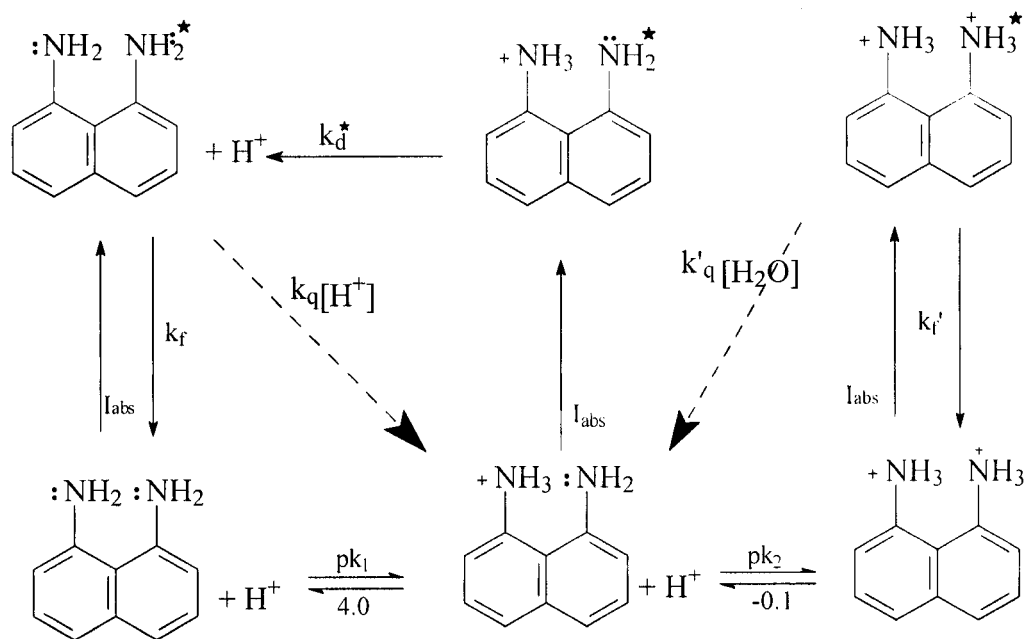
Table 3.18 Normal and natural lifetimes and extinction coefficients of 1-AN

Sample	Lifetime τ/ns	Quantum yield η	Nat. lifetime τ_0/ns	Ext. coeff. $\epsilon/\text{M}^{-1}\text{cm}^{-1}$
AN	18.2	0.490	37.1	9800
ANH⁺	45.0	0.327	137.6	6300
X-Form	2.0	0.065	30.8	8500

From table 3.17 and 3.18, the natural lifetimes and the extinction coefficients of 1,8-DAN and 1-AN are inversely proportional, as the Strickler-Berg equation is valid.

3.12 Kinetic Model of the Proton Transfer Reactions For 1,8-DAN

According to the preceding discussion, we propose the following scheme of the proton transfer reactions. As spectroscopic data suggest, the mono-cation form of 1,8-DAN in the excited state undergoes fast dissociation to the neutral form which gives the emission of the neutral form. Upon increasing the concentration of H^+ this form is quenched. On the other hand, the di-cation form of 1,8-DAN loses its excitation when a proton acceptor (i.e. water) is present. There is no equilibrium between the di- and mono-cation forms in the excited state i.e. it is a diabatic process, see scheme 3.1.



Scheme 3.1

Proton transfer reactions of 1,8-DAN in the ground and excited states.

Where

pK_1 & pK_2	Dissociation constants in the ground state.
k_d^*	Rapid dissociation constant of the mono-cation form in the excited state.
k_f & k'_f	Fluorescence rate constants, for neutral and protonated forms, respectively.
k_q & k'_q	Quenching rate constants, deactivation, for neutral and protonated forms, respectively.
I_{abs}	Absorption intensity, which indicate where excitation can be done.

3.13 1,8-DAN in Zeolite Y Sieves

Zeolite Y can be used as sodium form, NaY, or as protonated form, HY. NaY is the raw form of the zeolite Y. HY can be obtained by ion exchange with ammonium nitrate, NH_4NO_3 , at different H^+ ratios which depend on the NH_4NO_3 concentration.

The ion exchange process can be done as follows:



Three forms of zeolite Y are used: NaY, HY-34 and HY-96. The protonated form can interact with 1,8-DAN adsorbed on the surface of the zeolite, Figure 3.43. Loading levels of 1,8-DAN on the different forms of zeolite Y are reported in table 3.20.

The proton-transfer reaction between zeolite Y and 1,8-DAN has been studied by emission spectra. The fluorescence spectra of 1,8-DAN in the zeolite samples show either the neutral band or a mixture with the protonated band. 1,8-DAN/NaY shows the neutral band of 1,8-DAN. However, under higher energy excitation it shows the protonated band even though there is no proton, Figure 3.44. It shows some interesting effects with the aluminum, which is Lewis acid site, to give the higher energy band. 1,8-DAN/HY-34 shows both neutral band and the protonated band of 1,8-DAN, Figure 3.45. 1,8-DAN/HY-96 shows also both the neutral band and the protonated band of 1,8-DAN. However, under higher energy excitation it shows the low energy band, Figure 3.46. Further studies beyond the scope of this thesis are needed to explain this behavior.

Table 3.19 Edge of unit cell and the number of unit cells per gram of zeolite Y⁶

Sample	Unit Cell edge a_0 / Å	No. Unit Cell per gram
NaY	24.686	4.7×10^{19}
HY-34	24.628	4.8×10^{19}
HY-96	24.410	5.2×10^{19}

Table 3.20 Loading level of the probe molecule 1,8-DAN

Sample	No. Unit Cell Per 0.22g⁺	No. Adsorbed Molecules	Loading Level[*]
NaY	1.03×10^{19}	3.50×10^{18}	0.340
HY-34	1.06×10^{19}	3.47×10^{18}	0.330
HY-96	1.14×10^{19}	4.12×10^{18}	0.361

⁺ Used mass of zeolite Y is 0.22 g

^{*} Loading level expressed as molecule/unit cell

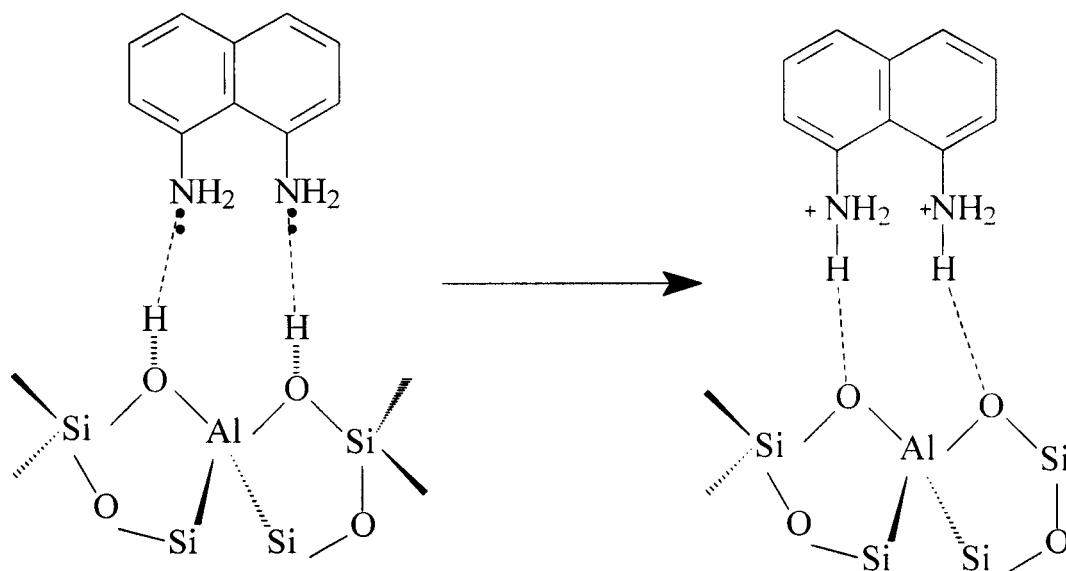


Fig. 3.43

Protonation process of 1,8-DAN adsorbed on zeolite Y at a Bronsted acid site

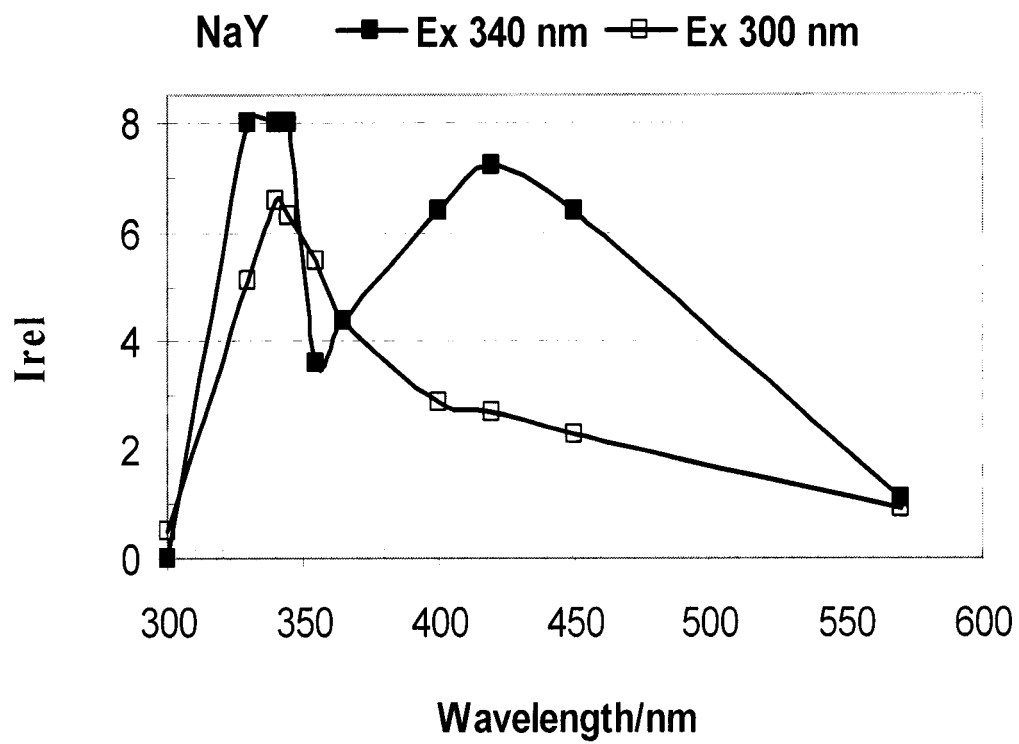


Fig. 3.44

Emission spectrum of 1,8-DAN/NaY

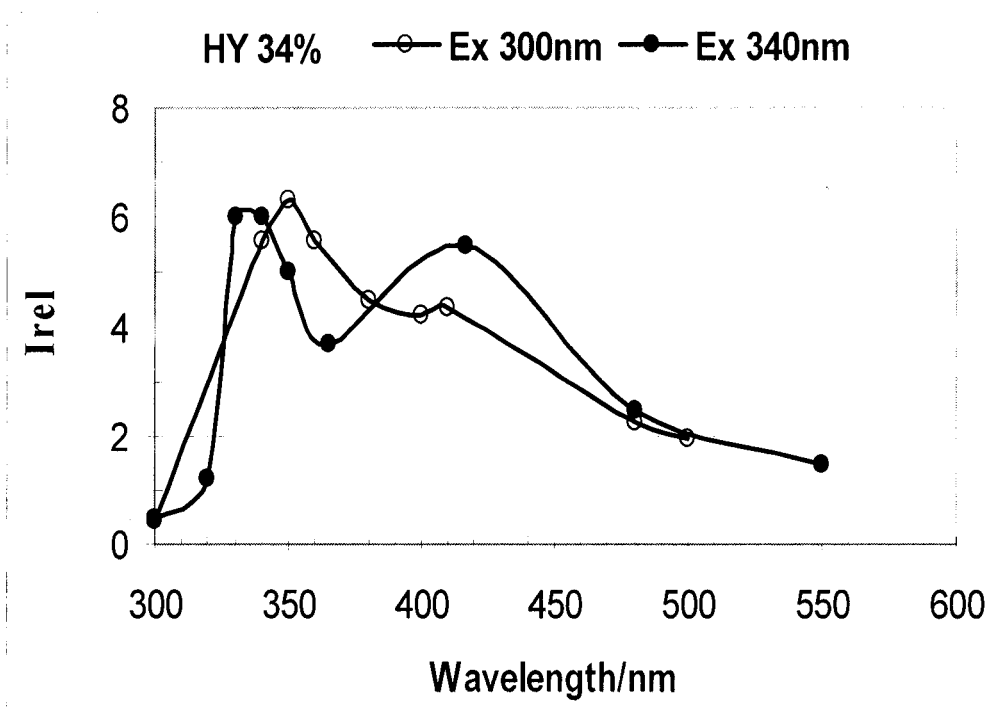


Fig. 3.45

Emission spectrum of 1,8-DAN/HY-34

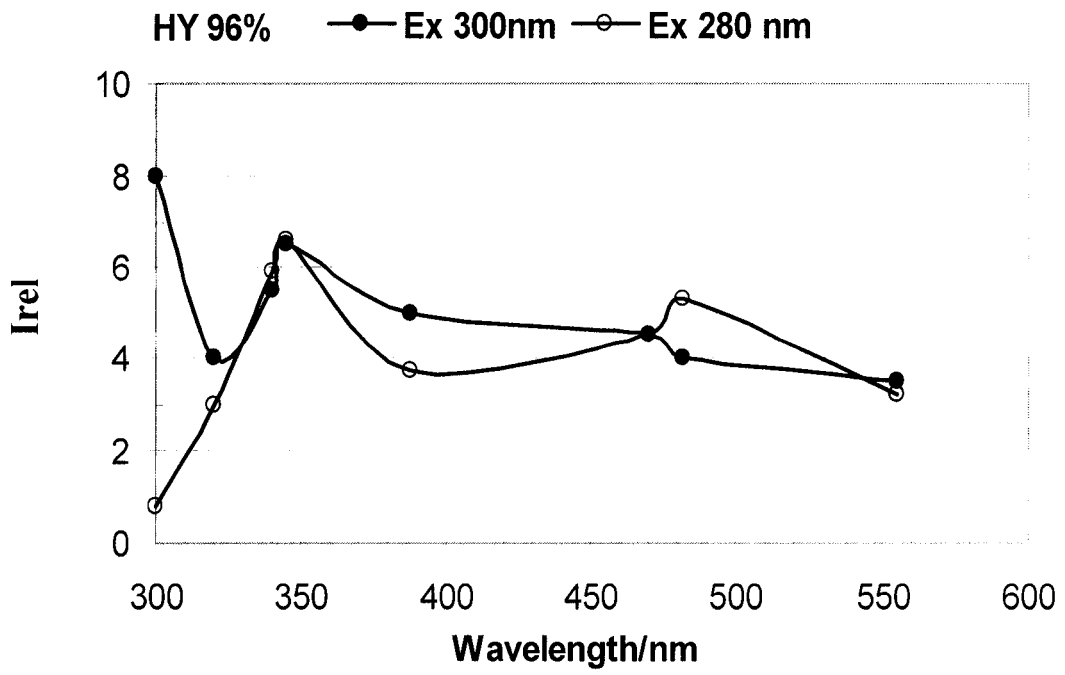


Fig. 3.46

Emission spectrum of 1,8-DAN/HY-96

CHAPTER IV

CONCLUSION

The proton-transfer reaction kinetics of 1,8-Diaminonaphthalene in acidic medium and in zeolite sieves was studied by means of absorption and emission spectra and by laser-induced picosecond spectroscopy. We found that there are three clear different forms of 1,8-DAN in the ground state, but only two different forms in the excited state.

The absorption of the mono-cation form of 1,8-DAN is found to be a mixture of two transitions, i.e. the neutral form transition and the di-cation form transition, which disproves the scheme which was proposed by Paul et al. i.e. the proton is shared between the two nitrogen atoms. However, the emission is found to be only from the neutral form, due to the fast dissociation of the mono-cation form once it is excited. The reaction of the excited neutral form with H^+ does not lead to an excited monoprotonated form (adiabatic reaction), rather to the unexcited monoprotonated form (diabatic quenching reaction).

Higher energy excitation of the mono-cation form gives a red shift emission due to solvent relaxation, as reported before. However, lower energy excitation of the mono-cation form gives the neutral emission which was not reported before.

There is a quenching effect upon increasing the acid concentration. It is observed from the emission spectra that the quencher for the neutral form is H^+ . Whereas, the quencher for the di-cation form is free H_2O molecules.

The neutral form and the mono-cation form of 1,8-DAN have similar exponential decays which confirms that only two forms are there in the excited state. On the other hand, the di-cation form has a bi-exponential decay which suggest the existence of a new form X. i.e. an adduct between the solvent molecules and the fluorophore molecules as shown for 1-Aminonaphthalene.

All dissociation and quenching rate constants have been determined, with good agreement of the Stern-Volmer plots using lifetime ratios and fluorescence intensity ratios as a function of $[H^+]$. The value of k_d^* is estimated to be in the order of $10^{17}s^{-1}$ based on the assumption that the pK^* of the mono-cation is the same like the pK^* of 1-Aminonaphthalene (1-AN). Quantum yields were determined for 1,8-DAN. The result found for the neutral form agrees well with the literature value.

A kinetics scheme for protonation/deprotonation of 1,8-DAN in the ground and excited states is proposed. According to the scheme, there is no equilibrium in the excited state between the different forms of 1,8-DAN i.e. no adiabatic processes are observed. Energy surface schemes for the mono- and the di-cation forms are proposed based on absorption and emission spectra.

The proton-transfer reaction kinetics between zeolite Y and 1,8-DAN has been attempted by laser-induced picosecond spectroscopy. The fluorescence spectra of 1,8-DAN in the zeolite samples show either the neutral or a mixture with the protonated form. Further studies beyond the scope of this thesis, are needed.

The excited state acid-base reaction is very sensitive to the presence or absence of water molecules and protons, which may make it a good choice to probe 1,8-DAN at catalyst surfaces with different acidity.

We estimate the hybridization of 1,8-DAN to be $SP^{2.2}$ for nitrogen, due to the delocalization of the lone pair.

REFERENCES

1. Caldin, E. ; Gold, V. Proton-Transfer Reactions. London: Chapman and Hall, 1975.
2. Bamford, C. ; Tipper, C. Comprehensive Chemical Kinetics. Proton Transfer, Vol. 8. Amsterdam: Elsevier, 1977.
3. Pine, E. ; Huppert, D. and Agmon, N. J. Chem. Phys. 1988, **88**, 5620.
4. Shizuka, H. Acc. Chem. Res. 1985, **18**, 141.
5. Tsutsumi, K. and Shizuka, H. Chem. Phys. Lett. 1977, **52**, 485.
6. El-Rayyes, A. ; Perzanowski, H. ; Barri, S. and Klein, U. J. Phys. Chem. A, 2001, **105(45)**, 10169.
7. El-Rayyes, A. Dissertation, Ph.D, KFUPM, 2001.
8. El-Rayyes, A. ; Perzanowski, H. ; Klein, U. and Barri, S. Catal. Lett. 2002, **78**, 161.

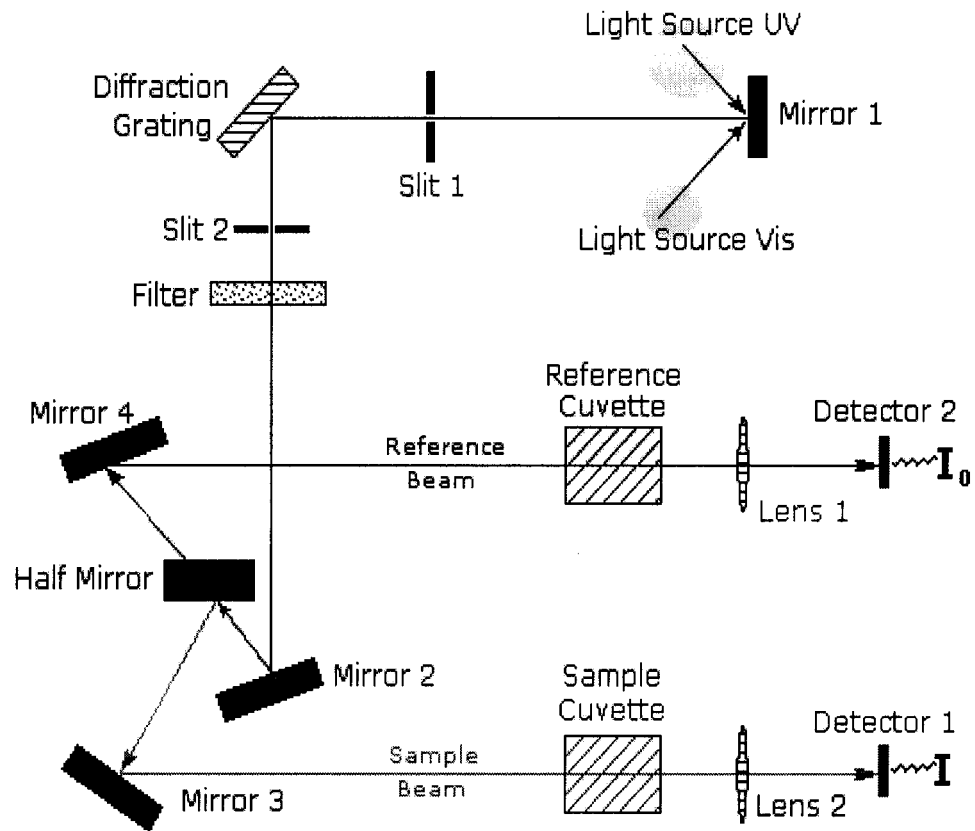
9. Paul; Sarpal and Dogra. Chem. Soc. Faraday Trans. 1990, **86(12)**, 2095.
10. Than Htun, M. Dissrtation, Ph.D, KFUPM,1994.
11. Than Htun, M. ; Suwaiyan, A. ; Baig, A. and Klein, U. J. Phys. Chem. A. 1998, **102**, 8230.
12. Than Htun, M. ; Suwaiyan, A. and Klein, U. Chem. Phys. Lett. 1995, **243**, 71.
13. Than Htun, M. ; Suwaiyan, A. ; Klein, U. Chem. Phys. Lett. 1995, **243**, 506.
14. Than Htun, M. ; Suwaiyan, A. ; Klein, U. Chem. Phys. Lett. 1997, **264**, 285.
15. Than Htun, M. ; Suwaiyan, A. ; Klein, U. Chem. Phys. Lett. 1995, **243**, 512.
16. Eigen, M. Discuss. Faraday Soc. 1954, **17**, 194.
17. Laidler, K. Chemical Kinetics. New York: Harper Collins, 1987.
18. Forster, T. Z. Electrochem. 1950, **54**, 531.
19. Weller, A. Prog. React. Kinet. 1961, **1**, 187.
20. Weller, A. Z. Phys. Chem. (Wiesbaden). 1958, **17**, 224.
21. Lee, La and Park. Organometallics. 1998, **17(17)**, 3648.
22. Zuber and Pruchnik. Reaction Kinetics and Catalysis Letters. 1976, **4(2)**, 281.

23. Lee, J. W. ; Park, D. S. ; Shim, Y.-B. and Park, S.-M. J. Electrochem. Soc. 1992, **139**, 3507.
24. Nasalska, A. and Skampska, M. J. Appl. Electrochem. 2003, **33(1)**, 113.
25. Bagheri, A and Nateghi, M. Indian J. Chem. A. 1998, **37A (7)**, 606.
26. Majid, S. ; El Rahzi, M. ; Amine, A. ; Curulli, A. and Palleschi, G. Microchimica Acta. 2003, **143(2-3)**, 195.
27. Sibi, Mukund P. Magnetic Resonance in Chem. 1991, **29(4)**, 400.
28. Cho; Moon; Ko; Lee; Kim; Yoon and Nam. J. Am. Chem. Soc. 2003, **125(41)**, 12376.
29. Cheung, Y. ; Lewis, D. ; Ridd, T. ; Gray, T. and Ioannides, C. Toxicology. 1997, **118(2, 3)**, 115.
30. Arnett, E. ; Venkatasubramanian, K. and McIver, R. J. Am. Chem. Soc. 1982, **104(1)**, 325.
31. Kakazai, B. and Melson, G. Inorg. Chim. Acta. 1968, **2(2)**, 186.
32. Kaupp G; Naimi-jamal M. And Stepanenko V. Weinheim an der Bergstrasse. 2003, **9(17)**, 4156.
33. Bar-Haim, G. ; Shach, R. and Kol, M. Chemical Communications Cambrige. 1997, **2**, 229.

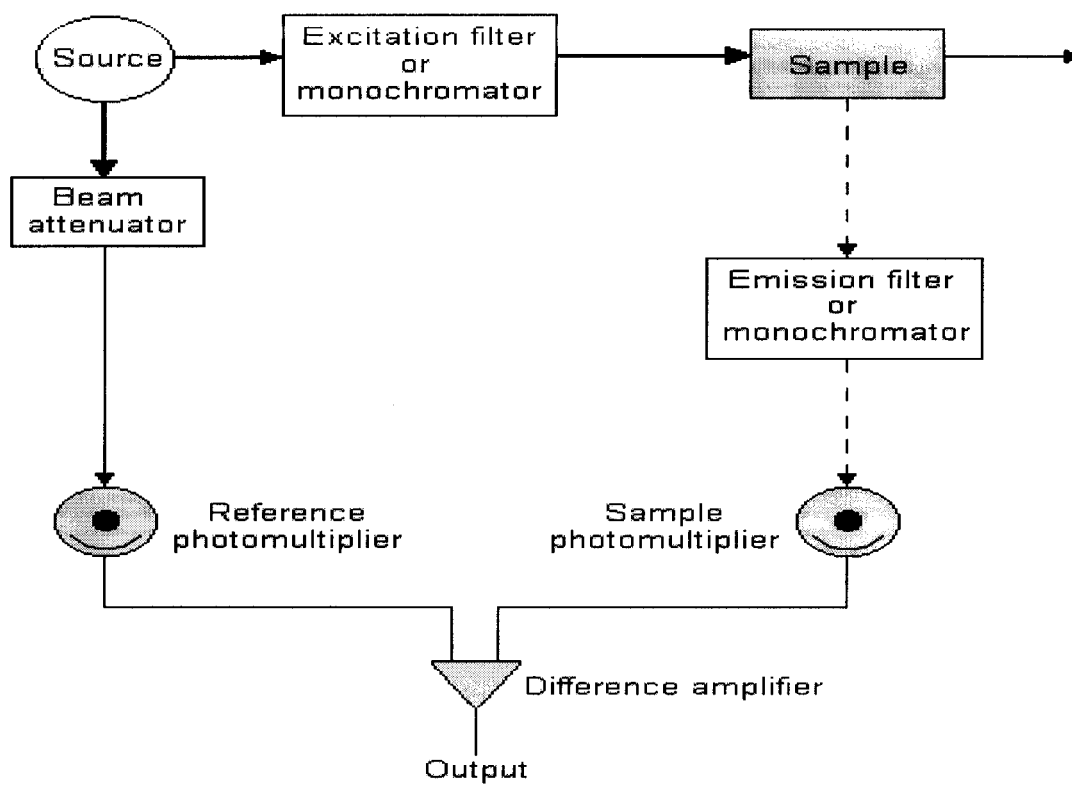
34. Pawelka and Zeegers-Huyskes. Spectroscopic Letters. 1990, **23(8)**, 1111.
35. Alder, R. ; Bryce, M and Goode, N. J. Chem. Soc. 1972. **4**, 477.
36. Llamas-Saiz, A. ; Foces-Foces, C. ; Martinez and Elguero, J. J. Chem. Soc. 1995, **5**, 923.
37. Davis, Christopher C. Lasers and Electro-Optics. New York: 1996.
38. Milonni, Peter and Ebery, Joseph. Lasers. New York: 1988.
39. Sheffield Hallam University (SHU) Site. Instrumentation, “<http://www.shu.ac.uk/schools/sci/chem/tutorials/molspec/lumin3.htm>”
40. Eastham, Derek. Atomic Physics of Lasers, 1986.
41. Price, G. Zeolite Page. “<http://www.personal.utulsa.edu/~geoffrey-price/zeolite/fau.htm>”
42. High Efficiency Cavity Dumper Instruction Manual. Spectra Physics, 1985.
43. Klein, U. and Hafner, F. Chem. Phys. Lett. 1976, **43**, 141.
44. Lakowicz, Joseph. Principles of Fluorescence Spectroscopy. New York: Plenum Press, 1983.

APPENDIX

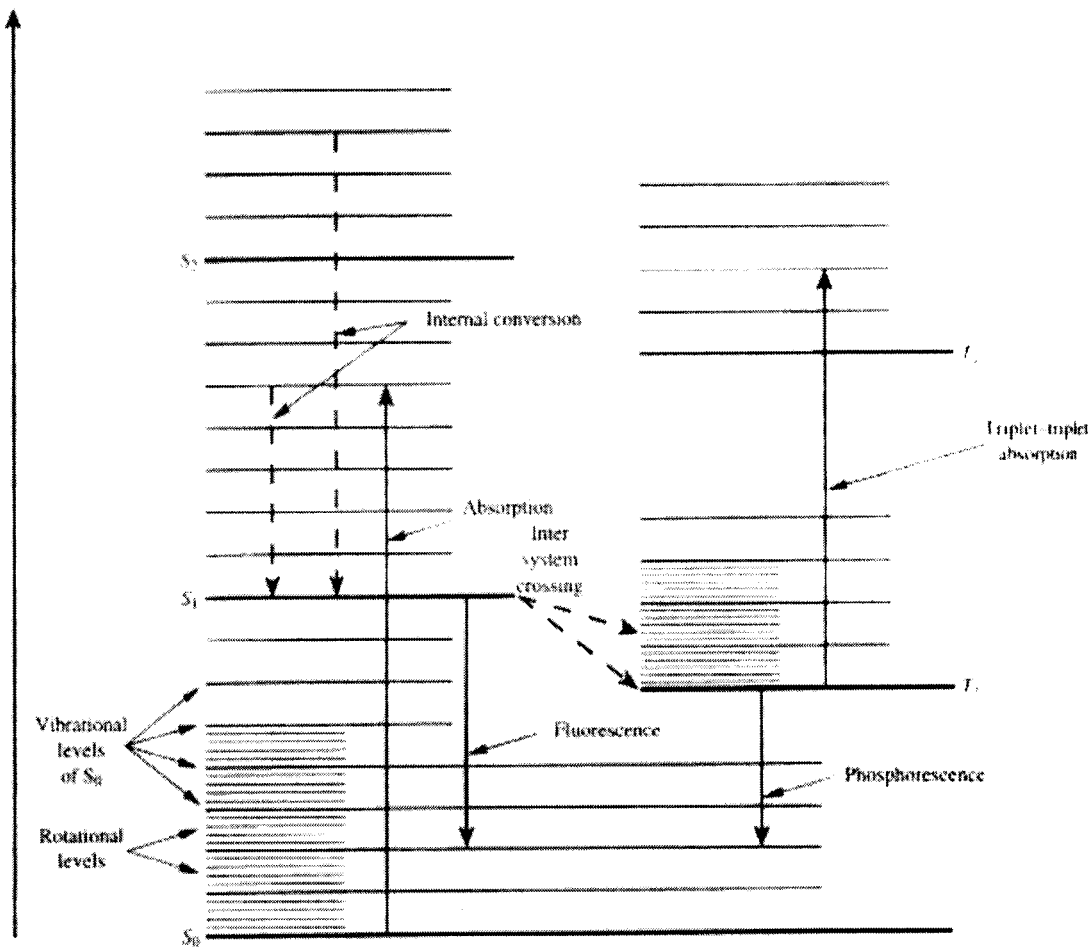
UV-Vis Spectrometer



Fluorometer / Spectrofluorometer



Jablonski Diagram of Energy Levels



Efficiencies and Power Levels of Lasers

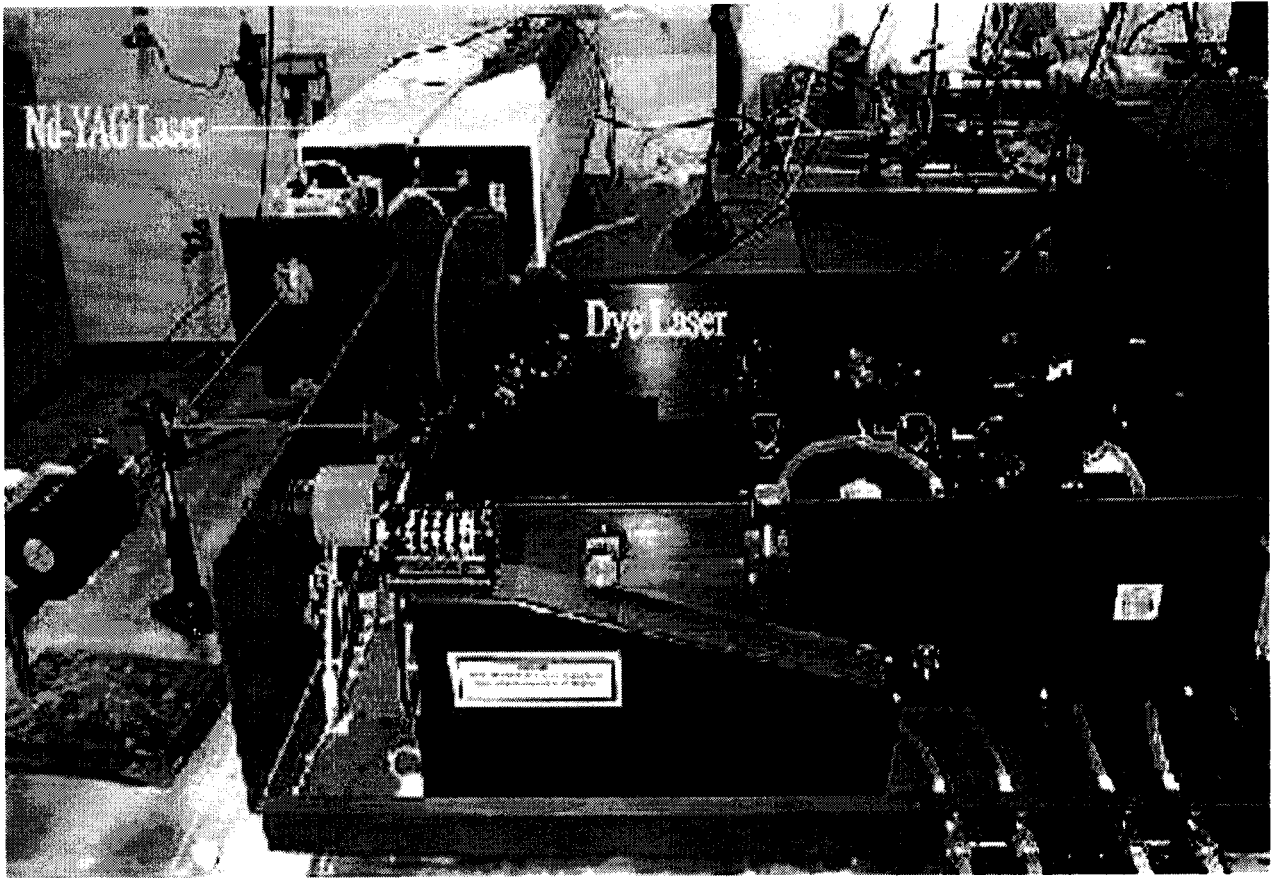
Type	Wavelength (μm)	Efficiency	Power levels available (W)	
			Pulsed	CW
CO ₂	10.6	0.01 - 0.02 (pulsed)	$> 2 \times 10^{13}$	$> 10^5$
CO	5	0.4	$> 10^9$	> 100
Holmium	2.06	0.03 (lamp) 0.1 (diode)	$> 10^7$	30
Iodine	1.315	0.003	$> 10^{12}$	-
Nd-glass, YAG	1.06	0.001 - 0.06 (lamp) > 0.1 (diode)	$\sim 10^{14}$ (10 beams)	$1 - 10^3$
* Color center	1 - 4	10^{-3}	$> 10^6$	1
* Vibronic (Ti Sapphire)	0.7 - 0.9	$> 0.1 \times \eta_p$	10^6	1 - 5
Ruby	0.6943	$< 10^{-3}$	10^{10}	1
He-Ne	0.6328	10^{-4}	-	$1 - 50 \times 10^{-3}$
* Argon ion	0.45 - 0.60	10^{-3}	5×10^4	1 - 20
* OPO	0.4 - 9.0	$> 0.1 \times \eta_p$	10^6	1 - 5
N ₂	0.3371	0.001 - 0.05	$10^5 - 10^6$	-
* Dye	0.3 - 1.1	10^{-3}	$> 10^6$	140
Kr - F	0.26	0.08	$> 10^9$	500
Xenon	0.175	0.02	$> 10^8$	-

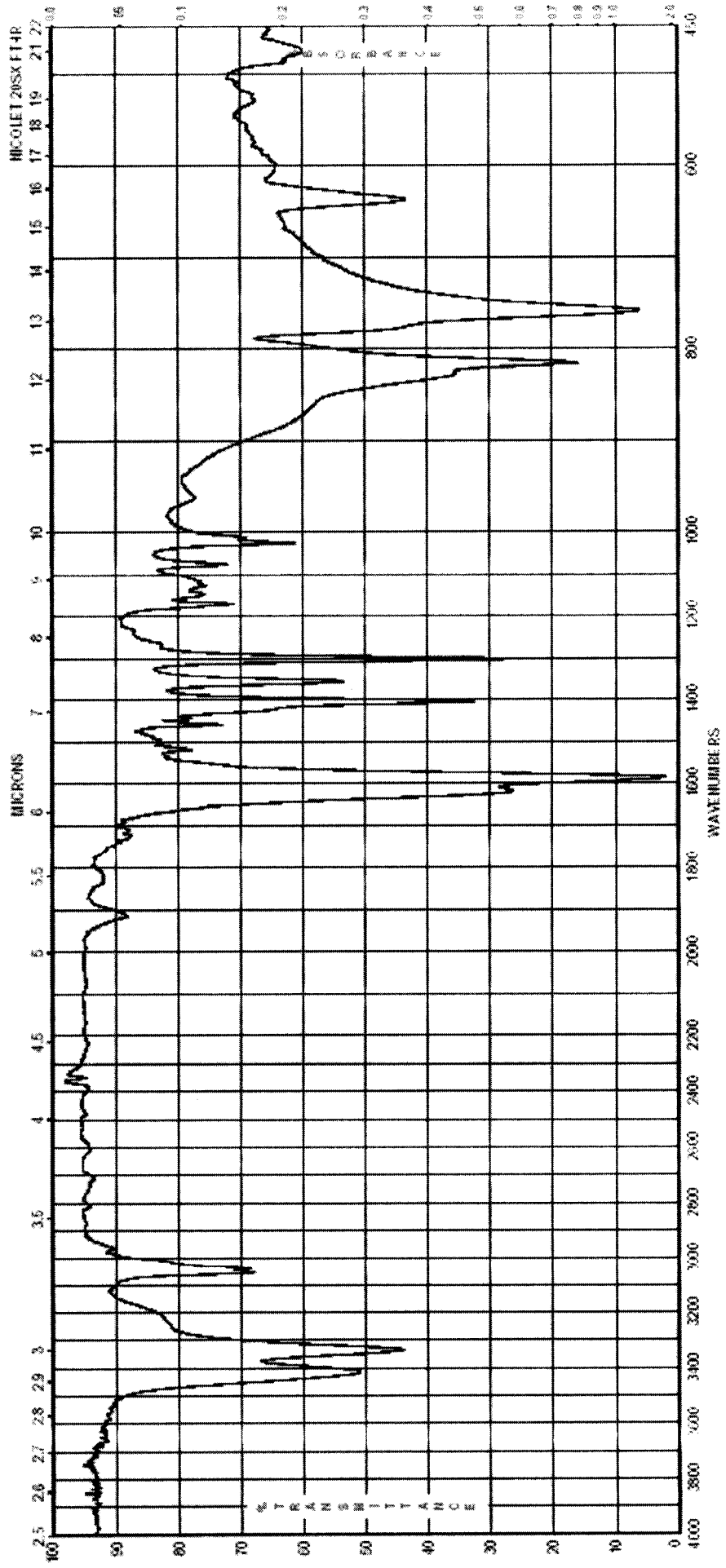
* = Tunable sources, η_p =pump laser efficiency

YAG stands for Yttrium Aluminum Garnet and OPO for Optical Parametric Oscillator

η_p is pump laser efficiency.

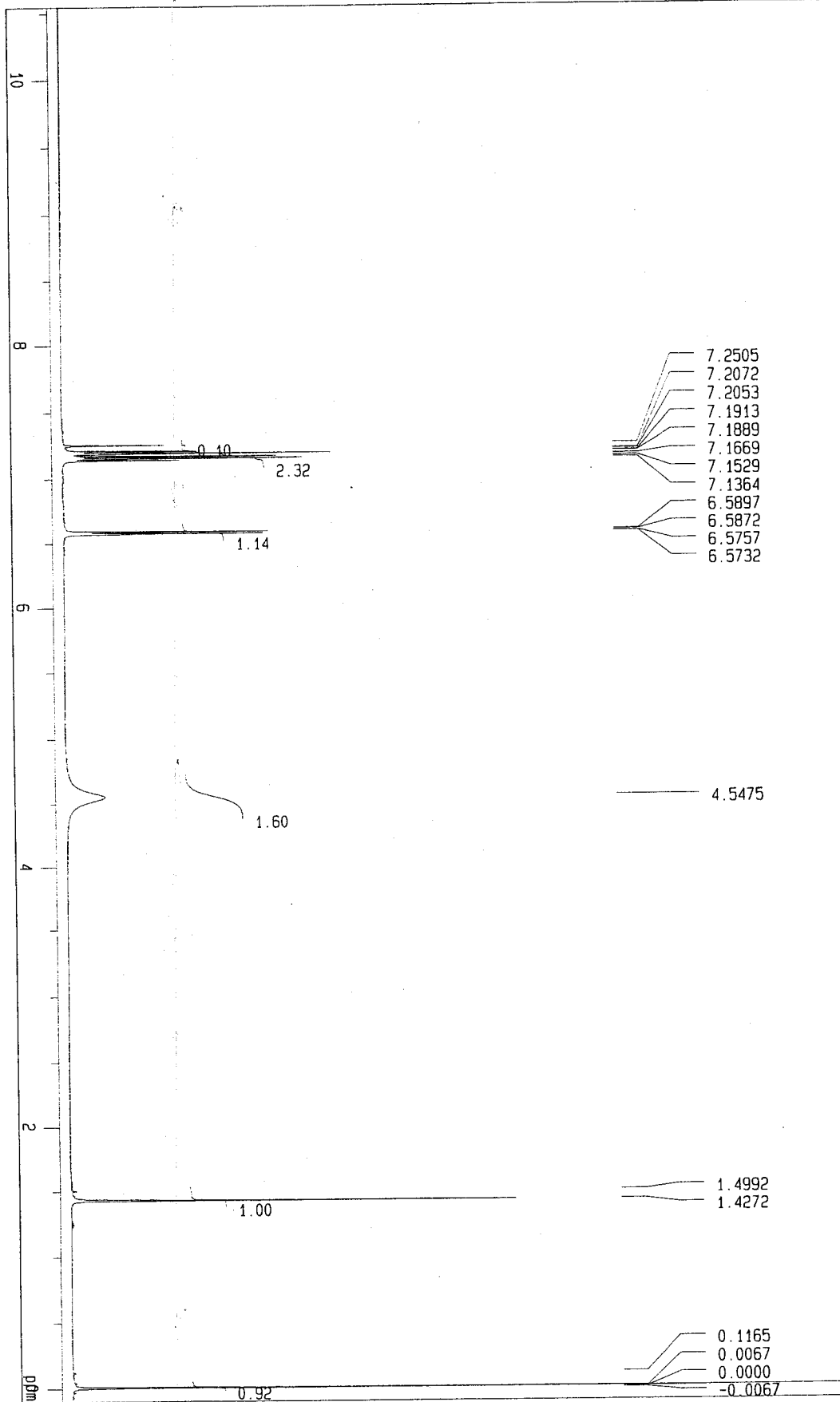
**Mode-Locked Nd:YAG Laser With A Cavity-Dumped
Synchronously Pumped Dye Laser**



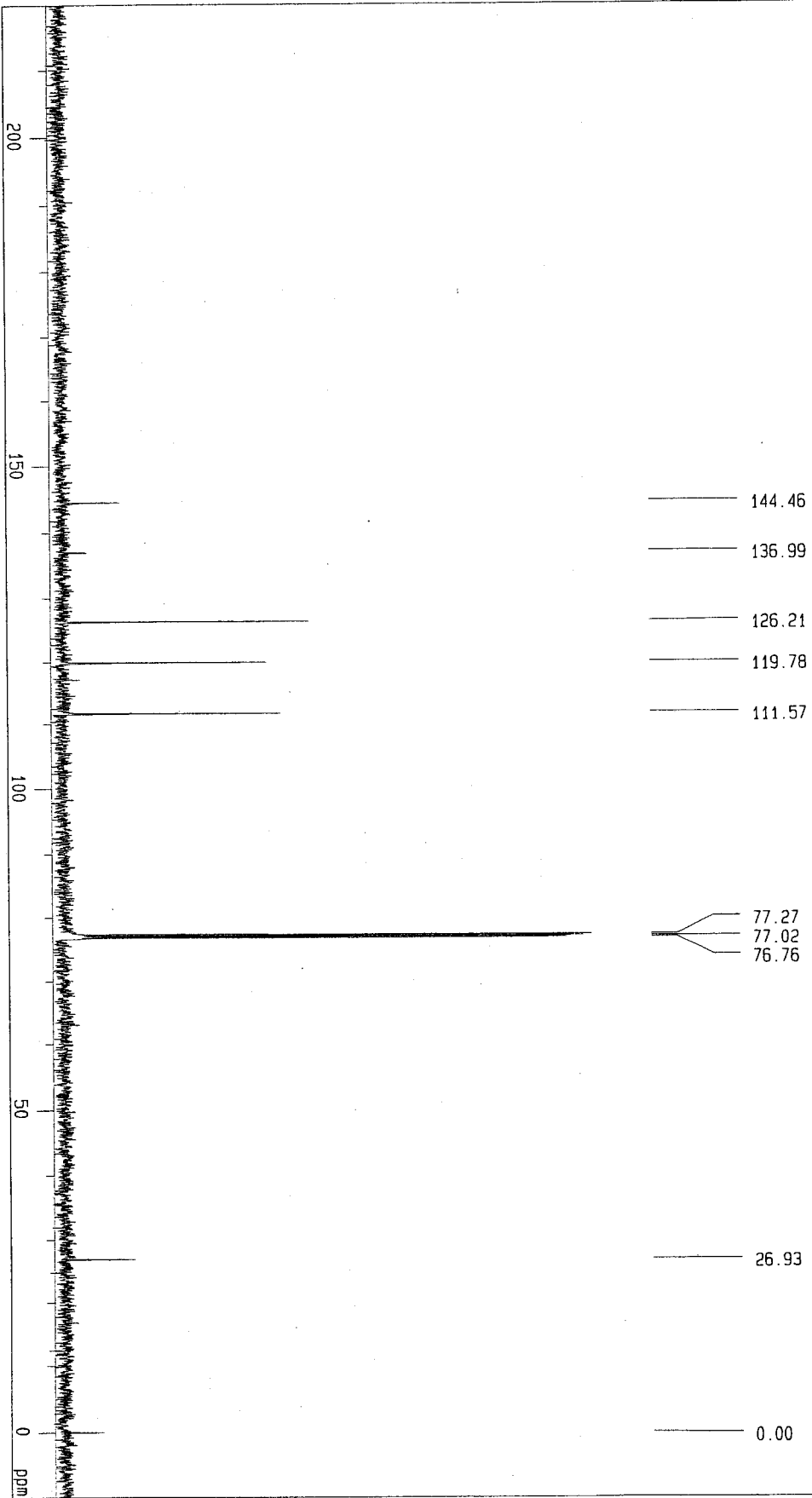


IR of 1,8-DAN

1H NMR 1, 8-DAN



13C NMR 1, 8-DAN



VITA

- Abdul-Rahman Faisal Al-Betar
- Joined King Fahd university of Petroleum & Minerals in 1997.
- Received Bachelor of Science (B.Sc.) degree in Chemistry from King Fahd university of Petroleum & Minerals in May 2002.
- Worked as Graduate Assistant (GA) at KFUPM.
- Received Master of Science (M.S.) degree in Physical Chemistry from King Fahd university of Petroleum & Minerals in May 2004.